

NOTE TO USERS

Page(s) missing in number only; text follows. The manuscript was microfilmed as received.

VII

This reproduction is the best copy available.

UMI[®]

RICE UNIVERSITY

EFFECTS OF MACROMOLECULAR CROWDING AND SMALL IONS ON THE FOLDING, STRUCTURE, AND STABILITY OF *DESULFOVIBRIO DESULFURICANS* FLAVODOXIN

by

Loren Stagg

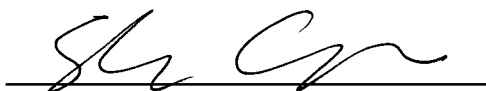
A THESIS SUBMITTED IN PARTIAL FULFILLMENT
OF THE REQUIREMENTS FOR THE DEGREE

DOCTOR OF PHILOSOPHY

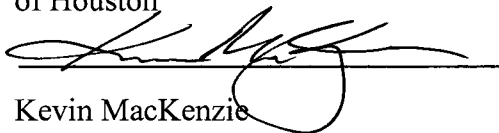
APPROVED, THESIS COMMITTEE



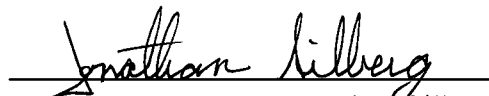
Pernilla Wittung-Stafshede, Chair,
Adjunct Professor, Biochemistry and Cell
Biology



Margaret Cheung
Assistant Professor, Physics, University
of Houston



Kevin MacKenzie
Assistant Professor, Biochemistry and
Cell Biology



Jonathan Silberg
Assistant Professor, Biochemistry and
Cell Biology



Bonnie Bartel
Professor, Biochemistry and Cell Biology



Jane Tao
Assistant Professor, Biochemistry and
Cell Biology

HOUSTON, TEXAS

UMI Number: 3425260

All rights reserved

INFORMATION TO ALL USERS

The quality of this reproduction is dependent upon the quality of the copy submitted.

In the unlikely event that the author did not send a complete manuscript and there are missing pages, these will be noted. Also, if material had to be removed, a note will indicate the deletion.



UMI 3425260

Copyright 2010 by ProQuest LLC.

All rights reserved. This edition of the work is protected against unauthorized copying under Title 17, United States Code.



ProQuest LLC
789 East Eisenhower Parkway
P.O. Box 1346
Ann Arbor, MI 48106-1346

ABSTRACT

EFFECTS OF MACROMOLECULAR CROWDING AND SMALL IONS ON THE FOLDING, STRUCTURE, AND STABILITY OF *DESULFOVIBRIO DESULFURICANS* FLAVODOXIN

by

Loren Stagg

The intracellular environment in which most proteins fold and function contains a range of biomolecules that results in significant volume exclusion, thus contrasting to the dilute buffer conditions common to most *in vitro* studies. In addition to intracellular macromolecular crowding, cells are ionic in nature, and although the Hofmeister series of ions has its origin in a work from 1888, much is still unclear concerning how small, charged ions affect protein properties. This thesis summarizes *in vitro* work assessing the effects of macromolecular crowding and small ions on the biophysical properties of a model protein – *Desulfovibrio desulfuricans* flavodoxin. Flavodoxin is a small (15.7 kDa), single domain, cytoplasmic protein with α -helical and parallel β -sheet secondary structural elements arranged in one of the five most common protein folds (the flavodoxin-like fold).

Using a range of biophysical/spectroscopic methods (e.g., circular dichroism (CD), fluorescence, calorimetry, stopped-flow mixing) along with synthetic crowding agents (e.g., Ficoll and dextran), I have found that macromolecular crowding increases the secondary structural content of folded

flavodoxin (toward that found in the crystal structure), increases flavodoxin thermal stability, and affects both the accumulation of a misfolded intermediate and the rate of proper protein folding. Collaborative *in silico* simulations employing Gō-like modeling of apoflavodoxin in the presence of large, inert crowding agents agrees with my *in vitro* work and provides structural and mechanistic information with residue-specific resolution.

We also found that small cations and anions in physiologically relevant concentrations (≤ 250 mM) increase flavodoxin thermal stability significantly. Both cations and anions in higher concentrations (300 mM – 1.75 M) affect oppositely charged proteins similarly suggesting that surface electrostatic charge plays only a minor role in mediating ionic effects on protein thermal stability. At all ion concentrations, ionic effects on protein stability are correlated to ion hydration (and thus the Hofmeister series). Our work suggests a dominant role for the peptide bond in coordinating ions at higher concentrations. This thesis work suggests that the crowded and ionic nature of the intracellular milieu can elicit changes to the structure, dynamics, stability, and folding mechanism of proteins which may not be captured *in vitro* using dilute buffer conditions.

ACKNOWLEDGMENTS

This thesis summarizes a number of projects that would not have been possible without the collaborative and advisory efforts of many people for whom I am very grateful. In particular, my thesis advisor Dr. Pernilla Wittung-Stafshede gave guidance and insight for each of the works detailed in this document. Collaborative works within the Wittung-Stafshede lab included early studies with Dr. Michael Perham assessing the effects of macromolecular crowding on protein structure and equilibrium stability as well as two projects with Dr. Erik Sedlák probing the effects of small ions on protein thermal stability. Both Drs. Perham and Sedlák provided a wealth experimental and general knowledge.

All *in silico* work detailed in this thesis was performed by the lab of Dr. Margaret Cheung (Department of Physics, University of Houston). Without the simulation work performed by the Cheung group (Dr. Dirar Homouz, Antonios Samiotakis, and S.Q. Zhang), we would not have been able to propose precise structural and mechanistic details in our attempts to explain *in vitro* observations assessing macromolecular crowding effects. Recent simulation work was made possible thanks to the solving of the *D. desulfuricans* flavodoxin crystal structure by Drs. Yousif Shamoo and Megan Guelker.

In addition to published collaborative work, Drs. Kevin MacKenzie and Adina Maximciuc-Kilpatrick provided expertise in performing and visualizing 2D-

NMR experiments using flavodoxin and Ficoll 70 which is not detailed here. Drs. MacKenzie and Joff Silberg also served as valuable local mentors and advisors. In addition to the aforementioned Drs. MacKenzie, Silberg and Cheung, I would like to thank the other members of my thesis committee, Drs. Bonnie Bartel and Jane Tao for their encouragement and constructive advice. Last, I would like to thank other members of the Wittung-Stafshede lab for their encouragement and friendship – Dr. David Apiyo, David Culbertson, Faiza Hussain, Dr. Kathryn Luke, Agustina Rodriguez-Granillo, and Dr. Corey Wilson.

LIST OF PUBLICATIONS

Much of the work presented in this thesis is summarized in the following publications (published or in review).

- 1.) Perham, M.*, Stagg, L.*, and Wittung-Stafshede, P. (2007). Macromolecular crowding increases structural content of folded proteins. *FEBS Lett* 581, 5065-5069.
- 2.) Stagg, L., Zhang, S.Q., Cheung, M.S., and Wittung-Stafshede P. (2007). Molecular crowding enhances native structure and stability of α/β protein flavodoxin. *Proc Natl Acad Sci U S A* 104, 18976-18981.
- 3.) Sedláč, E.*, Stagg, L.*, and Wittung-Stafshede, P. (2008). Role of cations in stability of acidic protein *Desulfovibrio desulfuricans* apoflavodoxin. *Arch Biochem Biophys* 474, 128-135.
- 4.) Sedláč, E.*, Stagg, L.*, and Wittung-Stafshede, P. (2008). Effect of Hofmeister ions on protein thermal stability: Roles of ion hydration and peptide groups? *Arch Biochem Biophys* 479, 69-73.
- 5.) Homouz, D., Stagg, L., Wittung-Stafshede, P., and Cheung, M.S. (2009). Macromolecular crowding modulates folding mechanism of α/β protein apoflavodoxin. *Biophys J* 96, 671-680.
- 6.) Guelker, M., Stagg, L., Wittung-Stafshede, P., and Shamoo, Y. (2009). Pseudosymmetry, high copy number and twinning complicate the structure determination of *Desulfovibrio desulfuricans* (ATCC 29577) flavodoxin. *Acta Crystallogr D Biol Crystallogr* 65, 523-534.
- 7.) Stagg, L., Samiotakis, A., Homouz, D., Cheung, M.S., and Wittung-Stafshede, P. (2009). Residue specific analysis of frustration in folding landscape of repeat β/α protein apoflavodoxin (in review).

* denotes co-first-authored papers

TABLE OF CONTENTS

<u>CHAPTER 1: INTRODUCTION TO PROTEIN FOLDING AND THE INTRACELLULAR MILIEU</u>	<u>1</u>
PROTEIN FOLDING	1
THE NATIVE STATE	2
FOLD AND FUNCTION	4
COFACTOR-BINDING PROTEINS	5
PROTEIN FOLDING MECHANISMS AND THEORIES	7
EXPERIMENTAL STUDIES OF EQUILIBRIUM AND KINETIC FOLDING REACTIONS	11
THERMAL AND CHEMICAL EQUILIBRIUM DENATURATION	12
PHI-VALUE APPROACH FOR FOLDING TRANSITION STATE ANALYSIS	13
COMPUTATIONAL APPROACHES	16
FLAVODOXIN – A MODEL PROTEIN	19
THE FLAVODOXIN-LIKE FOLD	19
STRUCTURE, FUNCTION, AND COFACTOR	21
CURRENT KNOWLEDGE OF FLAVODOXIN FOLDING REACTIONS	23
SPECIFICS OF <i>DESULFOVIBRIO DESULFURICANS</i> (ATCC 29577) FLAVODOXIN	24
THE INTRACELLULAR ENVIRONMENT	25
MACROMOLECULAR CROWDING AND EXCLUDED VOLUME THEORY	25
SYNTHETIC CROWDING AGENTS	28
EARLY STUDIES: EXPERIMENTAL AND THEORETICAL	29
IONIC NATURE OF THE CELL	29
HOFMEISTER SERIES OF IONS AND PROPERTIES	30
<i>D. DESULFURICANS</i> IS HALOPHILIC	31
<i>D. DESULFURICANS</i> FLAVODOXIN IS NEGATIVELY CHARGED	32
PROJECT GOALS	32
<u>CHAPTER 2: MATERIALS AND METHODS</u>	<u>34</u>
THEORY	34
ABSORPTION AND FLUORESCENCE SPECTROSCOPY	34
CIRCULAR DICHROISM (CD) SPECTROSCOPY	36
DIFFERENTIAL SCANNING CALORIMETRY (DSC)	38
PROTEIN ENGINEERING (SITE-DIRECTED MUTAGENESIS)	40
EXPERIMENTAL	40
PROTEIN PURIFICATION	40
ION EXCHANGE	41
GEL FILTRATION (SIZE EXCLUSION)	43
THERMAL AND CHEMICAL EQUILIBRIUM EXPERIMENTS	45
KINETIC FOLDING DYNAMICS	48
THE AMINO ACID SEQUENCE OF <i>D. DESULFURICANS</i> FLAVODOXIN	51

**CHAPTER 3: EFFECTS OF MACROMOLECULAR CROWDING ON THE
STRUCTURE AND STABILITY OF FLAVODOXIN** **54**

INCREASE IN PROTEIN SECONDARY STRUCTURE COMPARED TO IN BUFFER	54
INCREASE IN THERMAL STABILITY	57
INCREASE IN CHEMICAL STABILITY	63
DISCUSSION	67
CORRELATION BETWEEN <i>IN VITRO</i> AND <i>IN SILICO</i> RESULTS	67
SIMILAR TRENDS FOUND WITH UNRELATED, ALPHA-HELICAL PROTEIN (VLSE)	69
SUMMARY	71

**CHAPTER 4: EFFECTS OF SMALL IONS ON STABILITY AND FOLDING OF
APOFLAVODOXIN** **75**

CATIONS IN [≤ 250 MM] AFFECT APOFLAVODOXIN THROUGH SPECIFIC INTERACTIONS	75
CATIONS INCREASE APOFLAVODOXIN THERMAL STABILITY	75
CATIONS INCREASE APOFLAVODOXIN CHEMICAL EQUILIBRIUM STABILITY	81
CATIONS MODULATE THE FOLDED STATE OF APOFLAVODOXIN	81
EFFECTS OF ANIONS ON THERMAL STABILITY	85
CATIONS AFFECT BOTH KINETIC FOLDING AND UNFOLDING RATES OF APOFLAVODOXIN	87
IONS IN LARGER AMOUNTS (> 250 MM) AFFECT STABILITY OF OPPOSITELY CHARGED PROTEINS (APOFLAVODOXIN AND CYTOCHROME C) SIMILARLY	87
EFFECTS OF IONS ON APOFLAVODOXIN AND CYTOCHROME C THERMAL STABILITY	89
CORRELATION OF ION EFFECTS WITH ION PROPERTIES	91
ION PARTITION COEFFICIENTS	91
SURFACE TENSION	93
PREFERENTIAL HYDRATION	95
CHARGE DENSITY	96
ROLE OF PEPTIDE BACKBONE	96
DISCUSSION	98

**CHAPTER 5: TIME-RESOLVED FOLDING MECHANISM OF APOFLAVODOXIN
AND ROLE OF MACROMOLECULAR CROWDING** **101**

ASSESSING FOLDING MECHANISM OF APOFLAVODOXIN	101
EFFECTS OF MACROMOLECULAR CROWDING ON FOLDING OF APOFLAVODOXIN	101
<i>IN VITRO</i> AND <i>IN SILICO</i> RESULTS SUGGEST CROWDING AGENT GEOMETRY AFFECTS FOLDING MECHANISM	104
RESIDUE-SPECIFIC ANALYSIS OF APOFLAVODOXIN FOLDING MECHANISM	108
EQUILIBRIUM STUDIES OF APOFLAVODOXIN VARIANTS	112
<i>IN VITRO</i> FOLDING ANALYSIS OF WILD-TYPE AND MUTANT APOFLAVODOXINS	115

DISCUSSION	120
<i>IN SILICO</i> DATA CORRELATES WITH <i>IN VITRO</i> RESULTS	120
COMPETING NUCLEI IN CENTRAL BETA-SHEET DRIVE APOFLAVODOXIN FOLDING	126
SUMMARY	129
<u>CHAPTER 6: SUMMARY, OVERALL PERSPECTIVE, AND FUTURE DIRECTION</u>	<u>136</u>
<i>IN VITRO</i> DATA SUGGESTS INTRACELLULAR CONDITIONS SIGNIFICANTLY MODIFY PROPERTIES OF APOFLAVODOXIN	136
EFFECTS OF MACROMOLECULAR CROWDING ON APOFLAVODOXIN PROPERTIES: PROPOSED MECHANISM, DISCUSSION OF CURRENT CROWDING THEORY, AND IMPLICATIONS FOR THE FUTURE	136
EFFECTS OF HOFMEISTER IONS ON APOFLAVODOXIN (AND CYTOCHROME C) STABILITY: PROPOSED MECHANISMS FOR ION-INDUCED PROTEIN STABILITY	141
FUTURE DIRECTION OF THIS PROJECT AND IMPLICATIONS FOR FUTURE <i>IN VITRO</i> WORK	145
REFERENCES	147
APPENDIX	171
EFFECTS OF MACROMOLECULAR CROWDING ON APOFLAVODOXIN FOLDING MECHANISM	171
EFFECTS OF CROWDING ON WILD-TYPE AND MUTANT APOFLAVODOXIN EQUILIBRIUM STABILITY	171
EFFECTS OF CROWDING ON KINETIC FOLDING/UNFOLDING OF WILD-TYPE AND MUTANT APOFLAVODOXINS	173

LIST OF TABLES

TABLE 3.1: SOMCD STRUCTURAL PREDICTION OF CROWDING EFFECTS ON APOFLAVODOXIN SECONDARY STRUCTURAL CONTENT	58
TABLE 3.2: THERMAL MIDPOINTS OF APOFLAVODOXIN WITH VARYING [FICOLL 70] AND BUFFER CONDITIONS	62
TABLE 4.1: THERMAL MIDPOINTS OF APOFLAVODOXIN WITH VARYING [GDM ⁺]	78
TABLE 4.2: THERMODYNAMIC PARAMETERS CALCULATED FROM UREA EQUILIBRIUM UNFOLDING OF APOFLAVODOXIN IN PRESENCE OF CATIONS	82
TABLE 4.3: $dT_M/d[ION]$ VALUES FOR APOFLAVODOXIN AND CYTOCHROME C	92
TABLE 5.1: FOLDING AND UNFOLDING RATES OF APOFLAVODOXIN IN VARIOUS [FICOLL 70] AND [DEXTRAN 70]	103
TABLE 5.2: EQUILIBRIUM THERMODYNAMIC PARAMETERS CALCULATED FOR WILD-TYPE AND MUTANT APOFLAVODOXINS	114
TABLE 5.3: KINETIC PARAMETERS CALCULATED FOR WILD-TYPE AND MUTANT APOFLAVODOXINS	118
TABLE A.1: EQUILIBRIUM THERMODYNAMIC PARAMETERS CALCULATED FOR WILD-TYPE AND MUTANT APOFLAVODOXINS IN PRESENCE OF 100 MG/ML FICOLL 70	172
TABLE A.2: KINETIC PARAMETERS CALCULATED FOR WILD-TYPE AND MUTANT APOFLAVODOXINS IN PRESENCE OF 100 MG/ML FICOLL 70	176

LIST OF FIGURES

FIGURE 1.1: CHEMICAL STRUCTURE OF PEPTIDE BOND	3
FIGURE 1.2: FIVE MOST COMMON PROTEIN FOLDS	6
FIGURE 1.3: FUNNEL-SHAPED FOLDING ENERGY LANDSCAPE	10
FIGURE 1.4: CHEMICAL STRUCTURES OF UREA AND GUANIDINIUM-CHLORIDE	14
FIGURE 1.5: ENERGY DIAGRAM OF PROTEIN FOLDING REACTION COORDINATE	14
FIGURE 1.6: ENERGY DIAGRAMS DEPICTING PHI-VALUES OF 1 AND 0	17
FIGURE 1.7: STRUCTURE OF <i>D. DESULFURICANS</i> FLAVODOXIN	20
FIGURE 1.8: CHEMICAL STRUCTURE OF FMN	22
FIGURE 1.9: CROWDED CONDITIONS OF THE CELL	27
FIGURE 1.10: DEPICTION OF EXCLUDED VOLUME	27
FIGURE 2.1: CHARACTERISTIC UV-VIS SPECTRUM	35
FIGURE 2.2: CHARACTERISTIC FLUORESCENCE SPECTRA	37
FIGURE 2.3: CHARACTERISTIC CD SPECTRA	39
FIGURE 2.4: CHARACTERISTIC DSC THERMOGRAM	39
FIGURE 2.5: SDS-PAGE OF FLAVODOXIN	44
FIGURE 2.6: CHARACTERISTIC CHEVRON PLOT	50
FIGURE 2.7: FLAVODOXIN SEQUENCE ALIGNMENT	53
FIGURE 2.8: THERMAL AND UREA EQUILIBRIUM DENATURATION OF WILD-TYPE AND D79N APOFLAVODOXIN	53
FIGURE 3.1: CROWDING EFFECTS ON FOLDED APO- AND HOLOFLAVODOXIN	56
FIGURE 3.2: CROWDING EFFECTS ON GDMCL-UNFOLDED APO- AND HOLOFLAVODOXIN	58
FIGURE 3.3: CROWDING EFFECTS ON THERMALLY UNFOLDED APO- AND HOLOFLAVODOXIN	59

FIGURE 3.4: CROWDING EFFECTS ON HOLOFLAVODOXIN THERMAL STABILITY	61
FIGURE 3.5: CROWDING EFFECTS ON APOFLAVODOXIN THERMAL STABILITY	61
FIGURE 3.6: CROWDING EFFECTS ON APOFLAVODOXIN CHEMICAL STABILITY (10 mM HEPES, PH 7)	64
FIGURE 3.7: CROWDING EFFECTS ON APOFLAVODOXIN CHEMICAL STABILITY (100 mM KPI, PH 7)	66
FIGURE 3.8: DEPICTION OF PERIODIC BOX	68
FIGURE 3.9: 2D ENERGY LANDSCAPE OF APOFLAVODOXIN WITH/WITHOUT CROWDING	70
FIGURE 4.1: ELECTROSTATIC MAP OF APOFLAVODOXIN	76
FIGURE 4.2: DSC OF APOFLAVODOXIN WITH GDM^+	78
FIGURE 4.3: APOFLAVODOXIN T_M VS [CATION]	79
FIGURE 4.4: UREA DENATURATION OF APOFLAVODOXIN WITH/WITHOUT GDM^+	82
FIGURE 4.5: FAR- AND NEAR-UV CD OF APOFLAVODOXIN WITH/WITHOUT GDM^+	84
FIGURE 4.6: ANS FLUORESCENCE VS [CATION]	84
FIGURE 4.7: APOFLAVODOXIN T_M VS [ANION]	86
FIGURE 4.8: CHEVRON PLOTS OF APOFLAVODOXIN WITH/WITHOUT CATIONS	88
FIGURE 4.9: APOFLAVODOXIN AND CYTOCHROME C T_M VS [ION]	90
FIGURE 4.10: APOFLAVODOXIN AND CYTOCHROME C $dT_M/d[ION]$ VS ION PARTITION COEFFICIENTS	94
FIGURE 4.11: APOFLAVODOXIN AND CYTOCHROME C $dT_M/d[ION]$ VS ION CHARGE DENSITY	97
FIGURE 5.1: CROWDING EFFECTS ON APOFLAVODOXIN FOLDING/UNFOLDING RATES	103
FIGURE 5.2: CHARACTERISTIC MISSING AMPLITUDE IN APOFLAVODOXIN FOLDING PHASE	105
FIGURE 5.3: FOLDING ROUTE ANALYSIS OF APOFLAVODOXIN WITH/WITHOUT CROWDING	107

FIGURE 5.4: MUTANT APOFLAVODOXINS	110
FIGURE 5.5: CD SPECTRA OF FOLDED WILD-TYPE AND MUTANT APOFLAVODOXINS	110
FIGURE 5.6: OVERLAY OF <i>D. VULGARIS</i> AND <i>D. DESULFURICANS</i> FLAVODOXIN STRUCTURES	111
FIGURE 5.7: THERMAL DENATURATION OF WILD-TYPE AND MUTANT APOFLAVODOXINS	113
FIGURE 5.8: UREA DENATURATION OF WILD-TYPE AND MUTANT APOFLAVODOXINS	113
FIGURE 5.9: FREE ENERGY OF UNFOLDING VS T_M FOR WILD-TYPE AND MUTANT APOFLAVODOXINS	114
FIGURE 5.10: CHEVRON PLOTS FOR WILD-TYPE AND MUTANT APOFLAVODOXINS	117
FIGURE 5.11: FREE ENERGIES OF UNFOLDING (KINETIC) VS FREE ENERGIES OF UNFOLDING (EQUILIBRIUM) FOR WILD-TYPE AND MUTANT APOFLAVODOXINS	118
FIGURE 5.12: DEPICTION OF CALCULATED MUTANT APOFLAVODOXIN PHI-VALUES	121
FIGURE 5.13: FOLDING ROUTE ANALYSIS OF WT, V33A, AND V88A APOFLAVODOXIN	124
FIGURE 5.14: DEPICTION OF FOLDING NUCLEI IN APOFLAVODOXIN	128
FIGURE 5.15: BURST CD SIGNAL (%) VS $ NB1 - NB4 $ FOR WILD-TYPE AND MUTANT APOFLAVODOXINS	128
FIGURE A.1: CHEVRON PLOTS USING LINEAR FITS FOR WILD-TYPE AND MUTANT APOFLAVODOXINS IN PRESENCE OF 100 MG/ML FICOLL 70	175
FIGURE A.2: CHEVRON PLOTS USING CURVED FITS FOR WILD-TYPE AND MUTANT APOFLAVODOXINS IN PRESENCE OF 100 MG/ML FICOLL 70	175

LIST OF ABBREVIATIONS

ANS: *1-anilino-8-naphthalene sulfonate*

C α -SCM: *C-alpha side-chain model*

CD: *Circular dichroism*

DSC: *Differential scanning calorimetry*

FMN: *Flavin mononucleotide*

GdmCl: *Guanidinium chloride*

SDS-PAGE: *Sodium dodecyl sulfate polyacrylamide gel electrophoresis*

SRB: *Sulfate reducing bacteria*

T_m: *Thermal midpoint*

CHAPTER 1: INTRODUCTION TO PROTEIN FOLDING AND THE INTRACELLULAR MILIEU

Protein folding

Proteins are truly the workhorses of living organisms as they perform countless tasks covering virtually every essential life function from detoxification, to electron transport, to locomotion. In the simplest terms, proteins are linear chains of amino acids linked covalently by peptide bonds. Over the last century, remarkable progress has been made describing the nature of proteins from the macro level down to the atomic level. The field of protein folding came about along with advances in technology (e.g., NMR spectroscopy and X-ray crystallography) allowing for investigations into protein structure.

From early in the 20th century, scientists began to attempt to explain folding characteristics of proteins such as stability (Wu, 1931). In 1968, Cyrus Levinthal proposed what is now commonly known as the “Levinthal paradox” when he determined that given the rotational freedom available to individual peptide groups, proteins could sample an almost infinite number of conformations, taking an astronomical amount of time to find the proper one (Levinthal, 1968). However, many proteins fold to the same, predictable three dimensional structure reversibly on the order of milliseconds to seconds (Chaffotte et al., 1992; Gruebele, 1999; Li and Scheraga, 1987; Sali et al., 1994). It is this innate ability of many proteins to unfold and fold reversibly that resulted in Anfinsen’s dogma (proposed by Christian Anfinsen) which suggests that all the information necessary for a protein to assume its proper three dimensional structure is

encoded in each protein's unique amino acid sequence (Anfinsen, 1973). *In vivo*, however, newly synthesized proteins may need the aid of chaperone proteins to properly fold (Fink, 1999; Hartl and Martin, 1995; Hartl et al., 1992; Rothman, 1989).

The native state

The unique three dimensional structure assumed by proteins is known as the native (or folded) state. The native state can be broken down into smaller pieces based on levels of complexity. At the lowest level of native state organization is the primary structure. The primary structure is simply the covalently-linked (by peptide-bond) (Fig. 1.1) amino acid sequence which, on its own, gives no structural information, but as Anfinsen explains (Anfinsen, 1973), the amino acid sequence contains all the necessary information for global folding events and is therefore an important part of the "native state." Each amino acid (residue) comprises an amino group, a carboxylic group, and a unique side-chain attached to a central carbon (one amino acid, proline, differs slightly in its structure).

The next level, secondary structure, gives information about the organization of local regions of amino acid residues. Typical secondary structures include α -helices, β -strands, and loops. α -helices are coil-like structures that form when the polypeptide backbone spirals with roughly 3.6 residues per turn. This structure is stabilized by hydrogen bonding between the C=O group of one peptide bond to the N-H group of another peptide bond 4 amino acids away in the primary sequence. β -strands are more planar than α -helices, and instead of

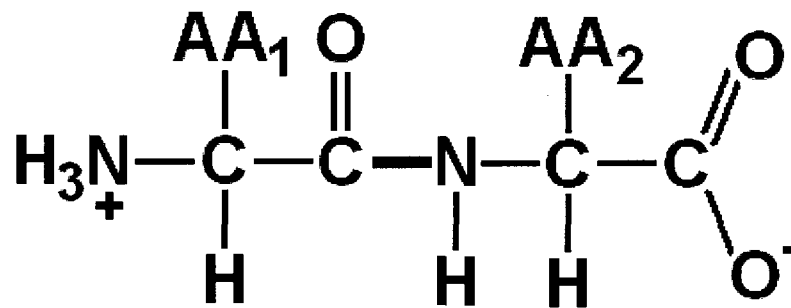


Figure 1.1 – Chemical structure of amino acids covalently linked by peptide bond (bold blue line). Also depicted are the side-chains of the two amino acids (AA₁ and AA₂).

forming interactions between amino acids near each other in primary sequence, amino acids in β -strands hydrogen bond to amino acids across space in other β -strands forming larger structures known as β -sheets. β -sheets may be parallel or anti-parallel depending on whether their individual β -strands align in similar N-terminus to C-terminus direction (parallel) or not (anti-parallel). Loop regions are less ordered than α -helices or β -strands and are thought of as being more dynamic.

The third level of organization is tertiary structure. The tertiary structure of a protein is usually what is being referred to as the native state or native fold. Tertiary structure describes the native topology of proteins as it includes all the secondary structural elements of the protein in the proper spatial arrangement. For monomeric proteins, the tertiary structure is the highest level order that can be described. Quaternary structure applies to multi-domain or multimeric proteins. The quaternary structure describes the spatial arrangement of the subunits that make up the native protein complex.

Fold and function

Proteins must fold to their characteristic, native state in order to perform their function (with the exception of intrinsically disordered proteins) (Wright and Dyson, 1999). In many cases, small, single-domain proteins need only fold to their characteristic tertiary structure to carry out their function. However, in other cases additional layers of complexity are necessary for proteins to function. Individual proteins (monomers) may need to form higher-order, oligomeric

complexes by binding to identical monomers (homo-oligomers) or different monomer proteins (hetero-oligomers). Examples of oligomeric proteins include the dimeric creatine-kinase M-line protein (Mani and Kay, 1976), the trimeric purine nucleoside phosphorylase (Edwards et al., 1973), and the tetrameric hemoglobin (Gibson et al., 1956). In many organisms, complex interactions between many proteins result in intricate molecular machinery that can carry out essential cellular functions such as DNA replication, signal transduction, protein expression, and organismal locomotion. Currently, it is estimated that between 650 and 10,000 protein folds exist (Koonin et al., 2002). The five most common protein folds include the flavodoxin-like, TIM-barrel, Rossmann, thiamin-binding, and P-loop hydrolase folds (Bollen and van Mierlo, 2005) (Fig. 1.2).

Cofactor-binding proteins

In addition to most proteins (excluding intrinsically disordered proteins) folding to a typical, native state in order to mediate protein-protein interactions, many proteins must bind other molecules (cofactors) to function. In fact, over 30% of proteins must bind a characteristic cofactor to carry out their cellular function (Bertini et al., 1994). Typical cofactors include metal ions or organic molecules, which may be bound either covalently or non-covalently. Often similar cofactors are bound either covalently or non-covalently depending on the protein. For instance, covalently bound cofactors include heme binding to cytochrome c (Moore, 1990) and flavin (FAD) bound to succinate dehydrogenase (Yankovskaya et al., 2003). Non-covalently coordinated cofactors include the

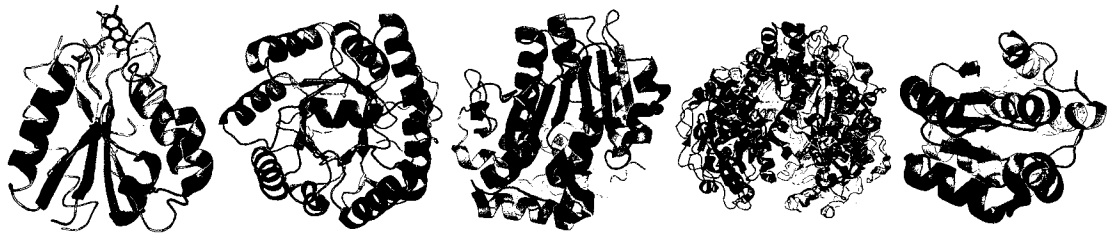


Figure 1.2 - The five most common protein folds. From left to right: the flavodoxin-like fold (pdb:1flv), the TIM-barrel fold (pdb:3chv), the Rossmann fold (pdb:3go4), the thiamin-binding fold (pdb:2qry), and the P-loop hydrolase fold (pdb:2dyp) (PyMol).

flavin mononucleotide (FMN) of flavodoxins (Sancho, 2006) and heme in the case of most globins (Hoy et al., 2007). Cofactor-binding proteins are involved in electron transport (e.g., ferredoxins that coordinate iron-sulfur clusters; (Fromme, 1996)), gas exchange (e.g., hemoglobin), metal transport (e.g., copper chaperones (Schaefer and Gitlin, 1999)), phosphorylation/dephosphorylation (e.g., CheY which coordinates Mg^{2+} (Hess et al., 1987)) and other essential cellular functions. Cofactors are often not synthesized within some organisms and therefore must be present in the organism's diet (vitamins, vitamin derivatives, and some metals (Goyer, 1997)). In addition to contributing to protein function, cofactors also generally engender increased stability in their native protein due to their specific binding to the polypeptide (e.g., heme coordinated to myoglobin (Hargrove et al., 1994), NAD(+) in the case of some DNA ligases (Georlette et al., 2003), and copper coordinated to azurin (Pozdnyakova et al., 2001). As proteins are often able to exist in states with or without cofactor present, these forms of the protein are known as "holo-" (with cofactor) or "apo-" (without cofactor) proteins.

Protein folding mechanisms and theories

As touched on earlier, Levinthal's paradox points to forces driving the folding of proteins via a mechanism or pathway. Differing opinions have since developed to describe the methods employed by proteins to fold from what is thought of to be an unstructured, dynamic polypeptide chain to a more structured, native state. One theory that arose to describe protein folding suggests that small areas (or nuclei) of unfolded polypeptide may conform to

their native arrangement thus providing a scaffold to drive the folding of the rest of the polypeptide (Wetlaufer, 1973). This theory became known as the nucleation (and later “nucleation-condensation”) theory and is still a popular protein folding theory (Djikaev and Ruckenstein, 2009). About the same time as the nucleation theory, Anfinsen proposed that protein folding occurred through the formation of stable interactions between “flickering” nuclei (Anfinsen, 1973).

Another theory to explain protein folding is based on the fact that nonpolar, hydrophobic amino acid side-chains are buried in the core of the protein while polar and charged residues decorate the solvent exposed surface. This theory is known as “hydrophobic collapse,” and it proposes that the spontaneous collapse of hydrophobic residues expels water molecules and drives the global folding of the protein (Hillson et al., 1999; Rhee et al., 2004). The hydrophobic collapse mechanism found its origins in the hypothesis posed by Kauzmann in the 1950s suggesting that nonpolar amino acid coordination must drive folding and determine stability, as proteins have a similar number of hydrogen bonds satisfied both in the native and unfolded states (Kauzmann, 1959). Kauzmann’s theory, which downplays the role of hydrogen bonding in protein folding, is contrary to others who pose a central role for intra-protein hydrogen bonding in productive folding (Baldwin, 2008; Rose et al., 2006). Another proposed protein folding mechanism is the diffusion-collision model proposed by Karplus and Weaver (Karplus and Weaver, 1976). This model proposes that each individual polypeptide chain has separate “microdomains” (such as dynamic helices) which

diffuse independently. The collisions of these microdomains in solution may cause microaggregation events or proper folding.

In contrast to folding pathways, a “New View” has been proposed to satisfy both the search for a thermodynamic energy minimum (proposed by Anfinsen) and also the relatively fast folding times of most proteins (as posed by Levinthal) (Sali et al., 1994). The New View has led to a common theory suggesting that protein folding should be envisioned as a search through a conformational energy landscape populated by multiple folding routes all in search of a thermodynamic energy minimum – the native state. Folding theory in terms of the New View has been proposed to refute the reality of the Levinthal paradox as the large difference between the enthalpies of the folded and unfolded states conformationally biases the polypeptide’s search for the native state making it unnecessary to sample all possible orientations (Dobson and Karplus, 1999). Since the formation of this New View, the folding energy landscape has most often been described as funnel-like (Chan and Dill, 1998) (Fig. 1.3). The width of the funnel-shaped energy landscape (lateral axis) describes the number of available chain conformations at a particular energy level (vertical axis). In many cases, proteins fold through complex mechanisms with intermediate states that may be described as local energy minima in the energy landscape making the funnel appear more rugged (Bryngelson et al., 1995; Leopold et al., 1992). Folding from the high energy, unfolded state to the low energy, native state must proceed through an energy barrier (the rim of the funnel) described as the “transition state.”

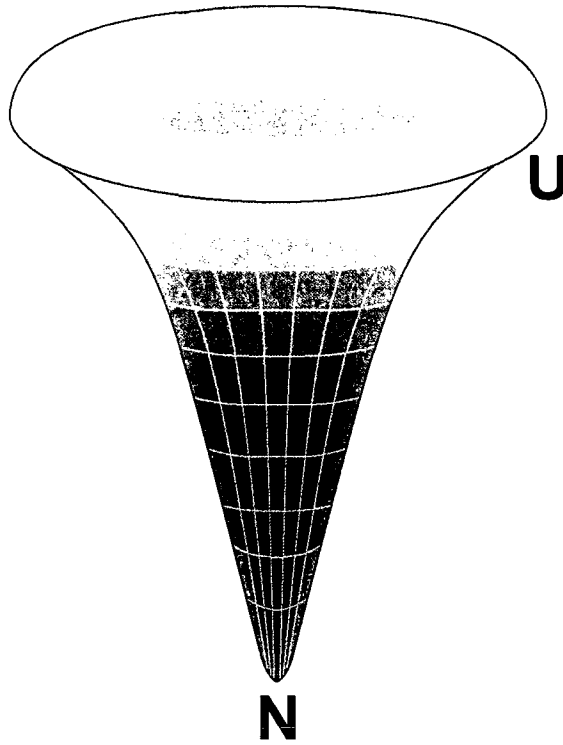


Figure 1.3 –Depiction of funnel-like energy landscape of protein folding with the width of the funnel representing conformational freedom (number of possible conformations; entropy) and the y-axis representing free energy. At the top of the energy landscape is the unfolded state (U), the rim of the energy landscape represents the transition state, and the bottom of the energy landscape represents the native state (N).

Experimental studies of equilibrium and kinetic folding reactions

Experimental protein folding studies can be isolated into two groups, equilibrium and kinetic studies, where structural changes to the protein are monitored through techniques such as spectroscopy (equilibrium and kinetics) and calorimetry (equilibrium). Methods for studying protein folding have advanced from isolating proteins from natural sources to the introduction of recombinant technology allowing for the expression and purification of proteins of interest. Equilibrium studies can best be understood assuming a two-state system where only two major subsets of individual protein molecules exist – native and unfolded proteins. In equilibrium studies, the test protein of interest is observed under conditions where the relative populations of native and unfolded protein are presumed to be unchanged over the duration of the experiment. Two-state equilibrium unfolding approximations are often found to be accurate, especially in the case of small proteins (Schellman, 1987), where protein unfolding resembles a single phase transition due to a high energy barrier between folded and unfolded proteins resulting in cooperative or “all-or-none” behavior (Shakhnovich and Finkelstein, 1989). In these cases, hydrophobic exposure is accompanied by large changes in both the enthalpy and entropy of the system resulting in the observed cooperative nature of the transition (Lumry and Biltonen, 1966). In the case of larger or multi-domain proteins, two-state approximations are often incorrect, as these proteins are likely to populate intermediate species corresponding to the folding or unfolding of individual domains (Privalov, 1982; Wetlaufer, 1973). The data collected from equilibrium

protein folding experiments gives the researcher information about the relative difference in energies of the native and unfolded states of the protein of interest (free energy) or more qualitative stability metrics such as the midpoint of protein unfolding under denaturing conditions. In contrast to equilibrium studies, kinetic studies involve rapid changes in the experimental conditions favoring the opposite conformational state (folded or unfolded) resulting in structural changes that can be observed over time. Kinetic experiments result in data that give information about the rates of protein folding, unfolding, and ligand binding. A collection of data from single-domain, globular, two-state proteins (~ 40 – 130 residues) shows that these proteins have a wide range of calculated free energies of unfolding (~ 5 – 50 kJ/mol) and folding rates extrapolated to zero denaturant (~ 1 – 10⁵ s⁻¹) (Grantcharova et al., 2001).

Thermal and chemical equilibrium denaturation

A number of different methods may be employed to tip the equilibrium of a protein system from native to unfolded (or vice versa). These methods include modulating temperature, pressure, pH, and concentration of chemical denaturants. The most often employed of these methods have become thermal and chemical denaturation. Thermal unfolding of polypeptides can best be explained by changes in enthalpy and entropy between the folded and unfolded states of the protein. As implied from the classical equation for free energy:

$$\Delta G = \Delta H - T\Delta S \quad (\text{Eq. 1.1})$$

the free energy of unfolding (ΔG) is related to be the change in enthalpy (ΔH) and entropy (ΔS) of the system. Both entropy (as shown above) and ΔH (through ΔC_p as: $\Delta H = C_p \cdot dT$) are related to temperature. As ΔC_p has been shown to be relatively constant for proteins (Privalov and Khechinashvili, 1974), the free energy of unfolding of proteins has a parabolic relationship with temperature with a maximum ΔG at the point where ΔH and ΔS contributions are equal.

Chemical denaturation of proteins is most often achieved using one of two common denaturants – urea or guanidinium chloride (GdmCl) (Fig. 1.4). Although it is well established that increasing the concentration of these chemical denaturants causes polypeptides to unfold, the mechanism by which these small molecules affect the structural equilibrium of these proteins is less understood. It is not generally accepted whether these denaturants interact directly with proteins (Lim et al., 2009; Robinson and Jencks, 1965) or if they modulate the hydrogen-bonding network of water (Wetlaufer, 1964). However, recent models have been constructed to combine the contributions of both proposed methods (Street et al., 2006). Regardless of their mechanism of interaction with proteins, their non-specific effects make chemical denaturants useful in protein folding studies.

Φ -value approach for folding transition state analysis

As mentioned before, the high energy barrier between the unfolded and folded state of proteins is termed the transition state (Fig. 1.5). The transition state is only transiently populated and thus cannot easily be analyzed by

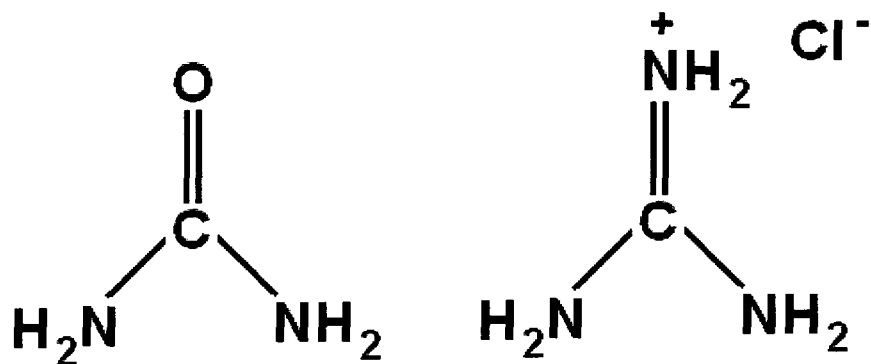


Figure 1.4 – Chemical structures of urea (left) and guanidinium chloride (right).

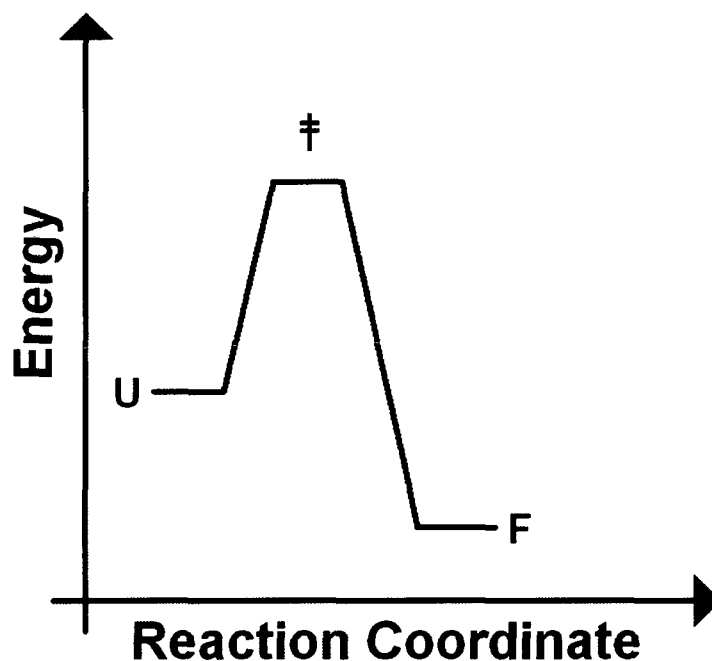


Figure 1.5 – Depiction of reaction coordinate for two-state protein folding. The free energy minimum is the folded state of the protein (F). The equilibrium free energy maximum is the unfolded state (U). Between the two equilibrium states is the high energy, transition state (‡) which does not populate at equilibrium. Progression down reaction coordinate can be thought of as gain of native-like contacts from U to F states. This reaction coordinate can be viewed as a cross-section of the folding energy landscape with the transition state (‡) sitting at the upper rim of the funnel.

equilibrium measurements but must be probed indirectly (Lindorff-Larsen et al., 2004). NMR techniques such as native state hydrogen exchange and relaxation dispersion have been used to assess kinetic intermediate structures (Bai, 2006; Englander et al., 2007; Korzhnev et al., 2004; Neudecker et al., 2006). One method that has been employed to analyze transition states is Φ -value analysis. Through protein engineering, it was first shown that one can analyze the transition state for unfolding (Matouschek et al., 1989) and later the transition state for folding (Fersht, 1990).

Φ -value analysis entails making a set of single, conservative point mutations (usually hydrophobic-to-alanine mutations) throughout the structure of a protein of interest and studying the effects of that mutation on the equilibrium and kinetic folding characteristics of the protein (Fersht and Sato, 2004). The Φ -values represent the change in stability of the transition state relative to the change in stability in the native state (Fersht and Sato, 2004). The change in energy of the transition state is calculated as:

$$\Delta\Delta G_{\ddagger \rightarrow u} = -RT \ln(k_{f,mut}^{H_2O} / k_{f,wt}^{H_2O}) \quad (\text{Eq. 1.2})$$

where $\Delta\Delta G_{\ddagger \rightarrow u}$ is the change in the energy of the transition state, $k_{f,mut}^{H_2O}$ is the folding rate of the variant protein extrapolated to zero denaturant, and $k_{f,wt}^{H_2O}$ is the folding rate of the wild-type protein extrapolated to zero denaturant.

Φ -values can then be calculated as follows:

$$\Phi_f = \Delta\Delta G_{\ddagger \rightarrow u} / \Delta\Delta G_{f \rightarrow u} \quad (\text{Eq. 1.3})$$

where $\Delta\Delta G_{f \rightarrow u}$ is the difference in the free energies of unfolding of the wild-type and variant proteins (usually calculated from equilibrium experiments). A Φ -value of 1 means the mutated residue contributes equally to the native and transition states (*i.e.*, wild-type side-chain forms native-like interactions in transition state) whereas a Φ -value of 0 means the mutated side-chain does not contribute to native-like interactions in the transition state (*i.e.*, wild-type residue is unfolded in transition state) (Fersht and Sato, 2004; Oliveberg, 2001) (Fig. 1.6). Φ -values between 1 and 0 (fractional Φ -values) imply different degrees of structure in the folding nucleus. Φ -value analyses of many two-state folding proteins have led to the classification of two types of folding-transition states - diffuse and polarized transition states (Sanchez and Kiefhaber, 2003). Diffuse transition states are typically described by fractional Φ -values spanning the whole of the tertiary structure of the protein whereas polarized transition states have distinct areas of the protein with Φ -values near unity. The protein chymotrypsin inhibitor-2 (CI2) was found to fold via a diffuse transition state (Itzhaki et al., 1995) while other proteins like a Src homology 3 (SH3) domain and protein L have been found to fold via polarized transition states (Kim et al., 2000; Northey et al., 2002).

Computational approaches

In addition to experimental procedures, the development of powerful computers has given rise to computational methods for studying protein folding. The use of supercomputers to simulate protein folding is very new as the first

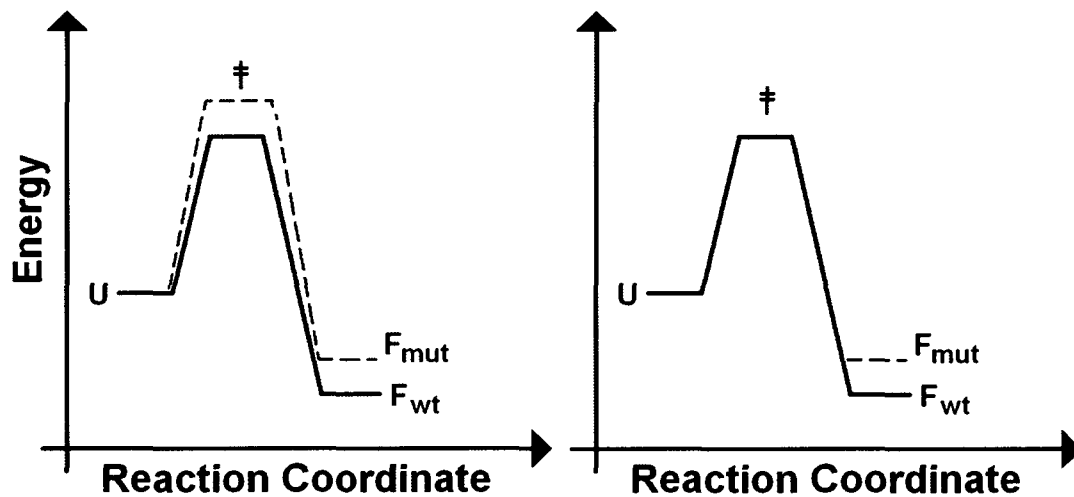


Figure 1.6 – Depictions of reaction coordinates for hydrophobic-to-alanine mutants yielding Φ -values of 1 (left) and 0 (right). In the left tile, the point mutation affects the folded state and transition state of the protein equally. In the right tile, the point mutation affects only the energetics of the folded state. Conservative nature of hydrophobic mutations allows for assumption that energetics of the unfolded state are not altered.

major breakthrough came in 1998 with the simulation of the folding of a 36-residue protein (Duan and Kollman, 1998). Today, there are two basic types of computer modeling for protein folding – all-atom simulations and coarse-grained modeling.

The difference in the two classes of models deals with the level of resolution of the models. In coarse-grained models, individual amino acid side-chains are usually replaced with a representative interaction center (Colombo and Micheletti, 2006). This simplification of the model system decreases the amount of necessary computing power and allows investigators to probe larger proteins. Gō-like models using the bead approach to describe polypeptides came about in the 1970s (Ueda et al., 1975; Ueda et al., 1978). This model uses a principle of minimal frustration (suggesting the foldable protein has evolved a primary sequence which minimizes conflicting interactions along the reaction coordinate toward proper folding) (Gulukota and Wolynes, 1994) and is able to construct relatively smooth, funnel-shaped folding energy landscapes (Clementi et al., 2000; Onuchic et al., 1997; Shea and Brooks, 2001). The structural Hamiltonian in such models may include parameters such as bond length and bond angle potentials (Cheung and Thirumalai, 2007) while simulations may be carried out using the Replica Exchange Method (REM (Hukushima and Nemoto, 1996; Sanbonmatsu and Garcia, 2002)) and the Langevin equation to ensure proper sampling (Veitshans et al., 1997). In contrast, all-atom simulations simulate each atom in the system. This allows investigators to gather information about a

protein at a much higher degree of resolution. However, the computational cost of such all-atom simulations in many cases makes certain protein systems more accessible by coarse-grained models (Clementi, 2008; Kolinski, 2004; Nielsen, 2004; Scheraga et al., 2007).

Flavodoxin – a model protein

A number of different species of flavodoxin are being used as model proteins. These include flavodoxins from *Azotobacter vinelandii*, *Anabaena*, *Chondrus crispus*, *Helicobacter pylori*, *Desulfovibrio vulgaris*, and *Desulfovibrio desulfuricans*. Properties of flavodoxins that make these proteins attractive to protein biophysicists include their relatively small size and the fact that they fold into a widely adopted tertiary structure.

The flavodoxin-like fold

Flavodoxins adopt the flavodoxin-like fold which, according to SCOP (Structural Classification of Proteins database; (Murzin et al., 1995)), is one of the five most common protein folds (TIM-barrel, Rossmann, thiamin-binding, and P-loop hydrolase folds) (Bollen and van Mierlo, 2005) (see Fig. 1.2) and is shared by sixteen protein superfamilies (Muller, 1992). This fold is characterized by a parallel β -sheet of five β -strands surrounded by five α -helices (although some flavodoxins, including *D. desulfuricans* flavodoxin, have four α -helices) (Hocker et al., 2002) (Fig. 1.7). The members of this group of proteins represent a vast array of amino acid sequences and functions that include electron-transfer proteins, catalases, lipases, and esterases (Muller, 1992). Information on



Figure 1.7 – Crystal structure of *D. desulfuricans* flavodoxin solved by Drs. Megan Guelker and Yousif Shamoo (one of two solved structures; pdb:3f6r). FMN cofactor shown in sticks (PyMol).

flavodoxin's folding behavior may be applied to other proteins with flavodoxin-like domains in an effort to better understand their folding properties. Such proteins include nitric oxide synthase, methionine synthase reductase, and cytochrome P450 reductase (Hall et al., 2001).

Structure, function, and cofactor

Flavodoxins are electron-transfer proteins that are found in prokaryotes and a few species of algae (Romero et al., 1996; Sancho, 2006). Their electron-transfer ability is generated by the noncovalent coordination of FMN (Helms and Swenson, 1991) (Fig. 1.8). Flavodoxins commonly replace ferredoxin in conditions of low-iron stress as a photosynthetic electron transport protein (Fillat et al., 1991; Maldonado et al., 1998). Under these conditions, flavodoxins transfer electrons from Photosystem 1 to ferredoxin-NADP⁺ reductase (FNR) by toggling between the semiquinone (one electron reduced) and hydroquinone (two electron reduced) forms of FMN (Nogues et al., 2005). Flavodoxins also serve a range of other functions, such as participating in nitrate reduction in *Azotobacter vinelandii* (by donating electrons to nitrate reductase) (Gangeswaran and Eady, 1996), aiding in the synthesis of biotin in *Bacillus subtilis* (by transferring electrons to Biol) (Stok and De Voss, 2000), and acting in the oxidation of pyruvate in *Helicobacter pylori* (likely as an electron acceptor for pyruvate:acceptor oxidoreductase) (Hughes et al., 1995) (reviewed in (Sancho, 2006)). As a result of the latter function, flavodoxin is being targeted for antibiotics against *Helicobacter pylori* (Cremades et al., 2005).

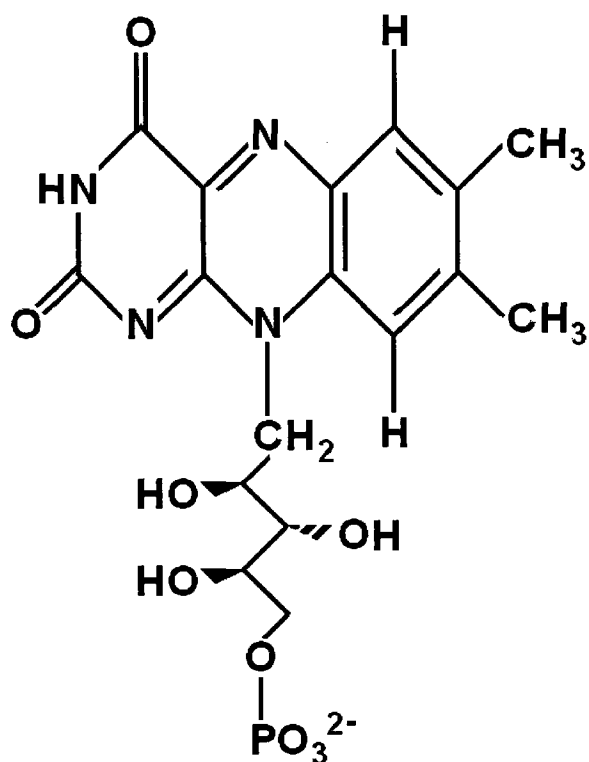


Figure 1.8 – Chemical structure of flavin mononucleotide (FMN; shown here as oxidized). The distinct regions of the molecule include the isoalloxazine ring (top), ribityl side-chain (middle), and phosphate moiety (bottom).

Two types of flavodoxins have been identified: short- (e.g., *D. desulfuricans* and *Desulfovibrio vulgaris*) and long-chain (e.g., *Anabaena* and *Azotobacter vinelandii*) flavodoxins. The difference between the two is that long-chain flavodoxins have a loop of approximately 20 amino acids interrupting the fifth β -strand of the core β -sheet (Muller, 1992). The finding that the 20-residue insertion is not required for flavodoxin function suggests that the long-chain variants may have preceded the short-chain flavodoxins evolutionarily (Lopez-Llano et al., 2004; Sancho, 2006).

Current knowledge of flavodoxin folding reactions

Most of the studies of flavodoxin folding reactions have been restricted to the apo-form of the protein as to not complicate the contributions of FMN in the folding process (Bollen et al., 2006; Bollen et al., 2004; Bueno et al., 2006; Campos et al., 2004; Fernandez-Recio et al., 2001; Lopez-Llano et al., 2006). Folding of apoflavodoxins has been studied in some detail, and it is clear that the time-resolved process is not a simple two-state reaction. A pathway involving an essentially off-pathway intermediate has been proposed for many apoflavodoxins including *D. desulfuricans*, *Anabaena*, and *A. vinelandii* (Apiyo and Wittung-Stafshede, 2002; Bollen et al., 2004; Bueno et al., 2006; Engel et al., 2008; Fernandez-Recio et al., 2001; Muralidhara et al., 2006; Nabuurs et al., 2008). This pathway implies that during folding, the protein first misfolds into unproductive structures (off-pathway intermediates) that must then unfold before attempting again to fold to the native state. The simplest version of this mechanism can be described in the following way:



The equilibrium unfolding of *D. desulfuricans* (in most cases) and *Anabaena* apoflavodoxins appear two-state (Apiyo and Wittung-Stafshede, 2002; Bueno et al., 2006; Stagg et al., 2007) while the equilibrium unfolding of *A. vinelandii* apoflavodoxin involves an intermediate species (Bollen et al., 2004). Currently, only one flavodoxin (*Anabaena* PCC 7119 apoflavodoxin; 24 % sequence identity to *D. desulfuricans* flavodoxin) has been subjected to Φ -value analysis (Bueno et al., 2006), and the transition state between U and F species for this long-chain flavodoxin has been described as diffuse involving native-like packing between α -helices and the core, β -sheet.

Specifics of Desulfovibrio desulfuricans (ATCC 29577) flavodoxin

D. desulfuricans flavodoxin is a short-chain flavodoxin of 148 amino acids (15.7 kDa) (Helms and Swenson, 1991). *D. desulfuricans* flavodoxin coordinates FMN through a combination of aromatic stacking interactions and hydrogen bonding (Lostao et al., 2000). Unlike some species of flavodoxin that undergo conformational change upon binding or release of FMN (e.g., *Chondrus crispus*) (Rogers and Sykes, 1990), *D. desulfuricans* and *Azotobacter vinelandii* flavodoxin have been found to have virtually identical structures in both apo- and holo-forms, except for increased loop dynamics in the absence of FMN (Genzor et al., 1996; Steensma and van Mierlo, 1998).

The folding of *D. desulfuricans* flavodoxin has been well characterized. As mentioned before, the folding reaction of apoflavodoxin is rather complex

involving the accumulation of an assumed off-pathway intermediate, however, folding of flavodoxin in the presence of FMN is faster than that of apoflavodoxin and appears to proceed along a two-state path (Apiyo and Wittung-Stafshede, 2002). FMN coordination to apoflavodoxin is mediated by aromatic stacking of the isoalloxazine ring to two aromatic residues (Trp60 and Tyr98) and hydrogen bonding of the ribityl side-chain of FMN to an N-terminal loop region (Genzor et al., 1996; Lostao et al., 2000; Muralidhara et al., 2006; Watenpaugh et al., 1972). It has also been suggested that the FMN-binding site of *D. desulfuricans* flavodoxin may be flexible enough to coordinate FMN dimers (Muralidhara and Wittung-Stafshede, 2003). In addition, it has been shown that inorganic phosphate elicits numerous effects on flavodoxin, including (a) speeding up the folding of apoflavodoxin, (b) increasing the affinity of apoflavodoxin for FMN, and (c) increasing the equilibrium stability of apoflavodoxin (Muralidhara et al., 2005).

The intracellular environment

Although protein folding studies are usually undertaken on purified recombinant proteins in dilute buffer solutions, the results of these studies are often used to explain *in vivo* phenomena. However, the conditions inside cells, where proteins are forced to fold and function, are drastically different than the conditions of most *in vitro* studies.

Macromolecular crowding and excluded volume theory

The cytoplasm of living cells resembles Jell-O more than water (Cheung, 2007; Vargas, 2003), because of the large amount of macromolecules in the cell.

The protein content of many cells alone accounts for 17-35% of the overall weight of the cell (Luby-Phelps, 2000). It is believed that between 30 and 40% of *E. coli* cells is volume occupied (Eggers and Valentine, 2001; Ellis and Minton, 2003), and that the overall concentration of macromolecular crowders in *E. coli* cells ranges from 300 to 400 mg/ml (Ellis, 2001a). Crowding agents *in vivo* include nucleic acids, proteins, lipids, and carbohydrates (Cheung et al., 2005; Zimmerman and Minton, 1993). The crowded nature of the cell has been beautifully demonstrated by cryoelectron tomography in the case of *Dictyostelium discoideum* (Medalia et al., 2002) (Fig. 1.9). The presence of large amounts of macromolecules in solution results in the “excluded volume effect” (Minton, 2000b) or “depletion force” (Asakura, 1954; Hall and Dobson, 2006), which simply poses that proteins in the cell have a significantly smaller portion of volume conformationally accessible to them than proteins in dilute solution (Fig. 1.10).

Macromolecular crowding has been proposed to affect both rates and equilibrium constants of macromolecular interactions (Ellis, 2001b), and studies on the volume exclusion effects of macromolecules began as early as the 1960s (Laurent, 1963). Crowding has also been speculated to affect the folding of proteins and nucleic acid chains as well as decreasing diffusion rates by up to ten times (Du et al., 2006; Ellis, 2001a). Aggregation is expected to be favored by macromolecular crowding, and this may in fact be one of the causes for the evolution of chaperones as these molecules may function to keep proteins from

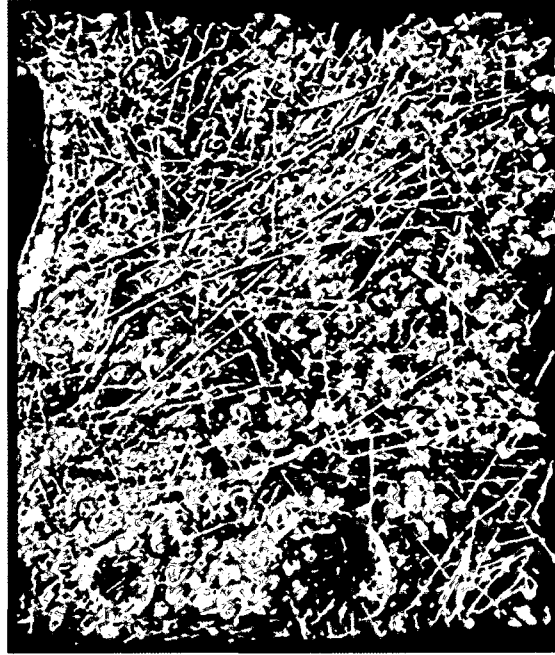


Figure 1.9 – From Medalia, O., Weber, I., Frangakis, A.S., Nicastro, G.G., and Baumeister, W. (2002). Macromolecular architecture in eukaryotic cells visualized by cryoelectron tomography. *Science* 298, 1209-1213. Reprinted with permission from AAAS. Cryoelectron tomography of *Dichtyostelium discoideum* shown with actin filaments (red), ribosomes (green), and membranes (blue).

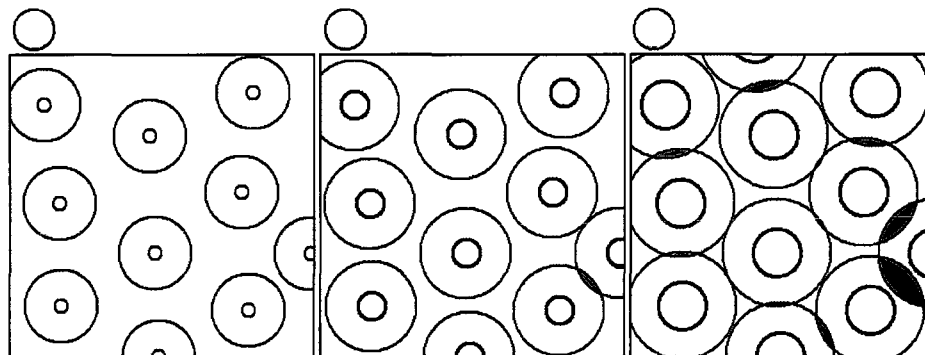


Figure 1.10 – Simplified depiction of excluded volume effects assuming spherical crowding agents (gray) and proteins (red). The three panels depict increasing crowding agent size (from left to right). Purple rings around crowding agents are the width of the radius of the protein. Thus in all three cases, the white area is the area accessible to the center of the protein. One can see that in the case of the larger crowding agents, most of the volume is excluded from the protein.

aggregating (Ellis and Minton, 2006). Macromolecular crowding is expected to stabilize proteins against thermal and chemical denaturation as a result of compaction of the unfolded state (less entropy) (Minton, 2000b). If these hypotheses are true, macromolecular crowding could alter the thermal and chemical midpoints of unfolding, rates of folding and unfolding, free energy of unfolding, and cofactor binding of proteins studied *in vitro*. It is because of these implications that theoreticians believe that addition of crowding agents should become common lab practice when studying biological molecules (Ellis, 2001a).

Synthetic crowding agents

Although little experimental work has been reported addressing effects of macromolecular crowding, a few synthetic agents have been identified as adequate reagents for crowding studies. The bulk of experimental crowding studies are being undertaken using inert polymers such as Ficoll, dextran, and polyethylene glycol (PEG) (Du et al., 2006). The inertness of these molecules is important for correlating results and theory because the excluded volume effect emphasizes steric repulsions (Ellis, 2001a; Minton, 2001). Ficoll 70 is a highly branched copolymer of sucrose and epichlorohydrin (Venturoli and Rippe, 2005). Dextran is a polymer of glucose monomers. Ficoll is believed to assume a spherical shape in solution, however, dextran is believed to behave more as a rod-like particle (Du et al., 2006).

Early studies: experimental and theoretical

Most investigations of the effects of crowded environments on protein stability have been computer simulations. For example, it has been proposed based on simulations that at all concentrations of crowding agent, the native state of the protein will be stabilized (Cheung et al., 2005). The effects of synthetic crowding agents on protein folding reactions have been tested experimentally *in vitro* only in a few cases. It has been shown that inert polymers stabilize lysozyme (Sasahara et al., 2003) and ribonuclease A (Tokuriki et al., 2004) against thermal and chemical perturbations *in vitro*. Also, it has been shown that cytochrome c is stabilized against thermal denaturation in the presence of dextran, and the stabilization effect increases with the size of the dextran molecules as well as with an increase in the amount of dextran in solution (Hall and Dobson, 2006). An interesting postulation suggests that the overall size of proteins could decrease as the excluded volume effect increases (Ping *et al.*, 2004). If this is true, the effects of crowding could change the overall packing and thus dimensions of folded proteins.

Ionic nature of the cell

In addition to the crowded nature of the cell, many bacterial cells (such as *Escherichia coli*) have devised systems of osmoregulation that often include the accumulation of ions (especially K^+) (Record et al., 1998a). It is believed that the intracellular concentration of K^+ *in vivo* (*E. coli*) is in the range of 100 mM to 1 M (Record et al., 1998b). In general, K^+ is favored over Na^+ in the cytoplasm by both prokaryotes and eukaryotes. This is evident in eukaryotes in that the

average cytoplasmic concentration of K^+ is ~159 mM while the concentration of Na^+ is only ~10 mM (Collins, 2006). Analogously, cytoplasmic levels of anionic species range from ~3 mM for chloride to ~20 mM for sulfates and up to 100 mM for phosphates (Di Stasio, 2004).

Hofmeister series of ions and properties

In 1888, Franz Hofmeister derived a series of ions based on their effects on the solubility of hen egg white proteins (Hofmeister, 1888). Since the creation of the Hofmeister series, it has been found that this series is also applicable to many other aspects of proteins. Generally, ions of the Hofmeister series can be divided into two classes based on interactions of the ions with water – kosmotropes and chaotropes. In general, kosmotropes are described as being “water loving” or coordinating water molecules more favorably. Chaotropes interact to a lesser degree with water. The majority of intracellular anions are kosmotropes (phosphates, sulfates, and carboxylates) whereas most intracellular cations are chaotropes (potassium and Lys/Arg side chains) (Di Stasio, 2004). Charge density of the ions also appear to play a role in the extent of their hydration and thus their classification as ions with high charge density tend to be kosmotropic and ions with low charge density tend to be chaotropic (Collins, 2004). It is believed that the major reason for pumping out Na^+ (kosmotropic) from the cell in favor of K^+ is because high levels of intracellular Na^+ would tend to interact strongly with the kosmotropic anions of the cell forming largely insoluble ion pairs (Collins, 1997).

D. desulfuricans is halophilic

Many organisms have developed the ability to survive in high salt environments, and are thus dubbed “halophilic.” Halophilic organisms are split into three classes based on optimal growth conditions: slight halophiles (2-5% NaCl), moderate halophiles (5-20% NaCl), and extreme halophiles (20-30% NaCl) (Ollivier et al., 1994). *Desulfovibrio desulfuricans* belongs to a family of bacteria known as sulfate reducing bacteria (SRB). SRB are mostly considered slightly halophilic as they thrive out in the open ocean where the average salinity is approximately 32-35 psu (about 3.5% NaCl) (Kerkar, 2005). One amazing, recent discovery is that *Desulfovibrio desulfuricans* (as well as *Desulfovibrio salexigens*) can grow in the Ribandar salt pans of Goa at conditions of salinity greater than 4 M salt (Kerkar, 2004). This suggests that *Desulfovibrio desulfuricans* has evolved a system of osmoregulation capable of dealing with such extreme conditions of salinity.

Although it is not known how *D. desulfuricans* compensates for life at high salt concentrations, initial research on SRB points to the accumulation of salts as the primary strategy for osmoregulation (Kerkar, 2005). The major internal cation in halophiles accumulating salts is believed to be K^+ , but at conditions of very high salt, the internal concentration of Na^+ is still believed to be in the molar range (Kerkar, 2005). Halophilic organisms have evolved two basic strategies for osmoregulating during salt stress. The first strategy (believed to be employed by SRB) is to accumulate K^+ in the cytoplasm in favor of Na^+ , and many halophilic

archaea have coupled this strategy with complex cellular machinery that functions even in conditions high salt (Dennis and Shimmin, 1997). The second strategy for osmoregulation employed by many halophiles is the production of compatible solutes in reaction to conditions of salt stress (da Costa et al., 1998).

D. desulfuricans flavodoxin is negatively charged

One interesting aspect of most species of flavodoxins is that they are highly negatively charged (Sancho, 2006). For example, the flavodoxin from *D. desulfuricans* has a net negative charge of -19 at pH 7 (pI = 4.1). This highly negative charge is a result of the many aspartate and glutamate residues decorating the surface of the protein. Interestingly, one of the major adaptations of halophilic organisms is the evolution of acidic proteins that can form and function at conditions of high salt that would precipitate most non-halophilic proteins (Mevarech et al., 2000). Flavodoxins are only found in some bacteria and oceanic algae; the flavodoxin gene was lost between algae and terrestrial plants (Zurbriggen et al., 2007). The fact that flavodoxins are primarily found in sea-bound organisms (conditions of approximately 3.5% NaCl) is likely the reason for the conservation of high negative charges across all species of flavodoxins (similar to proteins from halophilic organisms).

Project goals

Although much has been made about the crowded nature of the intracellular environment, relatively little is known through experimentation about the effects of macromolecular crowding on protein structure, stability, and kinetic folding

processes. We hypothesize that volume exclusion due to macromolecular crowding will result in increased *D. desulfuricans* flavodoxin thermal and chemical stability as well as increased flavodoxin folding rates. Our goal is to use a combined *in vitro* / *in silico* approach to test these hypotheses. In addition, I will use protein engineering techniques to produce a set of flavodoxin point mutants to probe the folding transition state of the protein both in buffer and under crowded conditions. The folding transition state of a short-chain flavodoxin has yet to be described, and no one has yet assessed the effects of macromolecular crowding on the structure of the folding transition state of a protein. As mentioned earlier, the intracellular milieu is also highly ionic. Less is known about the nature of the effects of cations on protein stability as anions have more profound effects on proteins. The highly negatively charged nature of flavodoxin gives us an excellent system in which to assess the effects of cations on protein stability. The combination of experiments probing the effects of macromolecular crowding and small ions on flavodoxin structure, stability, and folding kinetics will provide integral information toward a better understanding of the effects of the intracellular environment on protein biophysical properties.

CHAPTER 2: MATERIALS AND METHODS (THEORY AND EXPERIMENTAL)

Theory

Absorption and fluorescence spectroscopy

Proteins contain countless atoms that may populate different energy states (low to high). Incident light may promote atoms to convert from a low energy state to a higher energy state if the difference between the two energy states is identical to that of the incident photon. Scanning a particular biological sample with a wide array of different wavelengths of light produces a characteristic absorption spectrum. In proteins, individual amino acids (especially those with aromatic rings such as tyrosine, tryptophan, and phenylalanine) contribute to absorption which can be used to determine protein concentration and information about cofactors can often be gleaned by their characteristic absorption spectra (Fig. 2.1). Tyrosine, tryptophan, and cystine absorb light in the region between approximately 270 and 290 nm (Pace et al., 1995) while the peptide backbone absorbs light in the region between about 180 and 220 nm (Becklin and Desiderio, 1995).

In addition to absorption, some protein systems are amenable to fluorescence spectroscopy (Lakowitz, 1999; Stryer, 1968), which is a phenomenon that occurs when molecules return to their ground state from an excited state by emitting a photon of a longer wavelength than the incident photon. In proteins, tryptophan is an intrinsic fluorophore (and to a lesser degree, tyrosine). The intensity and

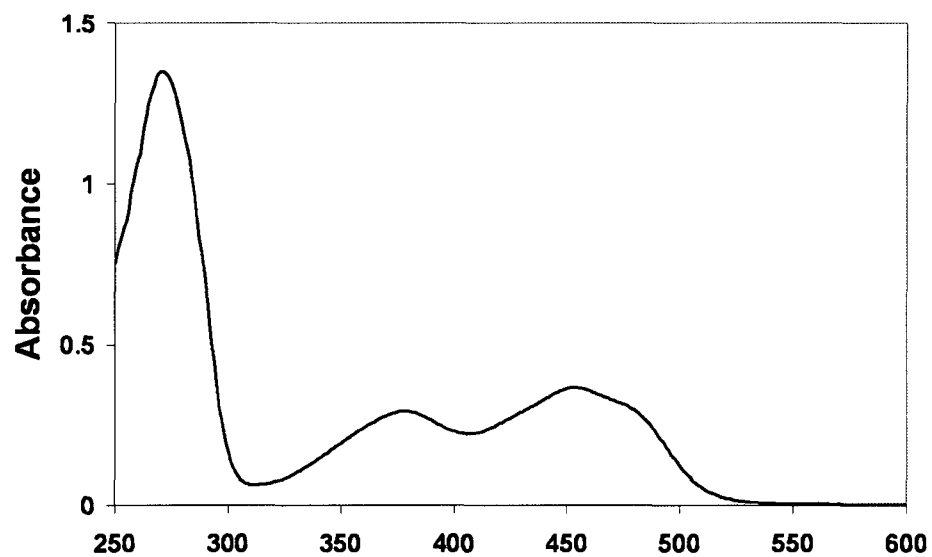


Figure 2.1 – Characteristic UV-Vis spectrum of wild-type holoflavodoxin. This spectrum features prominently a peak at approximately 275 nm (contributions from aromatic amino acids) and a double peak between 350 and 500 nm (contributions from FMN; oxidized).

peak of tryptophan fluorescence can give information about the environment of the fluorophore such as its degree of hydrophobic burial or solvent exposure (Chen and Barkley, 1998). In addition to tryptophan fluorescence, some cofactors (such as FMN) display characteristic fluorescence spectra that can provide information about their coordination to a host protein (Fig. 2.2).

Circular dichroism (CD) spectroscopy

CD is a method used in protein folding studies to determine the relative amount of secondary structure for a given protein of interest (Adler et al., 1973; Fasman, 1996; Kelly and Price, 1997; Woody, 1995). The theory behind CD is that chiral molecules (like proteins) absorb left and right circularly polarized light to different extents. The difference in the amount of left and right circularly polarized light ($\Delta A = A_L - A_R$) absorbed by a sample at a given wavelength is plotted over many wavelengths to give a characteristic spectrum. In most protein folding studies, CD signal is reported in ellipticity (Θ) with the units of degrees or millidegrees. There is a simple relationship between ΔA and Θ given by the equation: $\Theta = 32.98 \Delta A$ where Θ is in degrees (Kelly and Price, 1997). It should be noted that as most CD data is reported in millidegrees (mdeg), one millidegree is the result of the difference in absorption of left and right circularly polarized light by a chiral sample of approximately 3×10^{-5} absorbance units.

Far-UV CD (about 190 – 240 nm) gives information about the secondary structure of proteins as the absorbing group in this region is mostly the peptide bond. In this region, α -helices, β -strands, and unfolded proteins are all easily

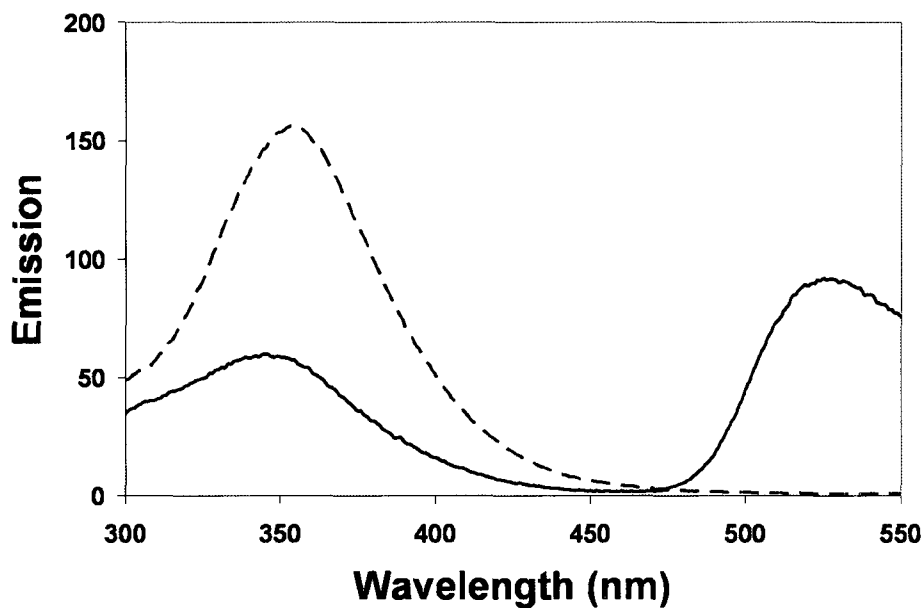


Figure 2.2 – Characteristic fluorescence spectrum of wild-type apo- (dashed) and holo-flavodoxin (solid) with excitation at 285 nm. For apo-flavodoxin, only the Trp60 fluorescence peak is seen. For holo-flavodoxin, two peaks are present: one peak at approximately 350 nm corresponds to intrinsic fluorescence from Trp60 (this peak is quenched by FMN coordination) and another peak at approximately 525 nm corresponds to FMN fluorescence.

differentiated based on their characteristic spectra. As flavodoxin is an α/β protein, its characteristic CD spectrum displays a mixture of α -helical and β -strand features (Fig. 2.3). As a result of the difference in the characteristic spectra of native and unfolded proteins, it is possible to follow the gain and loss (and therefore folding and unfolding) of secondary structural elements of proteins of interest using far-UV CD. In contrast to far-UV CD, near-UV CD (about 240 – 320 nm) gives information about the environment of aromatic amino acid side-chains (Trp, Tyr, and Phe). Shapes of near-UV CD spectra can provide additional information as to the rigidity of the fold, interactions between aromatic side-chains, and the number of aromatic amino acids (Kelly and Price, 1997).

Differential scanning calorimetry (DSC)

DSC, unlike spectroscopic techniques, gives direct information about the energetics of protein unfolding (Privalov, 1979; Privalov, 1982; Sanchez-Ruiz, 1992). In a typical DSC experiment, a purified, soluble protein (approximately ≥ 0.5 mg/ml) is placed in the sample chamber of the calorimeter with a buffer identical to that in the protein solution being placed in the reference chamber. The two cells are heated at a constant rate, and the difference in the amount of heat uptake (heat capacity; ΔC_p) for the two cells is plotted against temperature. The plot of heat capacity versus temperature often results in a single peak (phase transition) at a particular temperature (the melting point of the protein) (Fig. 2.4). Heat capacities of proteins are lower than the reference, buffer condition as water has a higher heat capacity than proteins (Cooper, 1999). In

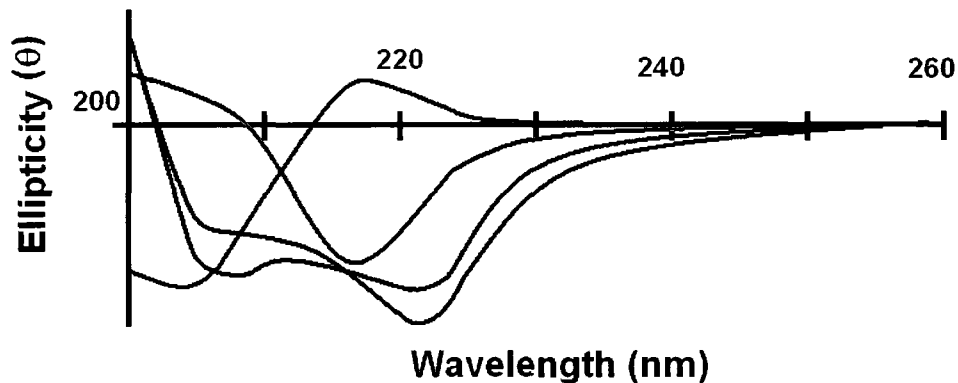


Figure 2.3 – Simplified representation of characteristic CD spectra of α -helical (blue), β -sheet (red), and unfolded (green) elements of proteins. In purple is a simplified representation of the characteristic spectrum of flavodoxin with its combination of α -helical and β -sheet secondary structural elements.

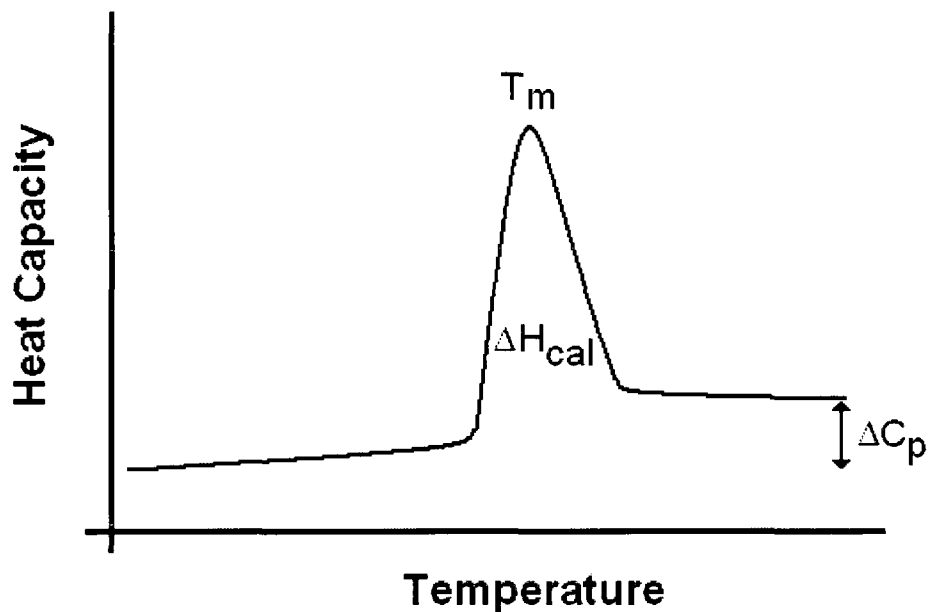


Figure 2.4 – Simplified representation of characteristic DSC thermogram for protein unfolding. Apparent in the unfolding thermogram are the pre-translational region (flat region at left), the unfolding transition (center peak), and the post-translational region (flat region to right). The y-axis plots heat capacity (C_p), the peak of the transition corresponds to the thermal midpoint (T_m), the change in heat capacity (ΔC_p) is represented in the offset of the native and unfolded baselines, and calorimetric enthalpy (ΔH_{cal}) can be calculated by integrating the area under the transition peak.

addition to the melting point (T_m), the calorimetric enthalpy of the unfolding event can be calculated by integrating the area beneath the peak, and the shape of the peak can provide information about the degree of complexity of the unfolding process.

Protein engineering (site-directed mutagenesis)

Breakthroughs such as polymerase chain reaction (PCR) and isolating and engineering specific lines of bacterial cells have allowed protein biochemists to make changes to existing proteins. One of the most often used protein engineering techniques is site-directed mutagenesis. Site-directed mutagenesis is used to make single point mutations to convert one amino acid of interest into another to determine the contribution of the original amino acid to structure or function. Site-directed mutagenesis is achieved by constructing two complimentary oligonucleotides containing the new codon of interest flanked by the wild-type DNA sequence. Through several rounds of PCR amplification, mutated plasmids are formed. The mutated plasmid is selected for using *DpnI* digestion. *DpnI* digests the original wild-type plasmid as it recognizes methylated DNA but not PCR amplified, mutant DNA.

Experimental

Protein purification

Flavodoxin was overexpressed in BL21(DE3) *Escherichia coli* cells from Stratagene. One L cultures were grown at 37 °C and shaking at 205 rpm until an $OD_{600} = 0.9$ was reached, at which point cells were induced with a final

concentration of 1.6 mM IPTG. Cells were then allowed to grow four more hours at initial growth conditions before harvesting by centrifugation. The resulting cell pellets from overexpressions were resuspended in approximately the same volume of buffer (20 mM sodium citrate, pH 5.2) as the dry pellet volume and stored at -80 °C. Cell pellets were thawed at room temperature, and all further steps were performed at 4 °C. Thawed cell pellets were passed through an 18 gauge needle before being broken using a cell disruptor (EmulsiFlex-G5; Avestin). Cells were broken by passing through the cell disruptor three times at approximately 15,000 psi. The resulting solution was centrifuged at 15,000 rpm (4 °C) for 15 minute intervals (discarding the pellet each time) until no pellet was visible. The supernatant was then filtered sequentially through 5 µm and 0.45 µm syringe filters from Fisher.

All buffers used for protein purification were filtered and degassed prior to use with an AKTA FPLC system (Amersham Pharmacia) in a cold box (Thermo) maintained at 4 °C.

Ion exchange

One of two anion exchange columns was used depending on the size of the starting cell pellet. For overexpressions involving ≤ 4 L, a 5 ml Mono-Q cartridge (GE Healthcare – Amersham Pharmacia) was used. For overexpressions greater than 4 L, a hand-poured 80 ml DEAE-Sepharose column (Pharmacia) was used. Columns were equilibrated using two column volumes of buffer B (20

mM sodium citrate, 2 M NaCl, pH 5.2) followed by two column volumes of buffer A (20 mM sodium citrate, pH 5.2) or until a UV baseline was reached.

Centrifuged and filtered cell lysates were loaded onto the column at a flow-rate (usually between 0.5 and 2 ml/min) that correlated to a backpressure below 0.3 MPa. As the FMN of flavodoxin was in its semi-reduced form at this point, a successful column loading resulted in a deep purple band at the top of the column. After loading the anion exchange column, the column was again washed in buffer A until a characteristic UV baseline was reached. Flavodoxin was eluted from the column using a gradient of 0→40 % buffer B at 0.5 ml/min over 150 minutes while collecting 4 ml fractions. The two species of flavodoxin (apo- and holo-forms) separate on the anion exchange column with apoflavodoxin eluting first.

SDS-PAGE was used to assess protein purity. SDS-PAGE was performed using 4-12 % Bis-Tris gels (Invitrogen) and Mark 12 molecular weight standard (Invitrogen). Peak fractions were pooled for both apoflavodoxin and holoflavodoxin. Fractions containing a mixture of both forms (as determined by SDS-PAGE and color) were included with the holo-protein. In order to ensure homogeneity of the holo-protein, exogenous FMN was added along with a small amount of potassium ferricyanide (to fully oxidize the FMN cofactor). Both apo- and holo-protein containing pools were centrifuged at 15,000 rpm to remove any insoluble impurities (or extra additive). Both proteins were then concentrated

using Viva Spin 20 3,000 MWCO (Sartorius) columns at 7,500 rpm down to approximately 2-4 ml.

Gel filtration (size exclusion)

After anion exchange, a 120 ml bed-volume Superdex 30 column (GE Healthcare – Amersham Pharmacia) was used for gel filtration. The column was equilibrated using two column volumes of gel filtration buffer (10 mM HEPES, pH 7). Before loading, all protein was centrifuged at 15,000 rpm to remove any insoluble particles. A 2 or 5 ml loop was used for sample injection depending on the volume to be loaded. When purifying both apo- and holo-forms of flavodoxin, the holoflavodoxin was loaded first to use its yellow color to visually assess the migration of the protein and the separation of exogenous FMN in the salt volume. Protein was eluted from the column using a flowrate of 0.5 ml/min (corresponding to a column pressure of 0.15-0.18 MPa) while collecting 5 ml fractions. After the salt volume of the holoflavodoxin load eluted, the second protein (if necessary) would be loaded and eluted as before. Peak fractions were diluted over approximately 40-60 ml from the original load volume.

Protein purity was assessed after elution using SDS-PAGE (Fig. 2.5). Peak fractions were pooled, centrifuged, and concentrated as before. Protein concentrations were determined using UV-Vis absorption of serial dilutions (e.g., 1:10, 1:20, 1:30, 1:40, and 1:50) of concentrated protein and molar extinction coefficients of $\epsilon_{280} = 11,460 \text{ M}^{-1} \text{ cm}^{-1}$ for apoflavodoxin and $\epsilon_{452} = 10,300 \text{ M}^{-1} \text{ cm}^{-1}$

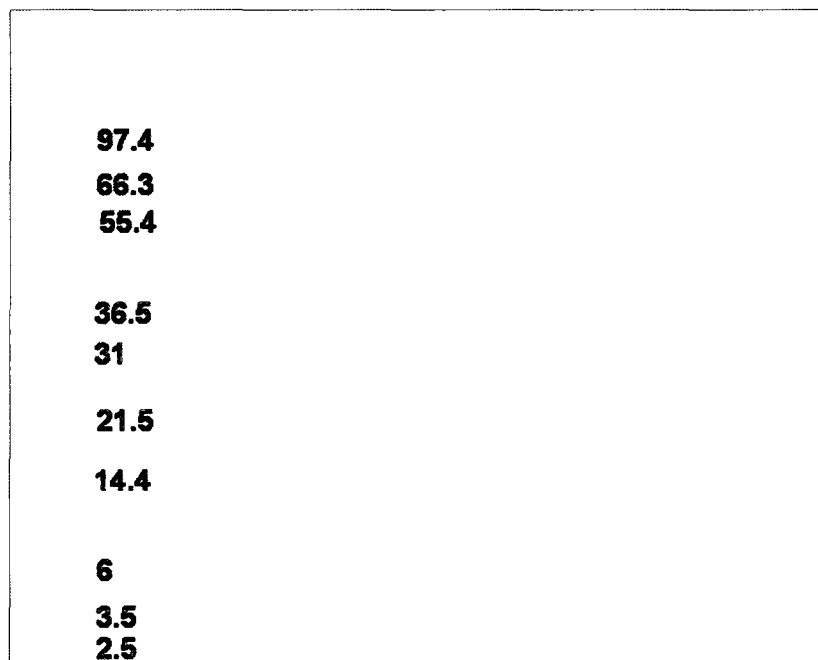


Figure 2.5 – Example of SDS-PAGE of purified flavodoxin after gel filtration. Far left lane is Mark 12 unstained standard with molecular weights (in kDa).

for holoflavodoxin. Fully FMN-loaded holoflavodoxin had a ratio of $A_{280}:A_{452}$ of ~ 3.7. Protein was stored at $-80\text{ }^{\circ}\text{C}$ in $700\text{ }\mu\text{l}$ to 1 ml aliquots.

Thermal and chemical equilibrium experiments

In all experiments, a protein concentration of $20\text{ }\mu\text{M}$ was used unless specified otherwise. All buffers were filtered and degassed and other reagents (chemical denaturant and synthetic crowding agents) were filtered before use to ensure that no impurities would contribute to experimental spectroscopic signals. High quality urea and Ficoll 70 were both purchased from Sigma, and dextran 70 was purchased from Amersham. To ensure equilibrium conditions in both thermal and chemical experiments, all samples were allowed to equilibrate for 30 minutes to 2 hours before measuring.

CD measurements were made using a Jasco J-810 instrument and temperature was maintained using a Jasco PTC-424S peltier. Far-UV CD measurements were performed using a 1 mm pathlength, and near-UV CD measurements were performed using a 1 cm pathlength. Fluorescence experiments were carried out using a Cary Eclipse fluorescence spectrophotometer and temperature was maintained using a Cary temperature controller.

For thermal equilibrium denaturations, sample cuvettes were stoppered to ensure that no solution evaporated at high temperatures. No scan rate dependence was found for flavodoxin between 0.1 and $2.5\text{ }^{\circ}\text{C}/\text{min}$, so unless

otherwise noted, thermal denaturation experiments were carried out using a 1.5 °C/min (90 °C/hr) rate. Temperature denaturation experiments performed using CD detection monitored changes in ellipticity at 222 nm unless otherwise specified. Data was fit to the following two-state equilibrium equation to approximate the thermal midpoint (T_m) adapted from (Luo et al., 1995; Maldonado et al., 2002):

$$S = [S_F + S_U e^{-(\Delta H (1 - T/T_m))/RT}] / [1 + e^{-(\Delta H (1 - T/T_m))/RT}] \quad (\text{Eq. 2.1})$$

where S is the observed signal, S_F is the signal in the folded state, S_U is the signal in the unfolded state, R is the gas constant, T is temperature, and T_m is the thermal midpoint. The original equation included a term for heat capacity (ΔC_p), however, this equation assumes a ΔC_p of zero (for simplification) as this assumption does not affect the calculation of an accurate T_m (the term of interest). For systems and experimental conditions where an accurate ΔC_p has been measured, the original fitting equation may be used effectively.

Thermal denaturation experiments performed by DSC were accomplished using a VP-DSC instrument. All buffers and samples were degassed at 15 °C for approximately 10 minutes prior to experiments. Sample concentrations varied between 40 and 100 μM protein ($\sim 0.5 - 2 \text{ mg/ml}$). Scan rates were maintained at 1.5 °C/min for heating and 1 °C/min for cooling.

Chemical equilibrium unfolding experiments were performed using reduced volume cuvettes for both far-UV CD and fluorescence. Unless specified

otherwise, all experiments were undertaken at 20 °C. Individual samples were made at approximately 0.25 M increments of denaturant, and in most cases, urea was the denaturant. Each sample was monitored by the averaging of two CD spectra scanning from 260 to 200 nm. For fluorescence experiments, samples were excited at 285 nm and monitored from 300 to 550 nm. As with CD experiments, each sample spectrum was the result of averaging of two spectra over the length of the full fluorescence scan. Chemical equilibrium unfolding experiments provide information about the difference in energies between the native and unfolded states at each denaturant concentration as shown here:

$$\Delta G_U = -RT \ln(K) \quad (\text{Eq. 2.2})$$

where ΔG_U is the Gibbs free energy of unfolding, R is the universal gas constant, T is temperature in Kelvin, and K is the equilibrium constant ($[U]/[N]$). Assuming a linear relationship between ΔG and [denaturant] in the transition of a denaturation curve, one can extrapolate ΔG to zero denaturant in order to approximate $\Delta G_U(\text{H}_2\text{O})$ as shown here (Greene and Pace, 1974):

$$\Delta G_U = \Delta G_U(\text{H}_2\text{O}) - m[\text{denaturant}] \quad (\text{Eq. 2.3})$$

where $\Delta G_U(\text{H}_2\text{O})$ is the Gibbs free energy of unfolding extrapolated to zero denaturant and m is the slope of the linear dependence of ΔG on denaturant concentration. m-values are presumed to give information about the change in solvent accessible surface area (ΔASA) between the native and unfolded states of proteins upon denaturation (Myers et al., 1995).

In practice, raw data can be fit directly to give thermodynamic information in chemical equilibrium unfolding experiments as shown here (Santoro and Bolen, 1988):

$$y = \{(y_F + m_F[D]) + (y_U + m_U[D]) * e^{-((\Delta G_U(H_2O)) - m[D] / RT)}\} / (1 + e^{-((\Delta G_U(H_2O)) - m[D] / RT)}) \quad (\text{Eq. 2.4})$$

where y is the observed signal, y_F is the signal of the folded state, y_U is the signal of the unfolded state, m_F is the slope of the pre-transitional baseline, m_U is the slope of the post-transitional baseline, m is the slope of the transition, $[D]$ is the concentration of denaturant, $\Delta G_U(H_2O)$ is the free energy of unfolding in water, R is the gas constant, and T is the temperature.

Kinetic folding dynamics

All kinetic experiments were performed on an Applied Photophysics π^* -180 stopped-flow mixer monitoring CD signal at 222 nm. Temperature was controlled using a Julabo F30-C peltier. For most experiments, the temperature was controlled at 20 °C. Either 1:5 or 1:10 mixing ratios were used, and samples were equilibrated 30 min to 2 hours. In all experiments (unless otherwise noted), a final concentration of 20 μ M protein was used. For all experiments, rates were determined using single exponential decays resulting from fits to the average of three to eight consecutive mixings (shots).

Plotting the natural logarithm of each of the rates determined by single exponential decays as a function of denaturant concentration gives the classical,

V-shaped, Chevron plot (Fig. 2.6). Experimental data can be fitted as followed to calculate folding and unfolding rates in zero denaturant (Maxwell et al., 2005):

$$\ln(k_{obs}) = \ln[e^{(A + m_F[D] / RT)} + e^{(B + m_U[D] / RT)}] \quad (\text{Eq. 2.5})$$

where k_{obs} is the observed rate, m_F is the slope of the folding phase, m_U is the slope of the unfolding phase, A is the natural logarithm of the folding rate extrapolated to zero denaturant ($\ln k_f^{H_2O}$), and B is the natural logarithm of the unfolding rate extrapolated to zero denaturant ($\ln k_u^{H_2O}$). This equation assumes a linear relationship of $\ln(k)$ versus denaturant concentration and allows for the fitting of an entire Chevron plot whereas it has its origins in equations for fitting the folding and unfolding phases individually (adapted from (Jackson and Fersht, 1991)):

$$\ln k_f = \ln k_f^{H_2O} - m_{kf}[D] \quad (\text{Eq. 2.6})$$

$$\ln k_u = \ln k_u^{H_2O} + m_{ku}[D] \quad (\text{Eq. 2.7})$$

Kinetic folding experiments (and to a lesser degree unfolding) were accompanied by the presence missing amplitude in the burst-phase (dead-time; approximately a few msec) of the stopped-flow mixer monitoring CD signal at 222 nm. Calculation of missing amplitudes was performed at each tested condition by dividing the amount of amplitude change recorded by the instrument by the amount of amplitude change expected as follows:

$$\% \text{ Miss. Amp. (Refolding)} = \{1 - [-a / (B_u + S)]\} * 100 \quad (\text{Eq. 2.8})$$

$$\% \text{ Miss. Amp. (Unfolding)} = \{1 - [(B_f + a) / -S]\} * 100 \quad (\text{Eq. 2.9})$$

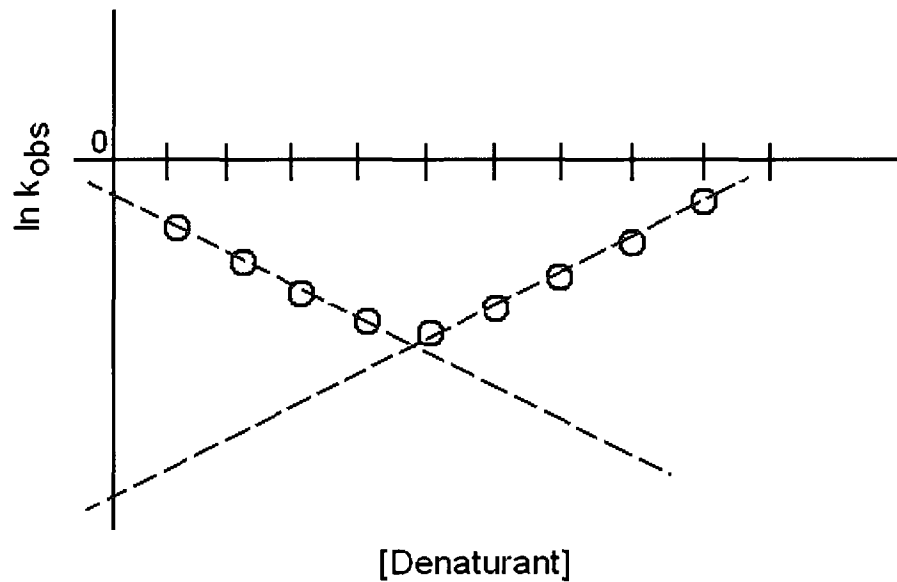


Figure 2.6 – Characteristic Chevron plot constructed from stopped-flow mixing experiments. Each data point represents the natural logarithm of the calculated rate constant derived by fitting experimental data to single exponential decays. The dashed red lines represent linear fits to the folding phase (left arm) and unfolding phase (right arm) which are extrapolated to zero denaturant to calculate folding and unfolding rates in water.

where a is the amplitude change observed in the kinetic trace (in mdeg), B_u is the signal of the unfolded baseline, B_f is the signal of the folded baseline, and S is the final signal observed for the particular kinetic trace. All data for missing amplitude calculation came from fits thus lessening the contribution of experimental noise. Calculation for the average missing amplitudes for individual proteins came from averaging the % missing amplitude of each data point in the linear portions of the folding phase of Chevron plots.

The amino acid sequence of D. desulfuricans flavodoxin

The flavodoxin gene was sequenced in 1990 (Helms et al., 1990). Our lab has subsequently worked with a pet-24c(+) plasmid expressing wild-type flavodoxin obtained from the lab that originally sequenced the flavodoxin gene. However, preliminary DNA sequencing of the plasmid revealed an apparent single-nucleotide mutation between the received plasmid and the original published sequence. The apparent mutation changed the originally published 79th codon from AAC (coding for asparagine) to GAC (coding for aspartic acid). We have come to believe that the original published sequence is incorrect, and the 79th amino acid should indeed be an aspartic acid. Sequence alignments of known flavodoxins show a conserved, acidic amino acid at position 79 (Fig. A.3).

In order to assess whether the 79th amino acid should indeed be Asp instead of Asn, I created a point mutation to return the plasmid to the published sequence. I then overexpressed the plasmid and purified D79N apoflavodoxin. Thermal and

chemical equilibrium experiments clearly show that the original published sequence of the protein codes for a less stable protein than the apparently mutated sequence (Fig. A.4). In light of the facts that flavodoxins have evolved with an acidic amino acid at position 79 and that Asp79 apoflavodoxin is more stable than Asn79 apoflavodoxin (assessed by both T_m and $\Delta G_U(H_2O)$), we believe that the wild-type sequence of *D. desulfuricans* (ATCC 29577) flavodoxin should include an aspartic acid residue at position 79.

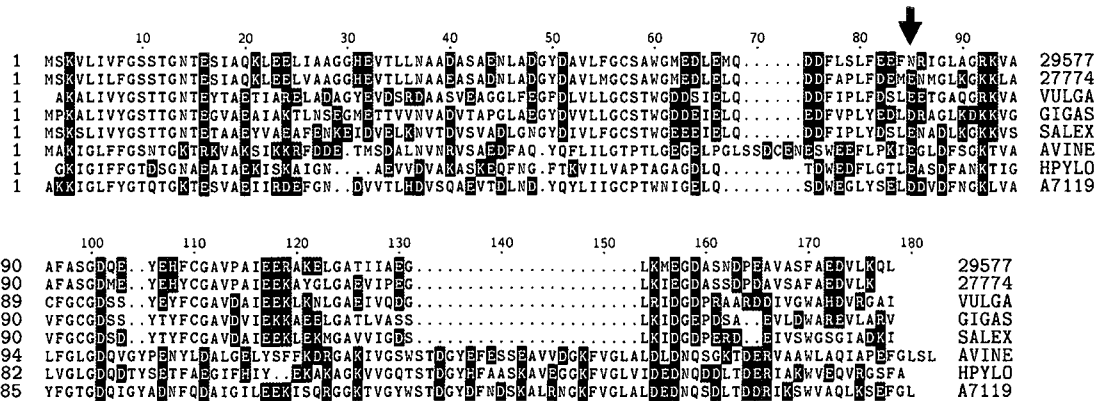


Figure 2.7 – Sequence alignment of various flavodoxins using Clustal W program. Charged residues are shown in red (-) and blue (+). Flavodoxins include those from *D. desulfuricans* ATCC 29577 (29577), *D. desulfuricans* ATCC 27774 (27774), *D. vulgaris* (VULGA), *D. gigas* (GIGAS), *D. salexigens* (SALEX), *Azotobacter vinelandii* (AVINE), *Helicobacter pylori* (HPYLO), and *Anabaena* PCC7119 (A7119). Conserved acidic residue at position 79 shifted here to residue 85 (red arrow). Figure adapted from Sedlák et al. (2008a).

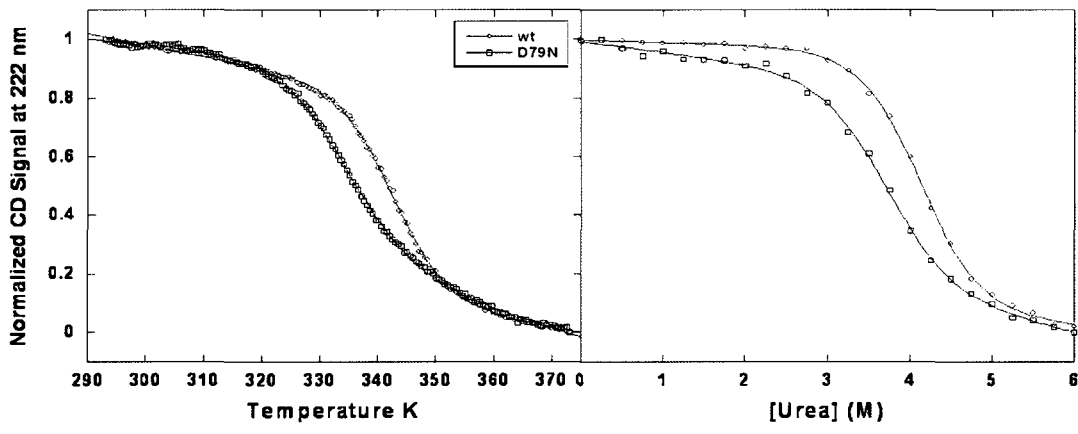


Figure 2.8 – Thermal (left) and urea denaturation (right) of the original published sequence (D79N) of apoflavodoxin (blue) and the sequence the Wittung-Stafshede lab has been using (wt) (red). “Wild-type” apoflavodoxin unfolds with a T_m of ~ 67.8 °C while D79N apoflavodoxin has a T_m of ~ 61.1 °C. $\Delta G_U(H_2O)$ values calculated for the two proteins were 26.4 kJ/mol for wild-type and 22.1 kJ/mol for D79N apoflavodoxin (100 mM KPi, pH 7, 20 °C).

CHAPTER 3: EFFECTS OF MACROMOLECULAR CROWDING ON THE STRUCTURE AND STABILITY OF FLAVODOXIN.

The results presented in this chapter include published (Homouz et al., 2009; Perham et al., 2007; Stagg et al., 2007) and unpublished material.

Increase in protein secondary structure compared to in buffer

Crowding theory suggests that biological processes that result in increasing the amount of available volume in a system will be promoted by macromolecular crowding (*i.e.*, compaction via conformational isomerization or intermolecular association) (Minton, 2005a; Minton, 2005b; Zhou, 2004; Zimmerman and Minton, 1993). As a result, it is reasonable to assume that macromolecular crowding could affect both the packing of the folded structure of a protein as well as increasing the stability of the protein against denaturation as compared to dilute buffer conditions.

In order to test these theories, I used both wild-type apoflavodoxin and holoflavodoxin in concert with synthetic crowding agents (especially Ficoll 70 and dextran 70) and assessed effects of crowding on both the folded structure and stability of flavodoxin. I used the synthetic crowding agents in the range of 0-400 mg/ml, which correlates with typical concentrations of macromolecular crowders *in vivo* (Ellis, 2001a). However, it should be noted that at higher concentrations of synthetic crowding agents (as at 100 mg/ml Ficoll 70 the calculated excluded volume ~ 50 %), it cannot be assumed that the shapes of the crowding agents are conserved or that the individual sugar polymers are not interpenetrating each other (close packing has been suggested for crowding agents above $\phi_c \approx 0.6$

(conditions of approximately 60 % volume exclusion) (Wenner and Bloomfield, 1999)).

Interestingly, I found that in the tested range of crowding conditions, the folded CD signal for both apo- and holoflavodoxin seemed to increase in the presence of crowding agents (10 mM HEPES, pH 7, 20 °C) (Fig. 3.1). For apoflavodoxin, I found that the negative CD signal of the protein in 200 mg/ml Ficoll 70 increased 10 % compared to in buffer alone and in 400 mg/ml Ficoll 70, the negative CD signal increased 15 % compared to the buffer condition. Similarly, large increases in folded CD signal were found for the holo-protein. At 200 mg/ml Ficoll 70, the CD signal of folded holoflavodoxin increased 24 %, and at 400 mg/ml Ficoll 70, the folded CD signal increased 33 % from the buffer condition.

Using the structural algorithm SOMCD (<http://geneura.ugr.es/cgi-bin/somcd/index.cgi>) (Unneberg et al., 2001), it was discovered that most of the secondary structural increases to apo- and holoflavodoxin in the presence of 400 mg/ml crowding agent occurred in α -helices. For example, in the case of apoflavodoxin, the helical content of the protein determined by SOMCD increases by approximately 20 % in 400 mg/ml Ficoll 70 compared to the buffer condition while the amount of random coil decreases by greater than 10 %. The changes to the secondary structural content of apoflavodoxin in the presence of 400 mg/ml Ficoll 70 makes the approximate secondary structural content of

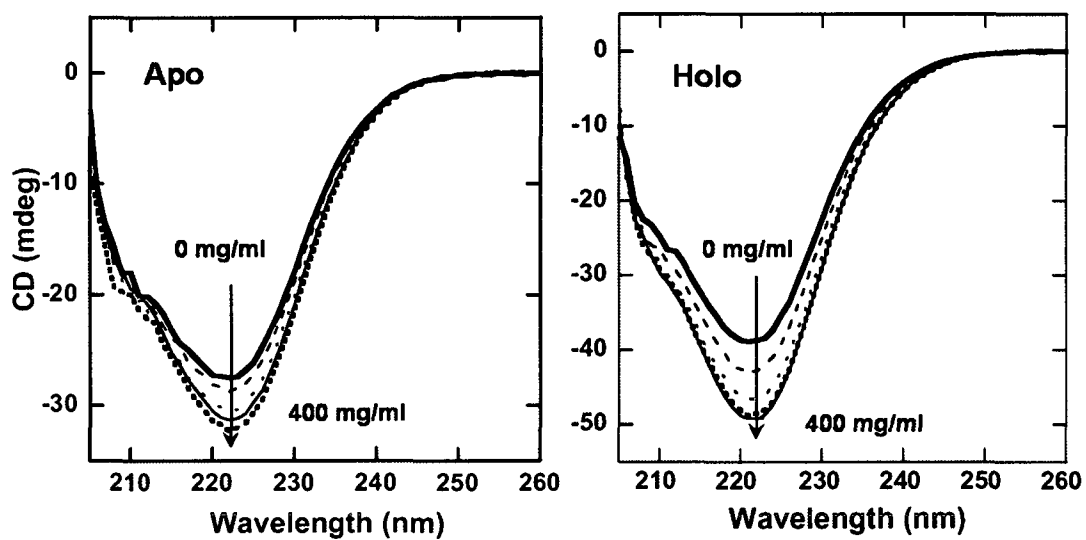


Figure 3.1 – Effects of increasing amounts of Ficoll 70 (0-400 mg/ml) on folded secondary structural content of apoflavodoxin (left) and holoflavodoxin (right) (10 mM HEPES, pH 7, 20 °C). Figures adapted from Perham et al. (2007) and Stagg et al. (2007).

apoflavodoxin (α -helices, β -strands, and loops) agree qualitatively with that of the crystal structure of *Desulfovibrio vulgaris* flavodoxin (a structural homolog) and the recently solved *Desulfovibrio desulfuricans* flavodoxin (Guelker et al., 2009) (pdb:3f6r) (Table 3.1). This suggests that the protein in buffer alone may be quite dynamic, especially in its outer, helical regions, and the inclusion of crowding agents tunes the structure more toward that of a crystal structure, which is of course determined under quite crowded conditions.

In contrast to the changes in secondary structure for apo- and holoflavodoxin in the folded state, the structure of unfolded protein seemed to be much less affected. For both apo- and holoflavodoxin unfolded by guanidinium chloride (GdmCl), the addition of Ficoll 70 (up to 400 mg/ml) elicited no difference in secondary structural composition (as evidenced by overlapping CD spectra) (Fig. 3.2). For apo- and holoflavodoxin unfolded thermally, there was a small increase in the amount of secondary structure as a result of increasing concentration of Ficoll 70 (Fig. 3.3). However, in all cases, the shapes of the CD spectra suggest that the protein is still unfolded, and the magnitude of change is lower than that seen for the folded proteins.

Increase in thermal stability

In order to assess the effects of excluded volume on flavodoxin stability, I used both Ficoll 70 and dextran 70 (in the case of holoflavodoxin) between 0 and 400 mg/ml coupled with monitoring CD signal at 222 nm. As expected, the

	% α -helix	% β -strand	% turn / random coil
<i>Experimental</i>			
Buffer	14 \pm 6	34 \pm 5	52 \pm 1
100 mg/ml Ficoll 70	25 \pm 13	33 \pm 6	42 \pm 5
400 mg/ml Ficoll 70	34 \pm 13	26 \pm 10	40 \pm 6
<i>Structure</i>			
2fx2 (<i>vulgaris</i>)	37	30	33
3f6r (<i>desulfuricans</i>)	40	20	40

Table 3.1 – SOMCD secondary structural predictions for apoflavodoxin (*experimental*) in buffer and in the presence of 100 and 400 mg/ml Ficoll 70 (10 mM HEPES, pH 7). Amount of calculated secondary structure in crystal structures of *D. vulgaris* and *D. desulfuricans* flavodoxins (*structure*) also shown.

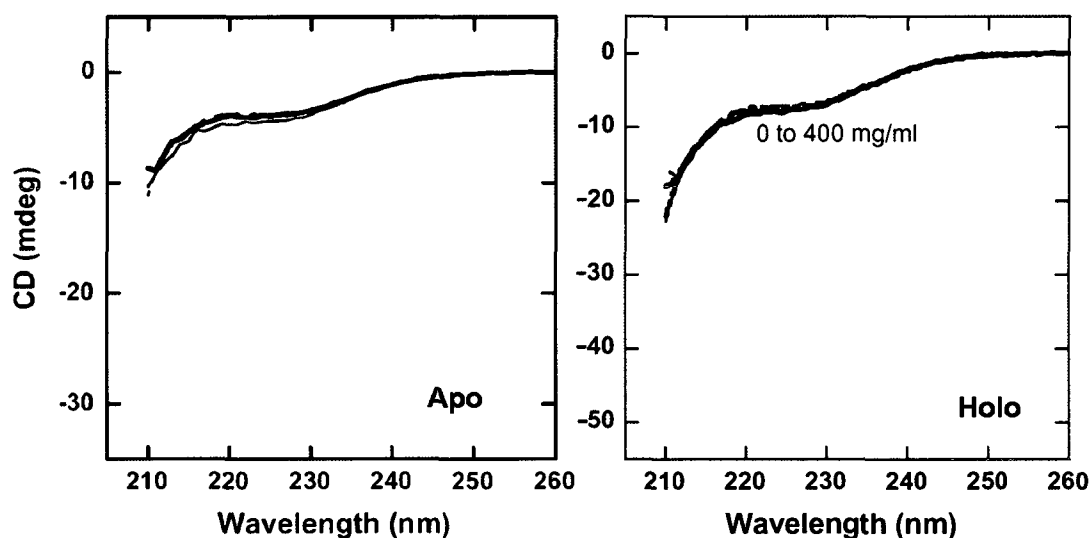


Figure 3.2 – Negligible effects of Ficoll 70 (0-400 mg/ml) on the secondary structure of 3 M GdmCl unfolded apoflavodoxin (left) and holoflavodoxin (right) (10 mM HEPES, pH 7, 20 °C). Figures taken from Perham et al. (2007) and Stagg et al. (2007).

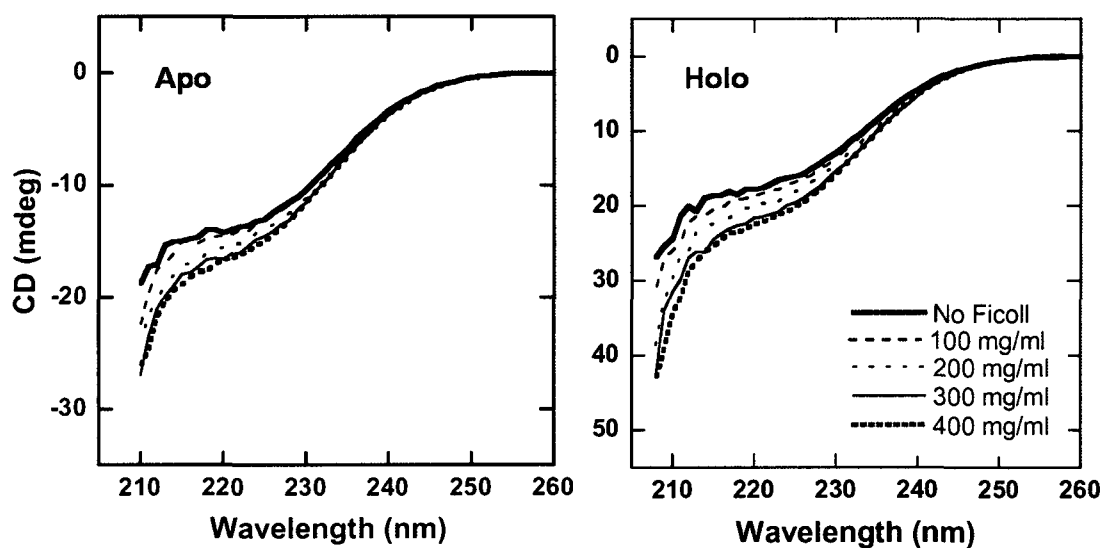


Figure 3.3 – Minor effects of Ficoll 70 (0-400 mg/ml) on secondary structure of thermally unfolded apoflavodoxin (left) and holoflavodoxin (right) (10 mM HEPES, pH 7, 95 °C). Although secondary structure increases, the spectral shape remains that of an unfolded polypeptide. Figures taken from Perham et al. (2007) and Stagg et al. (2007).

thermal stability of both apo- and holoflavodoxin (10 mM HEPES, pH 7) increased as a function of increased concentration of synthetic crowding agent (Figs. 3.4 and 3.5). Both Ficoll 70 and dextran 70 elicit significant increases in the T_m of holoflavodoxin. In the buffer condition, the T_m of holoflavodoxin was approximately 48 °C. Conversely, upon the addition of 400 mg/ml Ficoll 70, the T_m of holoflavodoxin increased to 64 °C. At 400 mg/ml dextran 70, the T_m of holoflavodoxin increased to 70 °C. The shapes of the thermal denaturation curves and later DSC experiments show that the unfolding event is two-state under the observed experimental conditions.

In the case of apoflavodoxin, the thermal midpoint increased from 45 °C in the buffer condition to 65 °C in 400 mg/ml Ficoll 70. Interestingly, I found that thermal stability was greatly modulated by buffer condition (Fig. 3.5) (Table 3.2). The T_m for apoflavodoxin increased by as much as 25 °C when changing buffers from 10 mM HEPES, pH 7 to 40 mM phosphate, 250 mM NaCl, pH 7. These data agreed with previous work showing that phosphate stabilizes flavodoxin (Muralidhara et al., 2005) as well as with our later work (Sedlak et al., 2008a; Sedlak et al., 2008b). Regardless of buffer effects, the T_m of apoflavodoxin under all buffer conditions increased with the addition of Ficoll 70. Only the magnitude of the stability change was affected by the buffer condition. In short, the effects of crowding on apoflavodoxin were more significant in buffers less stabilizing to the protein.

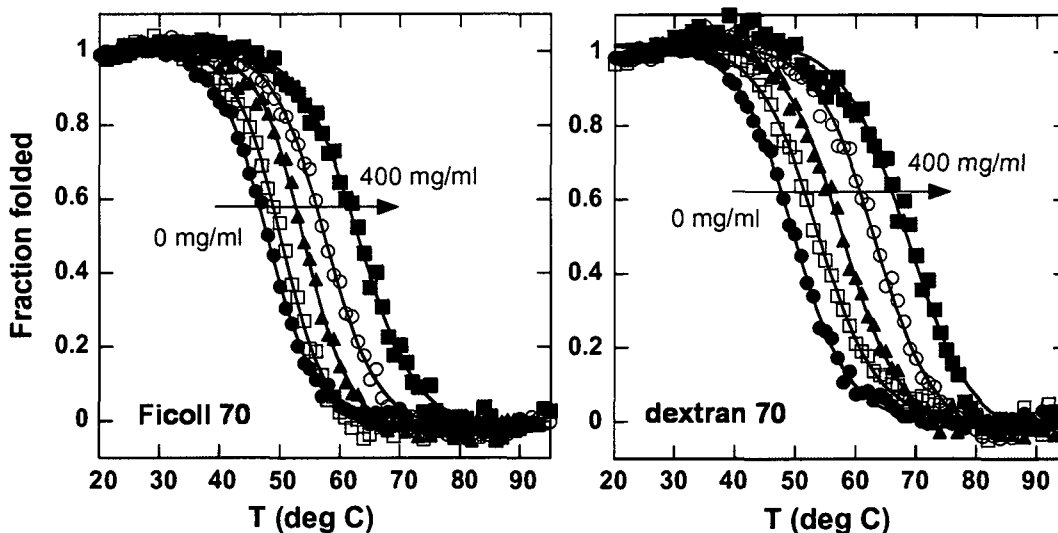


Figure 3.4 – Thermal denaturation of holoflavodoxin monitored by CD signal at 222 nm as a function of [Ficoll 70] (left) and [dextran 70] (right) (10 mM HEPES, pH 7). Figures taken from Perham et al. (2007).

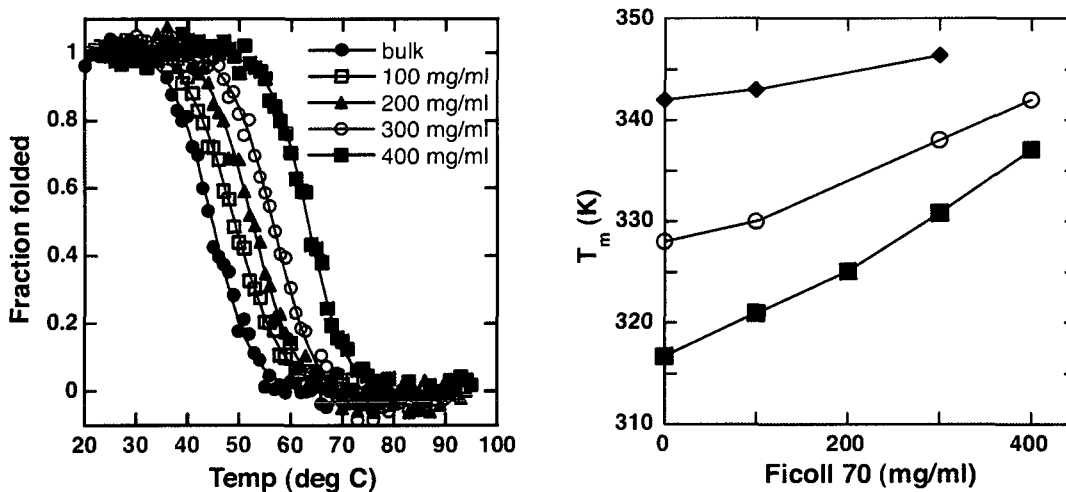


Figure 3.5 – Left panel shows increase of thermal stability of apoflavodoxin as a function of increasing [Ficoll 70] (0-400 mg/ml) as monitored by CD signal at 222 nm (10 mM HEPES, pH 7). Right panel shows the coupled effects of buffer (10 mM HEPES, pH 7, dark squares; 20 mM KPi, pH 7, open circles; and 40 mM KPi, 250 mM NaCl, pH 7, dark diamonds) and Ficoll 70. Figures taken from Staggs et al. (2007).

Buffer	Bulk	100 mg/ml	200 mg/ml	300 mg/ml	400 mg/ml
HEPES	317 ± 1	321 ± 1	325 ± 1	331 ± 1	337 ± 1
Phosphate	328 ± 1	330 ± 1	-	338 ± 1	341 ± 1
Phosphate + NaCl	342 ± 1	343 ± 1	-	346 ± 1	-
Simulation	365	372 (at $\phi_c = 25\%$)			

Table 3.2 – Thermal midpoints for apoflavodoxin with various amounts of Ficoll 70 for *in vitro* experiments monitored by CD 222 nm in three buffer conditions (10 mM HEPES, pH 7; 20 mM KPi, pH 7; and 40 mM KPi, 250 mM NaCl, pH 7) as well as T_m values determined *in silico*. Data for table from Stagg et al. (2007).

Increase in chemical stability

In accordance with experiments assessing the effects of crowding on flavodoxin thermal stability, we also expected that the addition of synthetic crowding agents to apoflavodoxin would increase the chemical equilibrium stability of the protein. As chemical equilibrium experiments by default require the addition of relatively large volumes of denaturant (in this case urea), high concentrations of crowding agent are not achievable. All urea denaturation curves were apparent two-state processes as verified by overlapping transitions monitored by both CD and fluorescence.

In the case of apoflavodoxin in 10 mM HEPES, pH 7, the addition of 150 mg/ml Ficoll 70 or dextran 70 increased the equilibrium stability of the protein. The protein in buffer alone exhibited a very low free energy of unfolding (only 4.4 kJ/mol – calculated by two-state fits), however the free energy of unfolding increased to 7.2 kJ/mol in the presence of 150 mg/ml Ficoll 70 and 8.9 kJ/mol in the presence of 150 mg/ml dextran 70. The slopes of the unfolding transitions appeared relatively unchanged with the addition of crowding agent, however, the urea unfolding midpoint ($U_{1/2}$) noticeably increased upon the addition of 75 and 150 mg/ml crowding agents (Fig. 3.6).

In agreement with the effects of phosphate on apoflavodoxin thermal stability, I found that the free energy of unfolding of apoflavodoxin in 100 mM KPi, pH 7 is 26.4 kJ/mol compared to 4.4 kJ/mol in 10 mM HEPES, pH 7. The calculated free

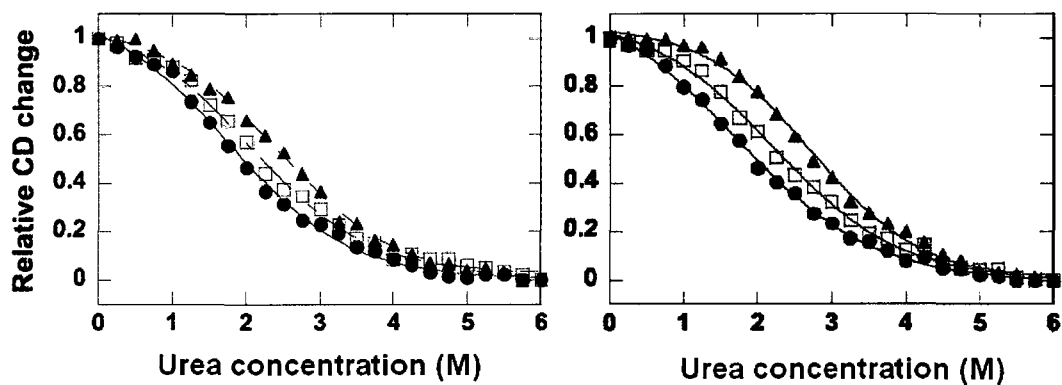


Figure 3.6 – Urea denaturation of apoflavodoxin with 0 (filled circles), 75 (open squares), and 150 mg/ml (filled triangles) Ficoll 70 (left panel) and dextran 70 (right panel) monitored by CD signal at 222 nm (10 mM HEPES, pH 7, 20 °C). Figure taken from Homouz et al. (2009).

energy of unfolding for apoflavodoxin (100 mM KPi, pH 7) increases, but not significantly, upon the addition of 100 mg/ml Ficoll 70. However, the urea midpoint of unfolding does increase from 4.3 M urea to 4.7 M urea upon the addition of 100 mg/ml Ficoll 70 (Fig. 3.7). The discrepancy in the more quantitative assessment of stability ($\Delta G_U(\text{H}_2\text{O})$) and the more qualitative assessment ($U_{1/2}$) could be attributable to a slightly more broad (lower m -value) slope in the transition region for apoflavodoxin in the presence of 100 mg/ml Ficoll 70.

Analyzing chemical denaturation curves quantitatively in the presence of macromolecular crowding agents is difficult, because it is unclear whether the synthetic sugar molecules uptake the chemical denaturant (a similar case to other three-component systems; (Bolen, 2001)). If in this case, urea is partitioned equally between the inside of Ficoll 70 molecules and the buffer, the apparent concentration of urea “felt” by apoflavodoxin molecules is accurately defined. However, if the urea molecules are effectively crowded by Ficoll 70 molecules, and partition only into the buffer, then the apparent concentration of urea “felt” by apoflavodoxin is higher than the assumed concentration and the effects of crowding are underestimated. If the second hypothesis were true for our system, then we would expect the cooperativity of the unfolding event (and thus the m -value) to appear to increase as the apparent concentration of denaturant “felt” by the protein would increase at increments greater than the

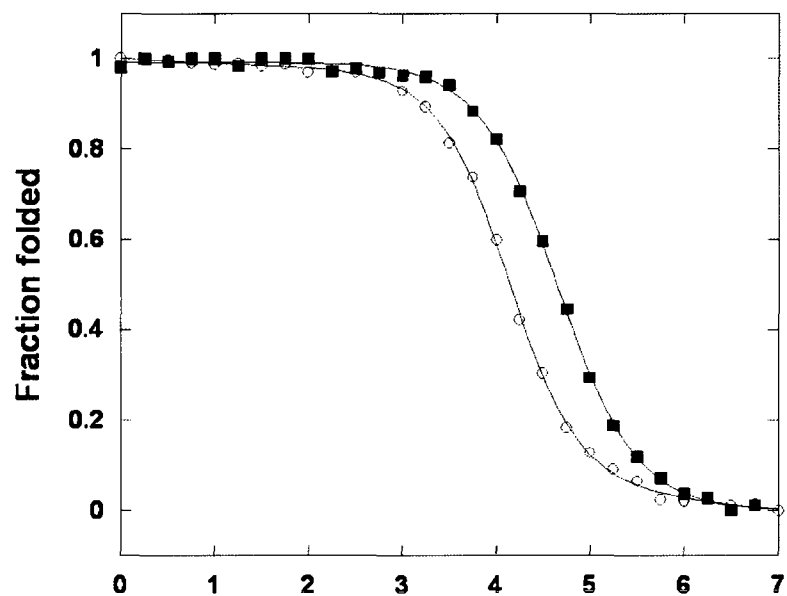


Figure 3.7 – Urea denaturation of wild-type apoflavodoxin in the absence (open circles) and presence (closed squares) of 100 mg/ml Ficoll 70 monitored by CD signal at 222 nm (100 mM KPi, pH 7, 20 °C).

assumed increments of the x-axis. We do not observe an increase in calculated m-values, and thus we believe that in the case of urea, denaturant molecules partition into both the buffer and the interior of the crowding agents.

Discussion

Correlation between in vitro and in silico results

In order to substantiate the results found in my *in vitro* experiments assessing effects of excluded volume on protein structure and stability, we collaborated with Dr. Margaret Cheung's group (University of Houston – Department of Physics) who specializes in biophysical simulations. Dr. Cheung's group used coarse-grained, C(α) side-chain modeling (C α -SCM) representing *Desulfovibrio vulgaris* flavodoxin (pdb:2fx2), which is homologous to *D. desulfuricans* flavodoxin (46 % identity), and a G δ -like interaction (where native, crystal structure interactions are attractive and non-native interactions are repulsive) to construct a free energy landscape. In C α -SCM simulations, each α -carbon is modeled as a bead and another bead is placed at the center of mass of the simulated amino acid. In addition, Ficoll 70 molecules were simulated as inert spheres with a radius of 55 Å (the calculated radius of Ficoll 70) (Fig. 3.8).

In agreement with *in vitro* data, simulations depicted a single thermal unfolding transition for apoflavodoxin that increased in the presence of spherical macromolecular crowding agents. The *in silico* T_m of apoflavodoxin increased by

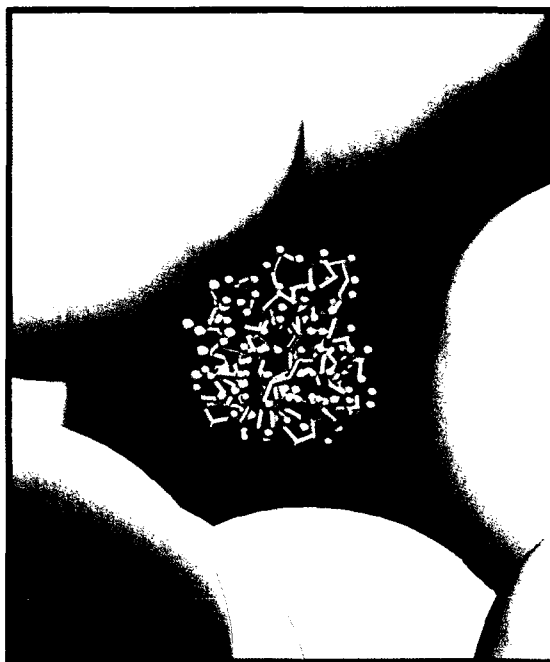


Figure 3.8 – Depiction of periodic box used by Cheung group in simulations of apoflavodoxin (blue chain and pink spheres) in the presence of Ficoll 70 (gray spheres). Figure taken from Stagg et al. (2007).

approximately 7 K from the buffer condition to a volume occupancy of 25 % ($\phi_c = 25\%$). 1D energy profiles of apoflavodoxin simulated at a temperature near the *in silico* thermal transition ($T = 360$ K) showed that the energy minimum of the folded state ensemble increased in terms of the fraction of native-like interactions (Q) with an increase in volume occupancy from $Q = 0.76$ (at $\phi_c = 0\%$) to $Q = 0.80$ at $\phi_c = 25\%$ and $Q = 0.82$ at $\phi_c = 40\%$ (not shown). Similarly, 2D energy landscapes for apoflavodoxin at 360 K showed clearly that the radius of gyration (R_g) of the folded-state ensemble shifted to a more compact (lower R_g) set of structures at $\phi_c = 25\%$ compared to in buffer (Fig. 3.9). Despite the decrease in R_g for the folded-state ensemble at $\phi_c = 25\%$, the shape parameters of the polypeptide remained virtually unchanged, suggesting that the compaction effects of the spherical crowding agent on apoflavodoxin were isotropic. Difference contact maps (at $\phi_c = 0\%$ and $\phi_c = 25\%$) suggested that the compaction event most likely occurs as surrounding helices squeeze in toward the central beta sheet and terminal helical fraying is decreased (not shown).

Similar trends found with unrelated, α -helical protein (VlsE)

In addition to work on the α/β protein, flavodoxin, Dr. Michael Perham also probed the effects of macromolecular crowding on the α -helical, elongated protein VlsE from *Borrelia burgdorferi* (Eicken et al., 2002; Homouz et al., 2008). In accord with the findings on the effects of synthetic crowding agents on flavodoxin structure and stability, Dr. Perham found that the secondary structural content of folded VlsE increased as a function of increasing [Ficoll 70]. He also

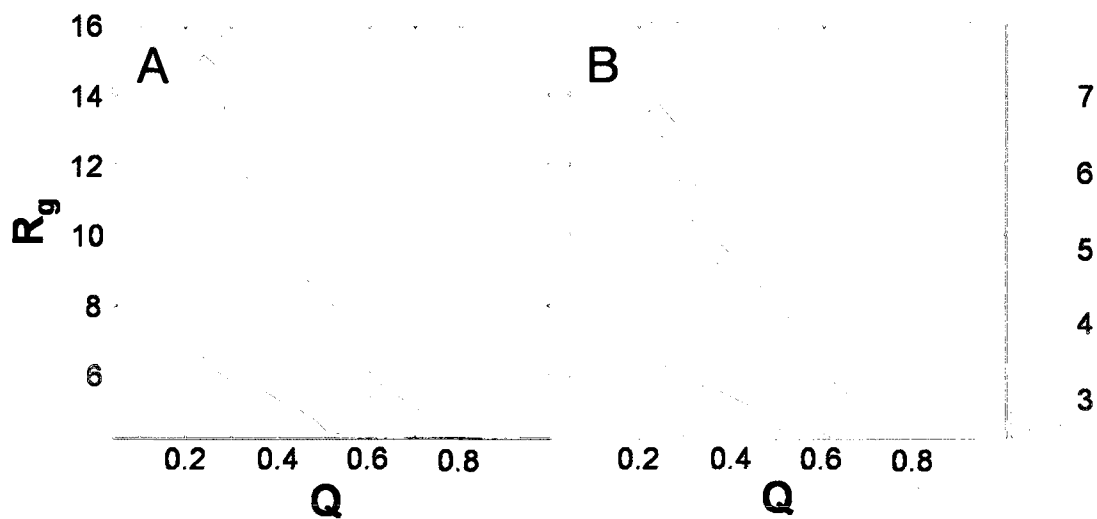


Figure 3.9 – 2D energy landscapes of apoflavodoxin at $T = 360$ K in bulk (A) and 25 % volume occupancy (B). R_g is radius of gyration in units of σ ($\sigma = 3.8$ Å), Q is fraction of native-like contacts, and color is scaled by $k_B T$. Figure taken from Stagg et al. (2007).

found that the thermal stability of VIsE increased approximately 6 °C upon going from the buffer condition (20 mM phosphate, pH 7) to 400 mg/ml Ficoll 70 (Perham et al., 2007). In contrast to my work on flavodoxin, it was found that at high concentrations of Ficoll 70, thermally unfolded VIsE adopted a non-native secondary structure that could best be approximated to a β -sheet/turn structure. Simulations by the Cheung group showed that the asphericity of VIsE in concert with spherical crowding agents may be the reason behind the adoption of non-native-like structures of VIsE under particular conditions of excluded volume and denaturant (Homouz et al., 2008). Interestingly, some of the non-native-like structures adopted by VIsE resulted in the exposure of an antigenic region (IR₆) (Liang et al., 1999) that is normally buried in the protein.

Summary

The increase in secondary structural content of two folded proteins (flavodoxin and VIsE) upon addition of synthetic crowding agents was not an expected phenomenon, as popular crowding theory predicted that only the energetics of the unfolded state would be affected (by compaction of the entropically favored, elongated polypeptide). In both cases (flavodoxin and VIsE), the addition of synthetic crowding agents in the range of 100-400 mg/ml elicited increases in the amount of calculated α -helical content and a decrease in the amount of random coil contribution. The SOMCD structural algorithm was used to calculate changes in flavodoxin secondary structure due to increased macromolecular crowding. This algorithm uses a set of 6 references (two α -helical, two β -sheet, and two random coil) and 39 training sets (proteins with

differing amounts of each secondary structure based on their crystal structures) from which to predict the secondary structural content of proteins of interest based on experimental CD data (Unneberg et al., 2001). For flavodoxin, the SOMCD structural algorithm calculated that the secondary structural content of the protein in the presence of 400 mg/ml Ficoll 70 very closely resembled the secondary structural content observed in the crystal structures of *D. vulgaris* flavodoxin (pdb:2fx2; a structural homolog) and *D. desulfuricans* flavodoxin (pdb:3f6r). These data suggest that excluded volume effects may effectively tune protein structures toward crystal structures (where molecules effectively crowd each other). Admittedly, the SOMCD data has considerable amounts of calculated error due in large part to the inability of obtaining reliable CD data in the range of ≤ 205 nm as a result of the absorbance of the synthetic crowding agents.

Observed changes to the folded state of flavodoxin due to the presence of macromolecular crowding agents as well as the global change in structure of at least one “intrinsically disordered” protein (FlgM) in the presence of both synthetic crowding agents and in the cell (Dedmon et al., 2002) suggest that significant structural changes may occur in proteins due to crowding. I do not claim that intrinsically disordered proteins are artifactual (due only to *in vitro* conditions). In fact, at least in the cases of two intrinsically disordered domains of human proteins, it has been shown that the presence of macromolecular crowding agents does not result in spontaneous folding (Flaugh and Lumb,

2001). However, in light of the fact that protein structures have been shown to vary to different degrees in the presence of macromolecular crowding, I would suggest that researchers probe the effects of volume exclusion on disordered proteins before classifying them as “intrinsically disordered.”

In contrast to changes in the secondary structural content of the folded state of flavodoxin, we found the secondary structure of chemically unfolded flavodoxin (3M GdmCl) to be completely unchanged upon addition of crowding agent. Thermally unfolded flavodoxin does appear to have slightly more secondary structure in the presence of crowding agents, however the shapes of the CD spectra do not change, suggesting that the protein is still globally unfolded. This suggests that energetic changes may occur both to the folded and unfolded states of the protein as a result of macromolecular crowding. Interestingly, for VlsE, Dr. Perham and Dr. Cheung's group found that relatively high concentrations of crowding agents in concert with certain denaturant conditions resulted in non-native-like structures to the protein that exposed the normally buried IR₆ antigen to solvent. Analogously, other groups have also observed changes in the unfolded state of proteins as a function of macromolecular crowding. Cytochrome c was found to adopt a molten globule state at low pH in the presence of crowding agents (Sasahara et al., 2003) and the intrinsically unstructured protein, FlgM, was found to fold under crowded conditions (Qu and Bolen, 2002).

As expected by crowding theory, both the thermal and chemical equilibrium stability of flavodoxin increases under conditions of macromolecular crowding. As hypothesized by Minton, it is possible that T_m values of soluble proteins could increase as much as 20 °C in the presence of physiological amounts of macromolecular crowding (Minton, 2000a). Others had seen modest increases in protein thermal stability as a function of increasing excluded volume. For example, the T_m of G-actin increased by 5 °C in 100 mg/ml PEG (Tellam et al., 1983) and the T_m of cytochrome c increased by 3.5 °C in 370 mg/ml dextran (Hall and Dobson, 2006). However, the T_m of flavodoxin in my studies was increased by approximately 20 °C, which correlates with Minton's hypothesis. Admittedly, flavodoxin is particularly sensitive to buffer content, and the degree to which the presence of crowding agents modulates the stability of the protein is dependent on buffer make-up (especially ionic concentration and presence of phosphate). However, in all buffer conditions, protein stability increases as a result of crowding.

CHAPTER 4: EFFECTS OF SMALL IONS ON STABILITY AND FOLDING OF APOFLAVODOXIN

The results presented in this chapter include published material (Sedlak et al., 2008a; Sedlak et al., 2008b).

Cations in [≤ 250 mM] affect apoflavodoxin through specific interactions

Cations increase apoflavodoxin thermal stability

It has long been accepted that salts can affect protein properties. As early as the late 1800s, the Hofmeister series of ions was being constructed based on the effects of certain salts on protein solubility (Hofmeister, 1888). Since then, it has been found that effects of ions on other protein properties often follow the Hofmeister series of ions. Salts may affect proteins either directly through binding or indirectly by modulating the structure of bulk water (Baldwin, 1996; Collins, 1997; Timasheff, 1992; Zhang et al., 2005). Anions in general elicit greater effects on protein properties than cations. In order to gain insight into the effects of cations on protein properties, one would hypothesize that a negatively charged protein would be the proper protein of choice. *D. desulfuricans* apoflavodoxin is a highly acidic protein (net charge of -19 at neutral pH) (Fig. 4.1), and the host organism has evolved to live in high salt environments (in certain cases greater than 4 M NaCl) (Kerkar, 2005).

Our original interest in studying the general effects of cations on apoflavodoxin stability arose from the surprising discovery that low concentrations (≤ 250 mM) of guanidinium chloride (GdmCl), which is normally a powerful denaturant, significantly stabilized apoflavodoxin against thermal

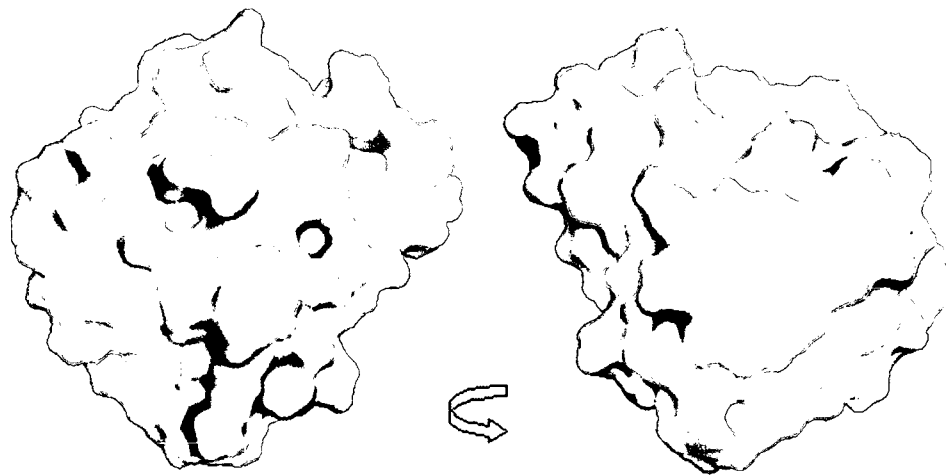


Figure 4.1 – Electrostatic surface map of apoflavodoxin using homology modeling of *D. desulfuricans* sequence on *D. vulgaris* structure with 3D jigsaw program. Negative residues are colored in red, positive residues are blue, and non-charged residues are white. Figure taken from Sedlák et al. (2008a).

denaturation (Fig. 4.2). Previous studies had shown that low concentrations of Gdm⁺ may elicit modest increases in protein stability (Bhuyan, 2002; Hagihara et al., 1993; Mayr and Schmid, 1993; Shukla et al., 2005). In order to assess the effects of cations on apoflavodoxin stability, we evaluated the effects of a range of chloride salts with monovalent cations spread across the Hofmeister series of ions. The chosen monovalent cations were Gdm⁺, NH₄⁺, Cs⁺, K⁺, Na⁺, and Li⁺ (listed here in order from most chaotropic to most kosmotropic). The reference buffer condition for all experiments was 10 mM HEPES, pH 7. Under these mildly stabilizing conditions, the thermal transition of apoflavodoxin appeared to be a simple, two-state mechanism (as indicated by agreement in CD, fluorescence, and DSC data) with a thermal midpoint centered at approximately 46 °C (which agrees very closely with earlier work (Stagg et al., 2007)). The thermal stability of apoflavodoxin increased greatly with additions of increasing amounts of Gdm⁺ up to 250 mM after which increasing Gdm⁺ concentrations destabilized the protein against thermal denaturation. At all tested Gdm⁺ concentrations between 0 and 1 M, thermal midpoints determined by the three detection methods were consistent (Table 4.1).

Extending the study to the other cations, we found that each cation stabilized apoflavodoxin against thermal denaturation in the studied concentration range. In fact, the dependence of the thermal midpoint of apoflavodoxin against the concentration of any given cation gave the appearance of a binding curve in each case suggesting specific binding events (Fig. 4.3). These apparent binding

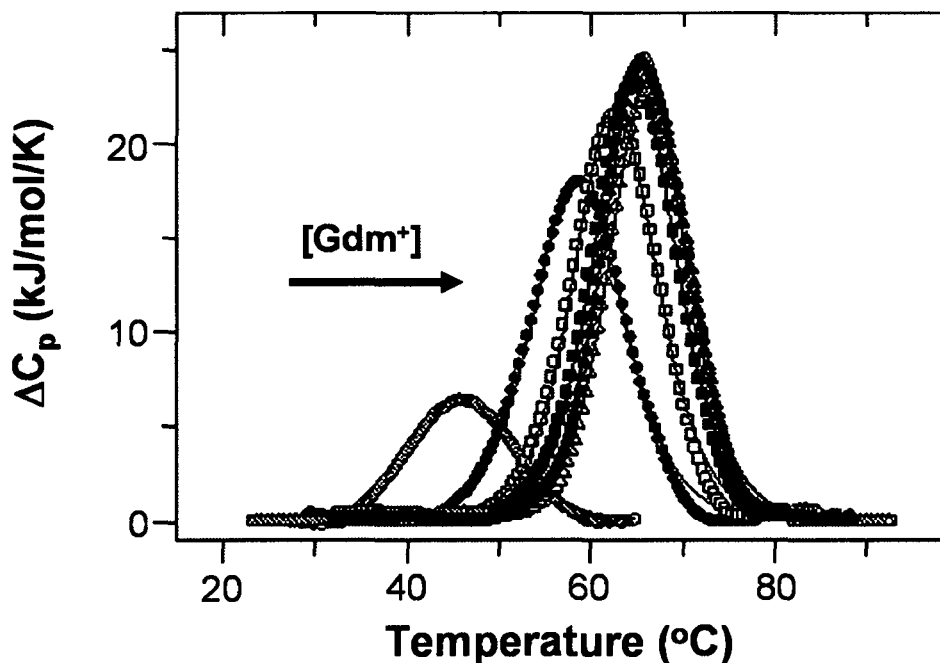


Figure 4.2 – DSC experiments of apoflavodoxin with varying concentrations of GdmCl (0, 10, 25, 50, 100 and 250 mM) showing an increase in thermal stability with increasing $[Gdm^+]$ (10 mM HEPES, pH 7). Figure adapted from Sedláč et al. (2008a).

$[Gdm^+]$ (mM)	$T_{m,CD}$ (°C)	$T_{m,F}$ (°C)	$T_{m,DSC}$ (°C)
0	45.9	46.2	46.2
10	58.5	58.1	58.7
25	62.4	61.7	62.7
50	64.5	64.6	64.9
100	66.4	66.2	66.2
250	66.9	66.5	65.8
500	65.4	64.4	64.3
1000	58.9	58.7	57.6

Table 4.1 – Thermal midpoints calculated for apoflavodoxin denaturation in the presence of varying amounts of Gdm^+ by three detection methods (CD, fluorescence, and DSC) (10 mM HEPES, pH 7).

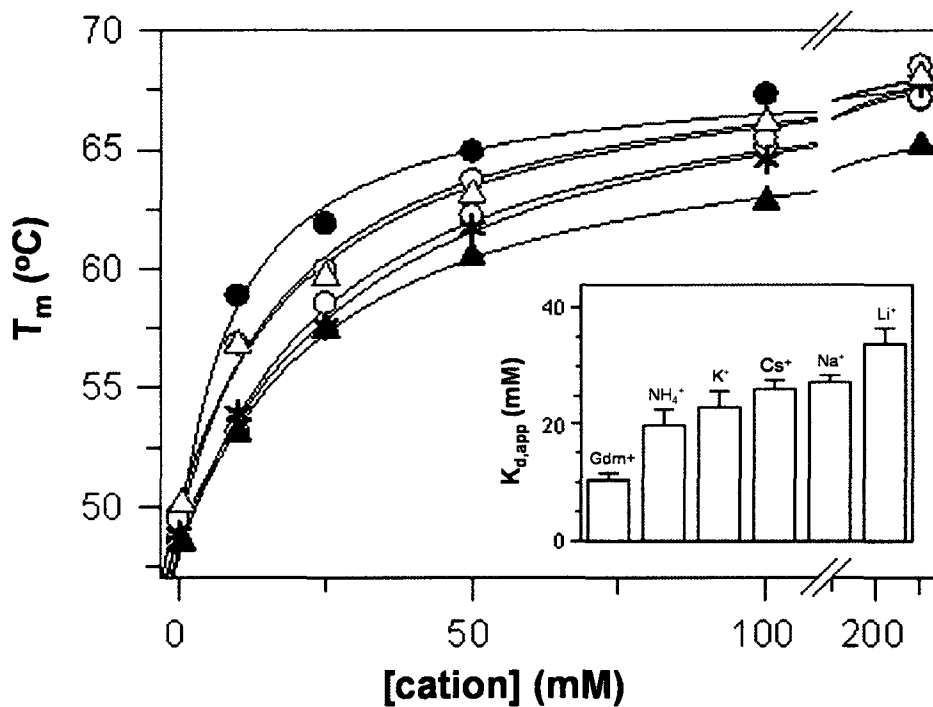


Figure 4.3 – Dependences of apoflavodoxin thermal midpoints (T_m) monitored by CD signal at 222 nm on Gdm⁺ (closed circles), NH₄⁺ (grey circles), Cs⁺ (closed triangles), K⁺ (open triangles), Na⁺ (open circles), and Li⁺ (asterisks) concentrations (10 mM HEPES, pH 7). Inset shows apparent dissociation constants ($K_{d,app}$) calculated for each ion based on apparent binding curves. Figure adapted from Sedláč et al. (2008a).

curves can be fit very simply to give apparent K_d values ($K_{d, app}$) as shown with the following equation:

$$S = \Delta S ([\text{cation}] / (K_{d,app} + [\text{cation}])) \quad (\text{Eq. 4.1})$$

where S is the measured parameter (in this case T_m), ΔS is the change in T_m from the reference value, and $K_{d, app}$ is the apparent dissociation constant for the studied cation. This equation assumes 1-to-1 binding. Interestingly, the calculated K_d values for the studied ions agree qualitatively with the position of the cations in the Hofmeister series (with chaotropic Gdm^+ binding with the most affinity and kosmotropic Li^+ binding with the least affinity). We believe that there are likely many non-specific binding sites for cations on the surface of apoflavodoxin (as was found for the phosphate anion; (Muralidhara and Wittung-Stafshede, 2003)). However, there may be a specific binding event between the studied cations and apoflavodoxin that engenders the significant increase in thermal stability. Δv values may be calculated for proteins in the presence of salts for which DSC data is available, and this parameter approximates the difference in the number of bound ions for the protein in the unfolded state relative to the native state. In the case of apoflavodoxin in the presence of Gdm^+ (0 – 100 mM), calculated Δv values (not shown) suggest that one fewer cation is present in the unfolded state relative to the native state (potentially dissociation of one specifically bound cation).

Cations increase apoflavodoxin chemical equilibrium stability

In the reference, buffer condition (10 mM HEPES, pH 7), apoflavodoxin has an extremely low free energy of unfolding in urea ($\Delta G_U(\text{H}_2\text{O}) = 4.4 \pm 0.7$ kJ/mol calculated by CD and 6.2 ± 0.4 kJ/mol calculated by fluorescence). In contrast, urea equilibrium unfolding of apoflavodoxin in the presence of 250 mM Gdm⁺ (Fig. 4.4) and all other studied cations dramatically increased the free energy of unfolding (Table 4.2). In addition to the increases in free energy of unfolding, the m-values (slope of transition region) for unfolding also increased in the presence of cations. This suggests an increase in the amount of exposed surface area between the native and unfolded states in the presence of cations. This is often explained as an increase in the “cooperativity” of unfolding (Uversky and Ptitsyn, 1996). In the case of apoflavodoxin unfolding as a function of the presence or absence of 250 mM [cation], we believe that the sizeable increase in the calculated m-values is a result of an increase in the rigidity of the native state of apoflavodoxin, thus resulting in a larger disparity between the solvent accessible surface area between the native state (which is presumably more compact in the presence of cations) and the unfolded state. Along with the increased free energy of unfolding and increased m-values, the urea unfolding midpoint of apoflavodoxin also dramatically increased in the presence of the studied cations.

Cations modulate the folded state of apoflavodoxin

The folded secondary structure of apoflavodoxin exhibited modest increases in CD signal (both near-UV and far-UV) as a function of increasing cation

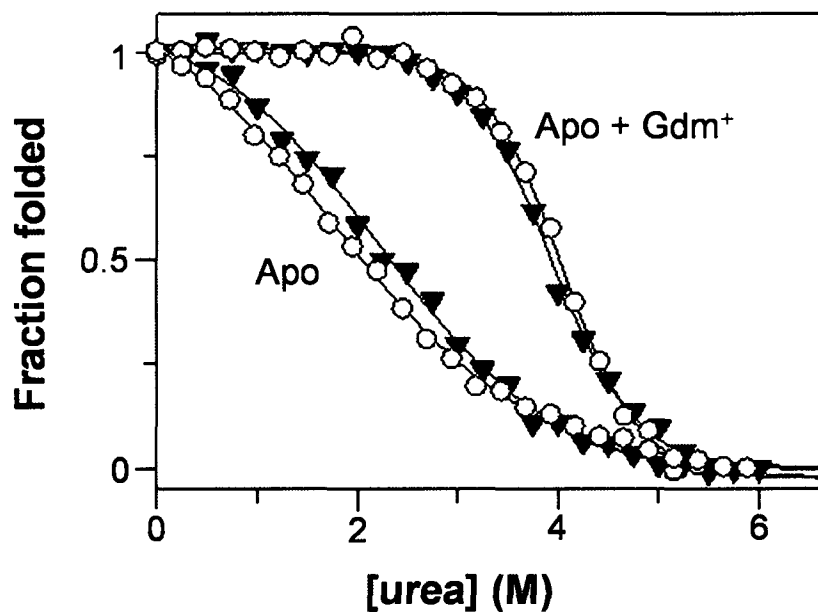


Figure 4.4 – Urea denaturation of apoflavodoxin monitored by CD signal at 222 nm (closed triangles) and fluorescence (open circles) in buffer alone and in the presence of 250 mM Gdm⁺ (10 mM HEPES, pH 7, 20 °C). Figure adapted from Sedlák et al. (2008a).

Cation	Method	ΔG_U (kJ/mol)	m (kJ/mol,M)	[Urea] _{1/2} (M)
-	CD	4.4 ± 0.7	2.5 ± 0.9	1.9
	F	6.2 ± 0.4	2.8 ± 0.1	2.3
Gdm ⁺	CD	25.2 ± 1.9	6.2 ± 0.2	4.0
	F	22.7 ± 0.7	5.8 ± 0.2	3.9
NH ₄ ⁺	CD	24.4 ± 2.3	6.0 ± 0.6	4.0
	F	21.8 ± 1.8	5.3 ± 0.5	4.1
Cs ⁺	CD	23.5 ± 1.2	5.3 ± 0.3	4.4
	F	24.7 ± 1.8	5.5 ± 0.4	4.5
K ⁺	CD	24.0 ± 0.8	5.5 ± 0.2	4.5
	F	23.5 ± 1.5	5.2 ± 0.3	4.5
Na ⁺	CD	26.9 ± 0.8	5.9 ± 0.2	4.5
	F	26.8 ± 1.3	5.9 ± 0.3	4.6
Li ⁺	CD	22.4 ± 0.8	5.4 ± 0.2	4.1
	F	29.0 ± 1.6	7.1 ± 0.4	4.1

Table 4.2 – Thermodynamic parameters calculated from urea equilibrium denaturation of apoflavodoxin in the presence and absence of 250 mM of the studied chloride salts (10 mM HEPES, pH 7, 20 °C) as monitored by CD and fluorescence (F). Data for table from Sedlák et al. (2008a).

concentration (Fig. 4.5). However, the spectral shape did not change from the buffer condition to increasing cation concentrations. As compared to changes in apoflavodoxin native structure in the presence of macromolecular crowding agents, the presence of salts increased the folded CD signal approximately 3-fold less.

However, as a result of the slight modulation of native structure, we decided to assess 1-anilino-8-naphthalene sulfonate (ANS) binding fluorescence with apoflavodoxin in the presence and absence of the studied cations. ANS is a fluorescent probe that binds to nonpolar solvent-exposed regions of proteins and is most often used to assess accumulation of intermediate protein species or changes in tertiary structure (Semisotnov et al., 1991). In the case of apoflavodoxin in the native state, ANS fluorescence shifted to shorter wavelengths and increased in intensity upon the increase in cation concentration. The amount of shift in wavelength and intensity varied for each cation with no apparent correlation to cation properties, however, again as with T_m values, the dependence of ANS intensity maxima (λ_{max}) on cation concentration gave the appearance of a binding curve (Fig. 4.6). Fitting these binding curves as before gave apparent K_d values. The K_d values calculated by ANS binding agree qualitatively with those determined by T_m values (with the exception of Cs^+). It is difficult to propose a mechanism explaining the changes in ANS fluorescence on the native state of apoflavodoxin as a function of increasing cation concentration.

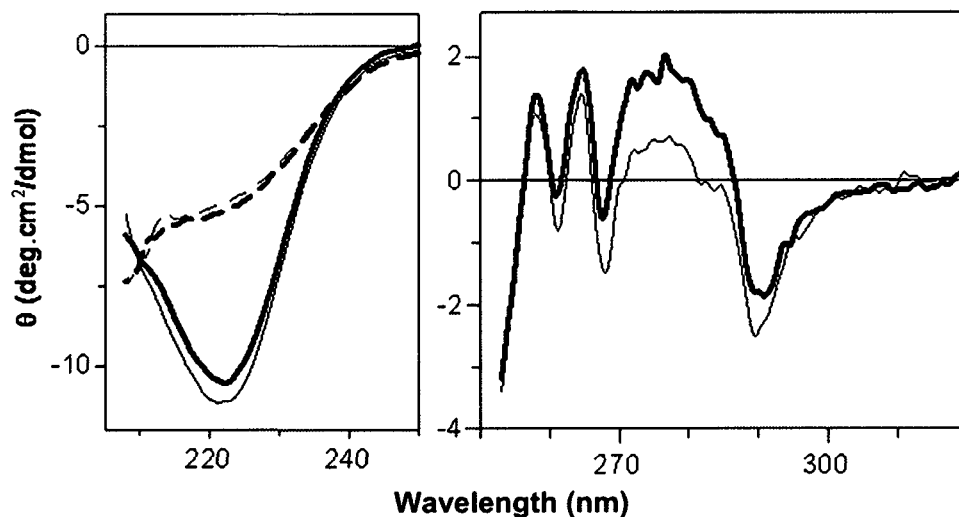


Figure 4.5 – Far- (left panel) and near-UV CD (right panel) of apoflavodoxin in buffer alone (bold lines) and in the presence of 250 mM Gdm⁺ (thin lines). Left panel shows native apoflavodoxin (solid lines) and thermally unfolded apoflavodoxin (dashed lines). Figure taken from Sedlák et al. (2008a).

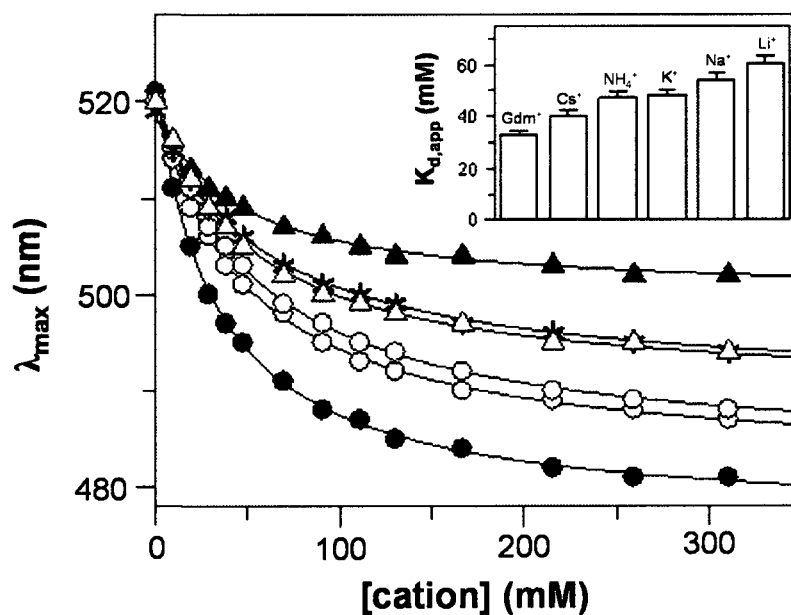


Figure 4.6 – Dependences of ANS fluorescence on [cation] for each of the studied cations (Gdm⁺, closed circles; NH₄⁺, grey circles; Cs⁺, closed triangles; K⁺, open triangles; Na⁺, open circles; and Li⁺, asterisks). Inset shows apparent dissociation constants ($K_{d,app}$) for each of the ions. Figure adapted from Sedlák et al. (2008a).

However, it is possible that ion screening may decrease the amount of charge-charge repulsions on the surface of the highly negatively charged protein creating a slightly more rigid fold with defined surface exposed non-polar ANS binding patches.

Effects of anions on thermal stability

In order to ensure that we were not overlooking the contribution of anions (in the above cases, Cl⁻) to apoflavodoxin stability, we assessed the effects of three anions on apoflavodoxin thermal stability. We chose SO₄²⁻, Cl⁻, and ClO₄⁻ (all present as sodium salts) because of their different positions in the Hofmeister series (with sulfate being highly kosmotropic, perchlorate being chaotropic, and chloride lying in the middle of the series). We found that in the cases of the studied anions at the concentrations of interest (≤ 250 mM), there is only a small change in the dependence of the T_m of apoflavodoxin as a function of the type of anion present (and all data overlaps at ≤ 100 mM) (Fig. 4.7). At higher concentrations, the dependence of T_m on the concentration and type of anion follows the Hofmeister series with sulfate being the most stabilizing and perchlorate being the most destabilizing. Our data suggest that at low anion concentrations (≤ 100 mM), the specific effects of Na⁺ on apoflavodoxin dominate, and only at higher salt concentrations do the Hofmeister effects of the anions come in to play.

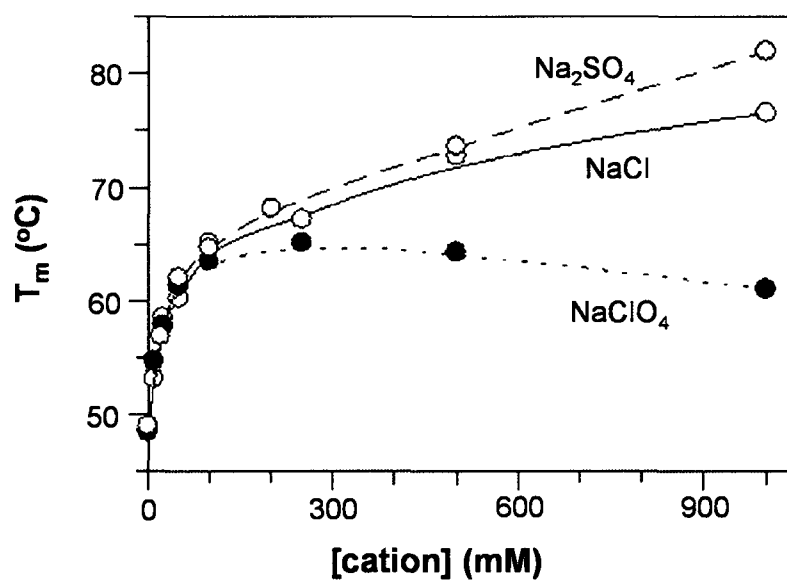


Figure 4.7 – Dependences of apoflavodoxin thermal midpoints (T_m) monitored by CD signal at 222 nm (10 mM HEPES, pH 7) on various anions (scaled to Na^+ concentration). Figure adapted from Sedlák et al. (2008a).

Cations affect both kinetic folding and unfolding rates of apoflavodoxin

In an attempt to correlate increases in chemical equilibrium stability of apoflavodoxin with kinetic effects, we assessed the kinetic folding rates of apoflavodoxin in the buffer condition along with in the presence of 250 mM GdmCl (chaotropic Gdm⁺ cation) and 250 mM LiCl (kosmotropic Li⁺ cation). Using stopped-flow mixing monitored by CD signal at 222 nm, we performed urea unfolding and refolding by dilution on apoflavodoxin under the three buffer conditions. As mentioned before (Eq. 1.4), apoflavodoxin folds via a complex mechanism involving an assumed off-pathway intermediate that populates during the dead-time of the stopped-flow mixer (approximately a few msec). However the missing amplitude in the burst-phase was not analyzed here. At the tested conditions, both Gdm⁺ and Li⁺ salts affected the kinetic folding and unfolding rates of apoflavodoxin similarly. Chevron (semilogarithmic) plots of all three kinetic experiments show that the folding rate of apoflavodoxin increases and the unfolding rate decreases with 250 mM Gdm⁺ and Li⁺ (Fig. 4.8).

Ions in larger amounts (> 250 mM) affect stability of oppositely charged proteins (apoflavodoxin and cytochrome c) similarly

Our previous work on the effects of cations on the stability of apoflavodoxin suggested that at low concentrations of cation, specific interactions between cations and apoflavodoxin are responsible for changes in protein stability. At higher concentrations of ions (where the Hofmeister series is expected to hold true), recent disagreements in the field of protein biophysics have occurred from

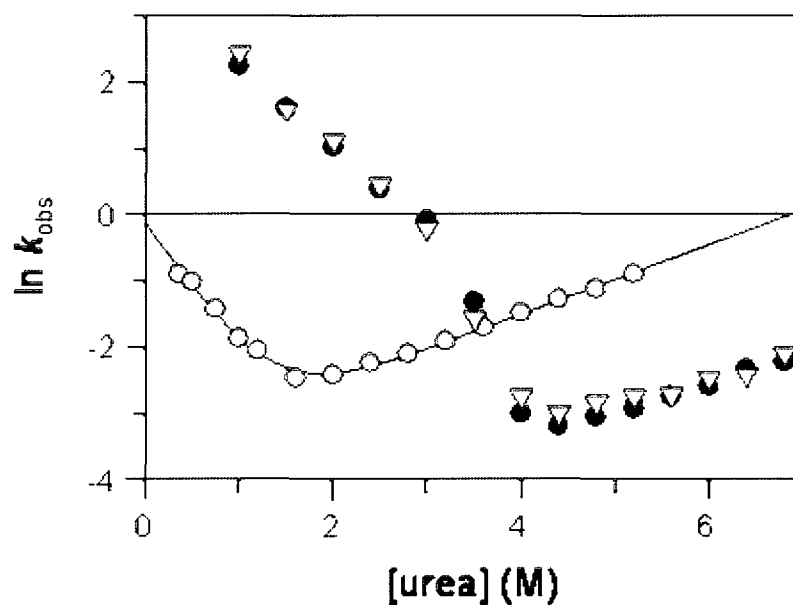


Figure 4.8 – Semilogarithmic, chevron plots of kinetic folding/unfolding of apoflavodoxin monitored by CD signal at 222 nm in buffer alone (open circles) and in the presence of 250 mM Gdm⁺ (closed circles) and Li⁺ (open triangles) (10 mM HEPES, pH 7, 20 °C). Folding rates calculated from single exponential step occurring after burst-phase.

opposing views of the effects of salts on proteins. One camp believes that the presence of salt modulates the hydration bonding network of water and affects protein properties indirectly. However, recent work using time-resolved infrared spectroscopy, X-ray absorption and X-ray Raman scattering studies, as well as pressure perturbation calorimetry suggests that the effects of ions in solution on the hydrogen bonding network of bulk water do not extend past the first hydration shell of the ions (Batchelor et al., 2004; Naslund et al., 2005; Omta et al., 2003). In order to assess the origin of Hofmeister effects on protein stability, we used a range of small ions in concert with two vastly oppositely charged proteins. As before, we used apoflavodoxin (- 19 net charge at pH 7), and we also used horse heart cytochrome c (+ 17 net charge at pH 4.5) (purchased from Sigma). In both cases, we assessed the dependence of the T_m values for both proteins on the type and concentration of six cations (Gdm^+ , Li^+ , Na^+ , K^+ , NH_4^+ , and Cs^+ ; all present as chloride salts) and seven anions (SO_4^{2-} , CH_3COO^- , Cl^- , Br^- , I^- , NO_3^- , and ClO_4^- ; all present as sodium salts).

Effects of ions on apoflavodoxin and cytochrome c thermal stability

Experiments using model polymers have shown that at conditions where the polymers are saturated by ions ($> \sim 200$ mM), there is a linear relationship between the thermal midpoint of the polymers and ion concentration (Baldwin, 1996). As expected, at the concentrations tested (300 mM – 1.75 M), the dependences of apoflavodoxin and cytochrome c T_m values on ion concentration are linear (Fig. 4.9). Reproducibility of T_m values was tested using reheating

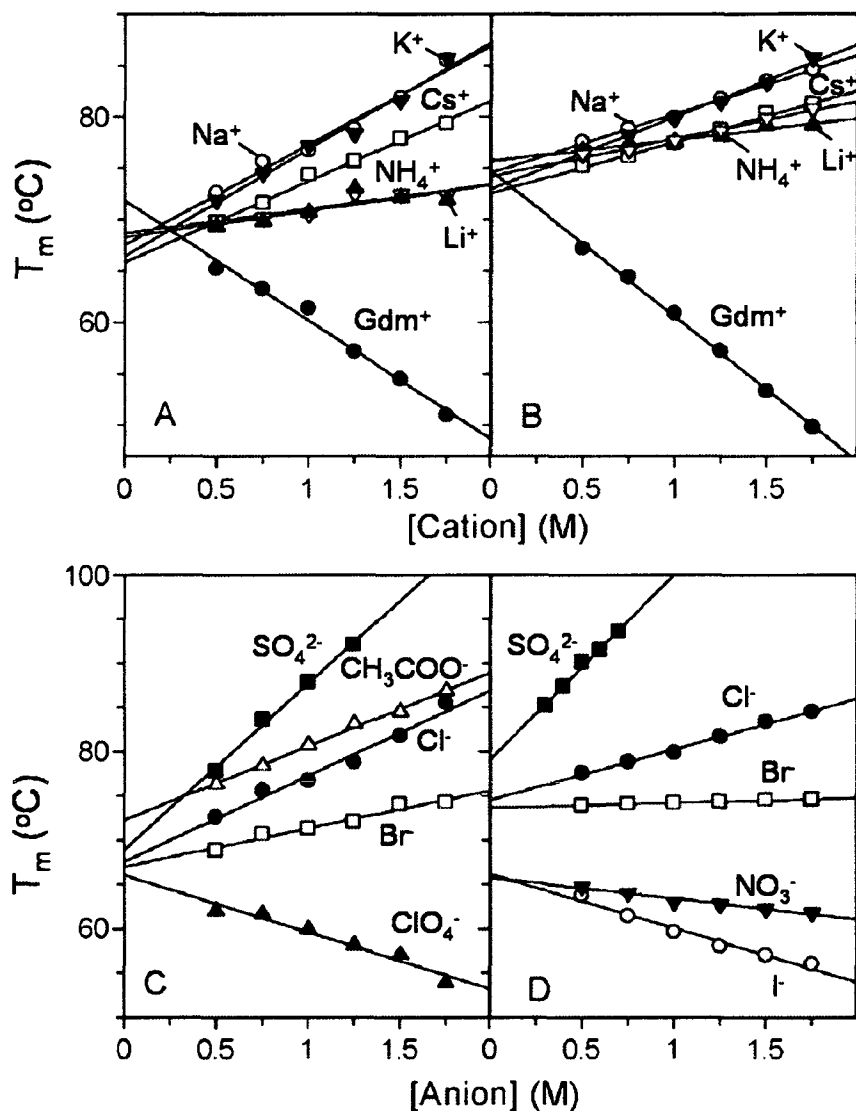


Figure 4.9 – Dependences of thermal transitions (T_m) of apoflavodoxin (left panels) and cytochrome c (right panels) monitored by CD signal at 222 nm on concentration of cations (top panels) and anions (bottom panels) (10 mM HEPES, pH 7). The counter ion for the studied anions is Na^+ while the counter ion for the studied cations is Cl^- . Figure adapted from Sedláč et al. (2008b).

experiments and in all cases the calculated T_m agreed within ± 0.5 °C of the original experiment. The linear slopes of the dependence of T_m values on ion concentration ($dT_m/d[\text{ion}]$) were used as a measure to assess the efficiency of each ion in modulating protein stability (Table 4.3). In the case of cations, all the studied cations stabilize both proteins in the tested concentrations with the exception of Gdm^+ . It has been well accepted that anions have greater effects on protein properties (e.g., protein solubility and stability) than cations (Collins, 2004). In agreement, our data shows that anions do have a greater effect on protein stability. In particular, sulfate ions greatly stabilize both proteins in comparison to the effects of any of the studied cations. Interestingly, the effects of both the set of cations and anions on both proteins are qualitatively very similar despite the vastly different surface charges of the two proteins.

Correlation of ion effects with ion properties

In an effort to pinpoint some of the properties of ions responsible for their Hofmeister effects on proteins, we attempted to correlate some of these intrinsic ion properties with our experimental $dT_m/d[\text{ion}]$ values for apoflavodoxin and cytochrome c. The values of intrinsic ionic properties used in correlations come from selected publications (Marcus, 1997; Pegram and Record, 2007).

Ion partition coefficients

One particularly interesting property of ions is the air/water partition coefficient. This coefficient describes the partitioning of dissolved ions into the air/water interface versus the bulk. We reasoned that ions that partition more

	Apoflavodoxin	r	Cytochrome c	r
<i>Anions</i>				
SO ₄ ²⁻	18.8 ± 1.2	0.996	21 ± 1.1	0.996
Cl ⁻	9.7 ± 0.8	0.987	5.7 ± 0.2	0.997
Br ⁻	4.3 ± 0.4	0.980	0.5 ± 0.0	0.993
NO ₃ ⁻	-	-	-2.4 ± 0.2	-0.983
I ⁻	-	-	-6.1 ± 0.5	-0.986
CH ₃ COO ⁻	8.4 ± 0.3	0.998	-	-
ClO ₄ ⁻	-6.4 ± 0.7	-0.977	-	-
<i>Cations</i>				
Li ⁺	2.5 ± 0.8	0.835	2.1 ± 0.2	0.976
Na ⁺	9.7 ± 0.8	0.987	5.7 ± 0.2	0.997
K ⁺	10.4 ± 0.8	0.988	7.1 ± 0.3	0.996
NH ₄ ⁺	2.4 ± 0.6	0.907	3.7 ± 0.2	0.992
Cs ⁺	7.9 ± 0.4	0.995	5.0 ± 0.2	0.997
Gdm ⁺	-11.6 ± 0.7	-0.993	-14.2 ± 0.3	-0.999

Table 4.3 $-dT_m/d[\text{ion}]$ values calculated using linear fits for apoflavodoxin (pH 7) and cytochrome c (pH 4.5) including correlation constants (r.) Data for table taken from Sedláč et al. (2008b).

into the air/water interface than the bulk may also accumulate preferentially around the surface of proteins relative to the bulk. This view is debatable as no clear correlation has been made, but it would hold true intuitively for well-defined surface regions on proteins with relatively low polarity. In fact, for anions, we find that the calculated $dT_m/d[\text{ion}]$ values for both apoflavodoxin and cytochrome c do correlate with anionic partitioning coefficients (Fig. 4.10). In the case of cations, there is an apparent correlation as well, however the position of the Gdm^+ partition coefficient may skew the correlation to appear stronger than it may be in reality. If our original hypothesis is correct stating that ions that partition preferentially into the air/water interface may also accumulate at the protein surface, then the correlation between $dT_m/d[\text{ion}]$ values and ion partition coefficients for apoflavodoxin and cytochrome c may suggest that direct protein-ion interactions mediate Hofmeister effects and not indirect effects of dissolved ions on the hydrogen-bonding network of the bulk.

Surface tension

The effects of ions on surface tension (γ) are directly related to the propensity of ions to partition to the air/water interface (Pegram and Record, 2007). As we have found a correlation between $dT_m/d[\text{ion}]$ and ion partition coefficients, it would stand to reason that we should also see a correlation between $dT_m/d[\text{ion}]$ and surface tension. In fact, we do find a correlation between $d\gamma/d[\text{ion}]$ and $dT_m/d[\text{ion}]$ (not shown). In general, we find that the more the ion increases surface tension, the more the ion stabilizes the proteins against thermal

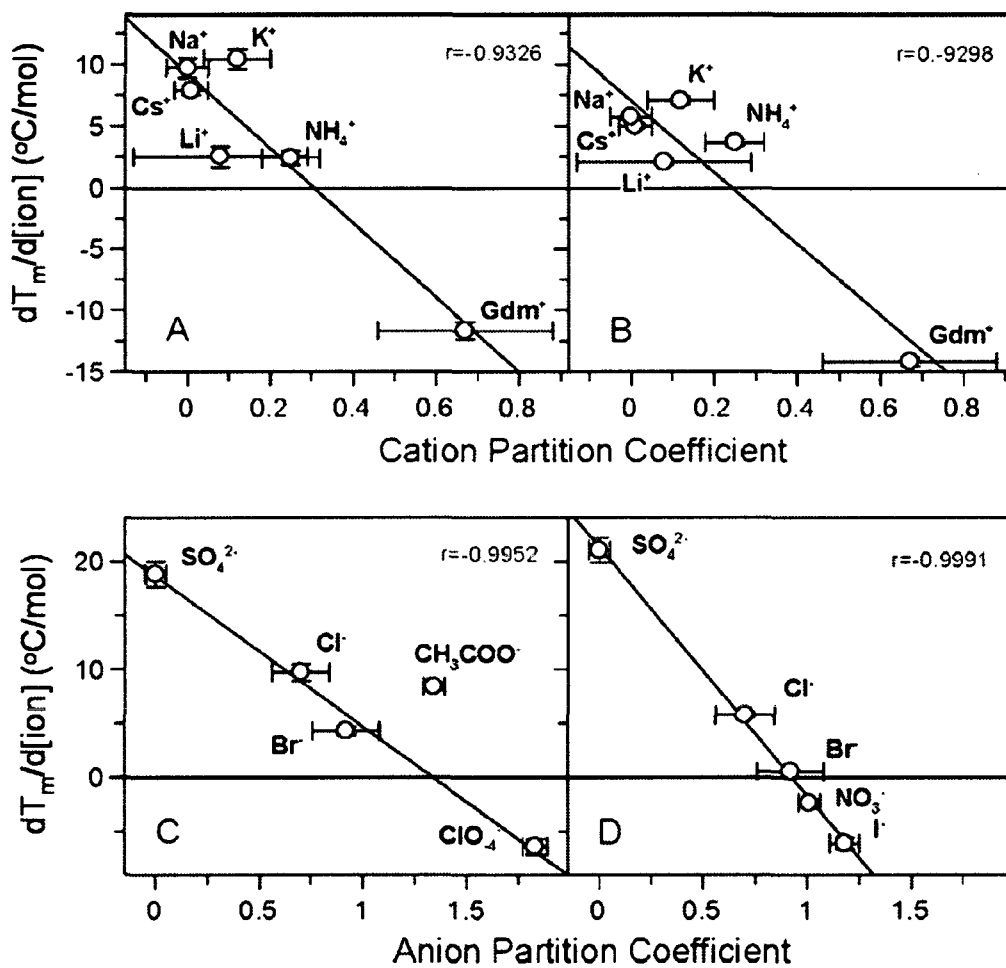


Figure 4.10 – Dependences of $dT_m/d[\text{ion}]$ for apoflavodoxin (left panels) and cytochrome c (right panels) on cation (top panels) and anion (bottom panels) partition coefficients. Linear correlation coefficients are noted in the top right of each panel. Error bars in x-direction from source data (Pegram and Record, 2007). Figure adapted from Sedláček et al. (2008b).

denaturation. Our results agree with a number of previous studies suggesting that ionic effects on surface tension modulates protein-ion interactions (Arakawa and Timasheff, 1982; Breslow and Guo, 1990; Jensen et al., 1995; Kaushik and Bhat, 1999; Lee and Timasheff, 1981). In the case of the ions tested in our study, all of the ions contribute positively to surface tension (meaning an increase in surface tension relative to bulk water). In light of the fact that Gdm^+ , I^- , NO_3^- , and ClO_4^- are destabilizing, effects of ions on surface tension is likely a contributing factor to protein stability but not the dominant factor.

Preferential hydration

Surface tension is one of the two properties of ions generally assumed to affect protein stability. The other factor is preferential hydration (Breslow and Guo, 1990).

$$\delta(\Delta G^0_{\text{stability}}) = \delta(\Delta G^0_{\text{cavitation}}) + \delta(\Delta G^0_{\text{solvation}}) \quad (\text{Eq. 4.2})$$

Above, the net free energy of stabilization depends on cavity formation (describing surface tension effects) and solvation (preferential hydration). In the cases of ions that destabilize proteins regardless of their increase in surface tension, the ions must affect the proteins through another mechanism. It is our belief, that in these particular cases, protein destabilization through direct protein-ion interactions (determined by ion preferential hydration) dominates the stabilizing effects of increased surface tension by the same ions. This hypothesis is well supported at least for Gdm^+ . Molecular dynamics approaches have shown that Gdm^+ can stack preferentially on the side-chains of planar amino acids (Arg, Trp, and Gln) as well as to a lesser extent on aliphatic side-

chains (Mason et al., 2007). Analogously, Gdm⁺ has also been suggested to bind directly to the peptide group (Courtenay et al., 2001; Courtenay et al., 2000).

Charge density

One intrinsic property of the tested ions for which there is a disparity between the effects of cations and anions is ion charge density. In the case of both apoflavodoxin and cytochrome c, there is a linear correlation between $dT_m/d[\text{ion}]$ and ion charge density only for the anions (Fig. 4.11). There is no apparent correlation between $dT_m/d[\text{ion}]$ and ion charge density for the tested cations. These findings do correlate with a number of other studies. In particular, vibrational sum frequency spectroscopy studies have shown that the ability of anions to orient water molecules at macromolecular interfaces is directly related to the position of the anion in the Hofmeister series while no correlation could be made for cations (Cacace et al., 1997). In addition, other studies have shown that charge density is a major determining factor in protein-ion interactions (Collins, 1997; Collins, 2006; Collins et al., 2007). The role of charge density (a hydration related parameter) in mediating protein-ion interactions in our study is further strengthened by the correlation between $dT_m/d[\text{ion}]$ and ion hydration entropies, viscosity coefficients, and ion hydration numbers (not shown).

Role of peptide backbone

Interestingly, the correlation between $dT_m/d[\text{ion}]$ and intrinsic ion properties for the studied ions were similar both for the negatively charged apoflavodoxin and the positively charged cytochrome c. Our data suggest that the electrostatic

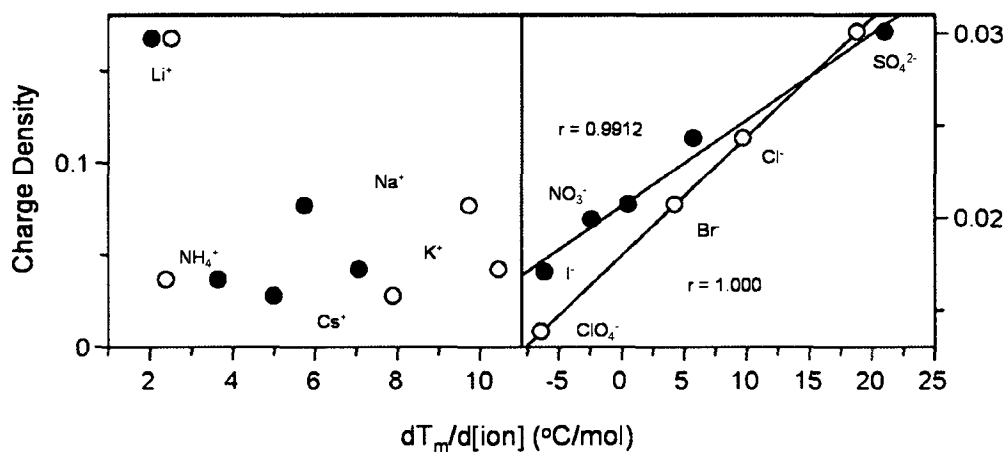


Figure 4.11 – Dependences of $dT_m/d[\text{ion}]$ for apoflavodoxin (closed circles) and cytochrome c (open circles) versus charge densities for studied cations (left panel) and anions (right panel). Figure adapted from Sedláček et al. (2008b).

surface potentials of the two proteins play only a minor role in the effects of ions on protein stability in the studied range. The major contributor to protein-ion interactions responsible for the increase in protein stability in the studied ion concentration range must be common to both proteins. Both surface exposed non-polar side-chains and peptide groups have been suggested to mediate protein-ion interactions (Nandi and Robinson, 1972a; Nandi and Robinson, 1972b; Von Hippel and Hamabata, 1973). In the case of apoflavodoxin and cytochrome c, the amount of exposed nonpolar surface is similar. Thus it is difficult to distinguish between effects of ions on nonpolar surfaces and the peptide group. However, we do believe it to be reasonable to assume a primary role for the peptide group due to the nature of peptide group hydration. The peptide group can be separated into two entities: the chaotropic (dehydrated) amide group and the kosmotropic (hydrated) carboxyl group. As mentioned earlier, anions are known to affect protein stability more strongly than cations. Anions can more readily bind to the chaotropic amide group, whereas cations (regardless of hydration) will find it more difficult to bind to the carboxyl with its well-formed hydration shell.

Discussion

Our studies on small ion effects on protein stability reveal a number of protein and ion properties that strongly modulate protein-ion interactions. In the case of negatively charged apoflavodoxin, low concentrations of cations (≤ 250 mM) appear to affect protein stability through specific binding. Low concentrations of cations elicit significant increases in apoflavodoxin thermal equilibrium stability,

chemical equilibrium stability, and kinetic folding rates while decreasing unfolding rates. Both dependences of T_m values and ANS binding on cation concentrations have the appearance of binding curves that result in the calculation of qualitatively similar $K_{d,app}$ values (with Cs^+ occupying slightly different positions). The calculated $K_{d,app}$ values for the studied cations appear to correlate with ion hydration and thus with the Hofmeister series. While the studied cations do slightly increase the secondary structure of the folded state of apoflavodoxin (far-UV CD), the changes are small in comparison with those found for macromolecular crowding agents.

Correlation between cationic effects on apoflavodoxin stability and cation hydration suggests direct protein-ion interactions which was also suggested for the apoflavodoxin from *Anabaena* (Maldonado et al., 2002). However, the degree to which cations stabilize halophilic, *D. desulfuricans* apoflavodoxin is greater than the effects seen for *Anabaena* flavodoxin. This suggests that *D. desulfuricans* has evolved to take advantage of high intracellular cation concentrations. As mentioned before, previous studies had shown that low concentrations of Gdm^+ may elicit modest increases in protein stability (Bhuyan, 2002; Hagihara et al., 1993; Mayr and Schmid, 1993; Shukla et al., 2005). However, in the case of *D. desulfuricans* apoflavodoxin, we found that the addition of 250 mM Gdm^+ increased the thermal midpoint of apoflavodoxin by 20 °C and the free energy of unfolding increased 5-fold in the presence of 250 mM Gdm^+ .

As specific binding of cations appears to be the major factor effecting negatively charged apoflavodoxin stability at relatively low ion concentrations, we chose a positively charged protein (cytochrome c) along with apoflavodoxin to assess the effects of higher concentrations of ions on protein stability. We found that regardless of surface electrostatic potential, the effects of individual cations and anions in the tested range (300 mM – 1.75 M) were similar for both proteins. $dT_m/d[\text{ion}]$ values for both proteins correlated linearly with ion air/water partition coefficients for both cations (weakly) and anions (strongly). Analogously, $dT_m/d[\text{ion}]$ values correlated well with ion effects on surface tension and with anion charge density. However, $dT_m/d[\text{ion}]$ values did not correlate with cation charge density or with ion polarizability. The fact that both cations and anions have similar effects on oppositely charged proteins suggests that binding events between ions and peptide groups could be the dominant factor determining the effects of salts on protein stability. Direct ion-peptide bond interactions have been previously suggested for model amides (Bello et al., 1966; Nandi and Robinson, 1972b). Also, the chaotropic (dehydrated) nature of the amide moiety of the peptide group could explain the greater effects of anions on protein stability. Our results suggest that even at high ion concentrations where the effects of ions have been hypothesized to result from an altered hydrogen bonding network in the bulk, direct protein-ion interactions still play a major role in modulating protein stability.

CHAPTER 5: TIME-RESOLVED FOLDING MECHANISM OF APOFLAVODOXIN AND ROLE OF MACROMOLECULAR CROWDING

The results presented in this chapter include published material (Homouz et al., 2009) as well as unpublished material (Stagg, Samiotakis, Homouz, Cheung, and Wittung-Stafshede. (2009). *Residue specific analysis of frustration in folding landscape of repeat β/α protein apoflavodoxin* (in review)).

Assessing folding mechanism of apoflavodoxin

Numerous species of apoflavodoxin have been studied, and it has been found that most apoflavodoxins fold through a complex, non-two-state mechanism involving an off-pathway intermediate (Eq. 1.4). Previous studies on *D. desulfuricans* apoflavodoxin came to the same conclusion (Muralidhara et al., 2006). Conversely, equilibrium unfolding of apoflavodoxin has been found to be two-state at all the experimental conditions discussed here.

Effects of macromolecular crowding on folding of apoflavodoxin

My previous work with macromolecular crowding agents (Ficoll 70 and dextran 70) and apoflavodoxin showed that the effects of excluded volume acted to increase the amount of secondary structure in the folded state of apoflavodoxin as well as increasing thermal stability. In addition, macromolecular crowding agents increased the stability of apoflavodoxin against urea denaturation. In an effort to assess the effects of macromolecular crowding on the kinetic folding mechanism of apoflavodoxin, I used stopped-flow mixing in the presence and absence of macromolecular crowding agents.

In the reference buffer condition (10 mM HEPES, pH 7), apoflavodoxin displays a very modest free energy of unfolding by urea denaturation of only 4.4

kJ/mol. However, upon the additions of 150 mg/ml Ficoll 70 or dextran 70, the free energy of unfolding increases to 7.2 and 8.9 kJ/mol respectively (as calculated by CD at 222 nm) (Fig. 3.6). Analogously, using stopped-flow mixing, I found that apoflavodoxin exhibited a very modest folding rate in the reference buffer condition. However, upon the additions of Ficoll 70 and dextran 70 at final concentrations of 75 and 150 mg/ml, apoflavodoxin folding rates significantly increased (approximately 2.5 fold increase at 150 mg/ml crowding agent) (Fig. 5.1) (Table 5.1). Unfolding rates decreased upon the addition of crowding agents, but only slightly. These findings suggest that the increase observed in equilibrium stability of apoflavodoxin in the presence of macromolecular crowding agents is most attributable to speeding up the folding rate. Our observation of faster folding rates for apoflavodoxin in the presence of macromolecular crowding agrees with theory and experimental work (Cheung et al., 2005; van den Berg et al., 2000) and likely has its origin in the destabilized nature of the unfolded state due to crowding. Although $\Delta G_U(\text{H}_2\text{O})$ values calculated from kinetic rates do not agree exactly with those calculated from equilibrium experiments (disagreement is expected in this case as a result of the off-pathway intermediate), the increase in $\Delta G_U(\text{H}_2\text{O})$ values as a function of increased concentration of crowding agents in the kinetic experiments does agree qualitatively with the equilibrium data.

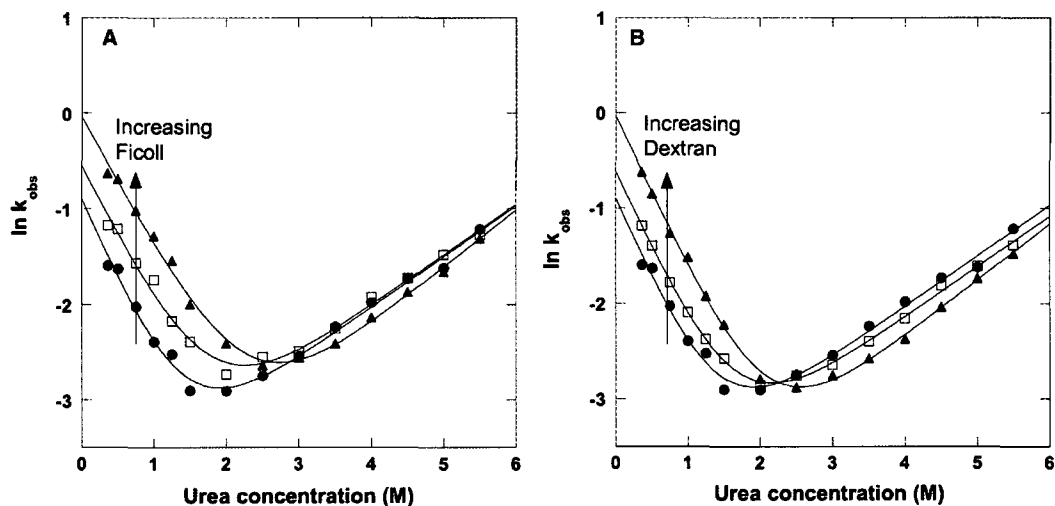


Figure 5.1 – Chevron plots of apoflavodoxin folding/unfolding monitored by CD signal at 222 nm in the presence of 0, 75, and 150 mg/ml Ficoll 70 (A) and dextran 70 (B) (10 mM HEPES, pH 7, 20 °C). Folding rates calculated from single exponential step occurring after burst phase. Figure adapted from Homouz et al. (2009).

Crowding Agent (mg/ml)	k_f (s ⁻¹)	k_u (s ⁻¹)
0	0.39 ± 0.02	0.016 ± 0.005
75 (Ficoll 70)	0.56 ± 0.02	0.016 ± 0.005
150 (Ficoll 70)	0.95 ± 0.02	0.010 ± 0.005
75 (dextran 70)	0.53 ± 0.02	0.014 ± 0.005
150 (dextran 70)	0.95 ± 0.02	0.009 ± 0.005

Table 5.1 – Folding and unfolding rates for apoflavodoxin in the presence and absence of various amounts of Ficoll 70 and dextran 70 calculated from fits to Chevron plots (10 mM HEPES, pH 7, 20 °C). Data for table from Homouz et al. (2009).

In vitro and in silico results suggest crowding agent geometry affects folding mechanism

Under the tested experimental conditions, I was able to observe (indirectly) the accumulation of the off-pathway intermediate in stopped-flow mixing experiments. The stopped-flow mixer has a dead-time of approximately a few milliseconds. In all cases, I observed missing amplitude in the dead-time of the experiment (suggesting a burst-phase intermediate) (Fig. 5.2). In short, this means that kinetic refolding traces do not start from the unfolded baseline amplitude at the zero time point. Instead, the kinetic folding traces start from a more negative CD signal. The simplest explanation in the case of an off-pathway intermediate is that the missing amplitude corresponds to the amount of secondary structure in the off-pathway intermediate. Conversely, the amount of missing amplitude could correspond to a mixture of different populations of structural states.

Interestingly, the amounts of missing amplitude calculated in the refolding phase of apoflavodoxin in the reference buffer condition and in the presence of 75 and 150 mg/ml Ficoll 70 were unchanged. In all of these cases, roughly 30 % of the expected amplitude was missing in the dead-time of the instrument. However, in the case of dextran 70, I found that about 75 % of the expected amplitude was missing in the dead-time of the instrument. This suggests that the shape of the crowding agent (Ficoll 70 is roughly spherical while dextran 70 is more rod-like) may have an effect on the folding mechanism of the protein.

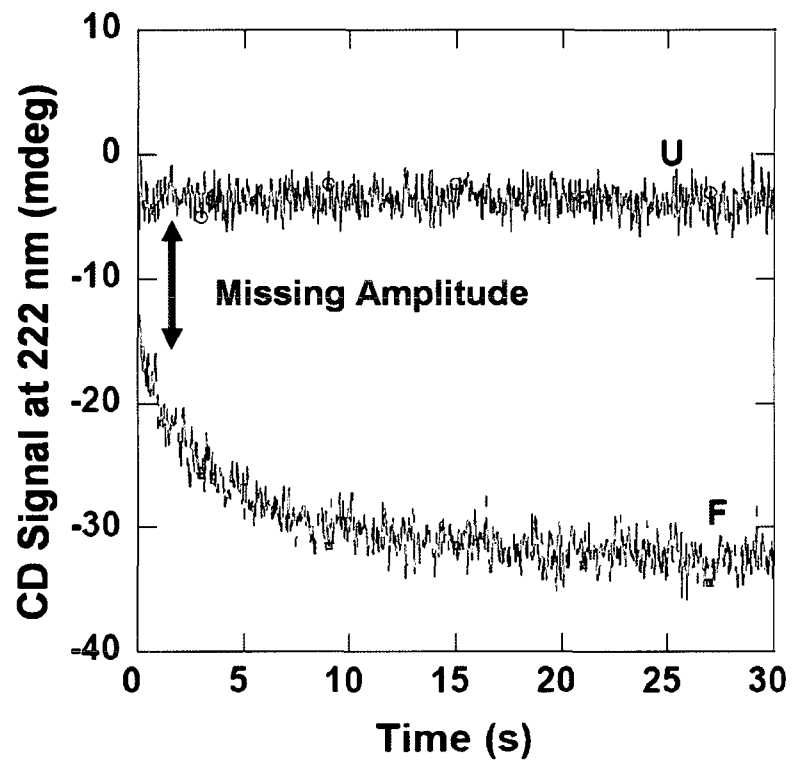


Figure 5.2 – Typical kinetic traces for apoflavodoxin unfolded baseline (black trace) and refolding (blue trace) showing missing amplitude (red arrow).

In order to gain more structural insight into the effects of crowding agents (and crowding agent geometry) on the folding mechanism of apoflavodoxin, we again collaborated with Dr. Margaret Cheung's group. Using coarse-grained models, Dr. Cheung and Dr. Dirar Homouz were able to simulate apoflavodoxin (with *D. vulgaris* apoflavodoxin; pdb:2fx2), Ficoll 70, and dextran 70 (as a dumb-bell shaped molecule). Using information from our previous collaboration, Drs. Cheung and Homouz chose to follow the evolution of native-like contacts for three structural elements of apoflavodoxin (β -strand 1, β -strand 3, and α -helix 1) along the reaction coordinate for the entire polypeptide. They found that the secondary structural elements of apoflavodoxin fold heterogeneously along a pathway with considerable topological frustration (especially in the early stages of folding; near the transition-state). In particular, native-like contacts in α -helix 1 form very early along the reaction coordinate. However, the individual strands in the central β -sheet compete for native contacts (Fig. 5.3).

In the buffer ($\phi_c = 0\%$) condition, native-like contacts in both β -strand 1 and β -strand 3 begin to form near the transition-state. However, in order for the entire polypeptide to continue along the reaction coordinate, β -strand 1 is forced to unfold while β -strand 3 continues to gain more structure. In the case of Ficoll 70 (at $\phi_c = 40\%$ with spherical crowders *in silico*), the folding pathway is very similar with only a slight change. In particular, β -strand 1 forms more native-like contacts near the transition state before unfolding and allowing β -strand 3 to gain structure. In the case of dextran 70 (at $\phi_c = 40\%$ with dumb-bell shaped

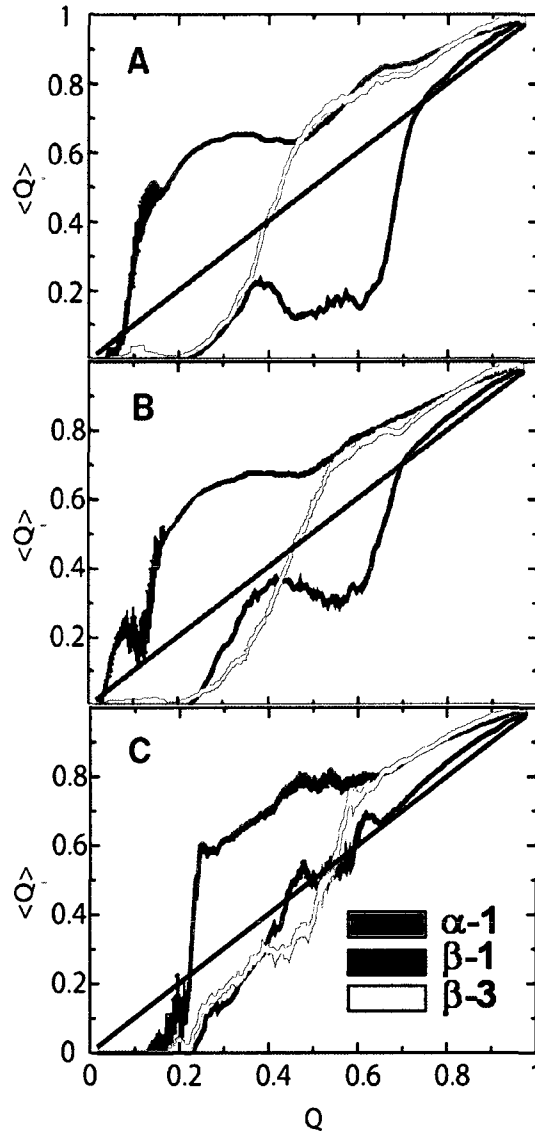


Figure 5.3 – Folding pathways of secondary structural elements of apoflavodoxin in buffer (A), 40 % spherical (Ficoll 70) crowding agents (B), and 40 % dumb-bell shaped (dextran 70) crowding agents (C) determined *in silico* where $\langle Q_i \rangle$ is the probability of forming native contacts in the secondary structural region of interest along Q (fraction of global native contacts). Folding of apoflavodoxin in bulk and 40 % Ficoll 70 appear similar with only slightly more early formation of β -1 in the case of Ficoll 70 (at $Q \approx 0.4$). Apoflavodoxin in 40 % dextran 70 appears to have more native-like contacts in unfolded state (Q starts at ~ 0.2) and folding in the β -sheet is relatively homogeneous for β -1 and β -3. Figure adapted from Homouz et al. (2009).

crowders *in silico*), the folding pathway is markedly different. In particular, β -strands 1 and 3 form native-like contacts homogeneously along the folding pathway instead of competing. Simulations also suggest that the unfolded state ensemble for apoflavodoxin in the presence of dextran 70 may start out with slightly more native-like contacts than the protein in buffer alone or in the presence of spherical crowding agents. This residual structure in the unfolded state could act as a scaffold from which to drive homogeneous folding.

Residue specific analysis of apoflavodoxin folding mechanism

Our previous work studying the apoflavodoxin folding mechanism along with information from other groups on the folding mechanisms of proteins adopting the flavodoxin-like fold (Bollen et al., 2004; Bueno et al., 2006; Hills and Brooks, 2008a; Hills and Brooks, 2008b; Kathuria et al., 2008; Melo et al., 2003) suggest that the α/β topology favors the formation of a misfolded, off-pathway species. The apparent ubiquitous nature of the folding mechanism of flavodoxin-like proteins leads to the suggestion that native-state topology may be the dominant factor in driving folding pathways. In order to gain more detailed information on the folding pathway of apoflavodoxin, I constructed a set of mutations (mostly hydrophobic-to-alanine) spanning the secondary structural elements of the protein in hopes of performing Φ -value analysis.

The mutations chosen for this study are Leu5Ala and Val7Ala (β -strand 1), Ala19Gly (α -helix 1), Val33Ala and Leu36Ala (β -strand 2), Val53Ala and Phe55Ala (β -strand 3), Leu74Ala (α -helix 2), Val88Ala (β -strand 4), Glu109Ala

(α -helix 3), Ile120Ala (β -strand 5), Leu124Ala (β -strand 5 / loop), and Val137Ala (α -helix 4) (Fig. 5.4). All chosen mutants are classical hydrophobic to hydrophobic mutations (with the exception of E109A), which are assumed to be “cavity forming” mutations that will not alter the energetics of the unfolded states of the variants relative to the wild-type protein. A number of other mutants were proposed for the study, however, the repeated presence of degradation fragments upon purification or non-native CD spectra made some mutants undesirable (Phe91Ala, Ile119Ala, and Ala141Gly). The native-like fold of all mutants was verified qualitatively by their ability to bind FMN and quantitatively by their native-like CD spectra (Fig. 5.5). Buffer conditions for the study of the mutants were chosen at 100 mM KPi, pH 7 after a number of the mutants lacked pre-transitional baselines in chemical equilibrium experiments in 20 mM KPi, pH 7.

In concert with my *in vitro* approach, Dr. Margaret Cheung (along with Dr. Dirar Homouz and Antonios Samiotakis) simulated each of the proposed mutants. Recently, Dr. Megan Guelker and Dr. Yousif Shamoo solved the structure of *Desulfovibrio desulfuricans* flavodoxin (pdb:3f6r) (Guelker et al., 2009) which folds to a very similar structure as *D. vulgaris* flavodoxin (pdb:2fx2) (Fig. 5.6). Although the crystal structure was solved with FMN coordinated, previous work has shown that the global fold of apoflavodoxin is conserved with the exception of more dynamics in the FMN-binding loops

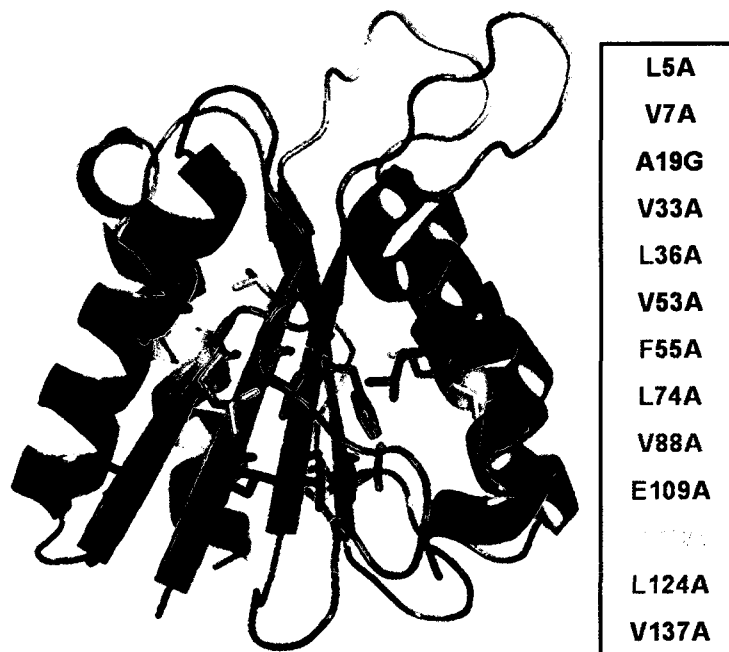


Figure 5.4 – Apoflavodoxin (3f6r) shown with positions of single point mutations (in stick) (PyMol).

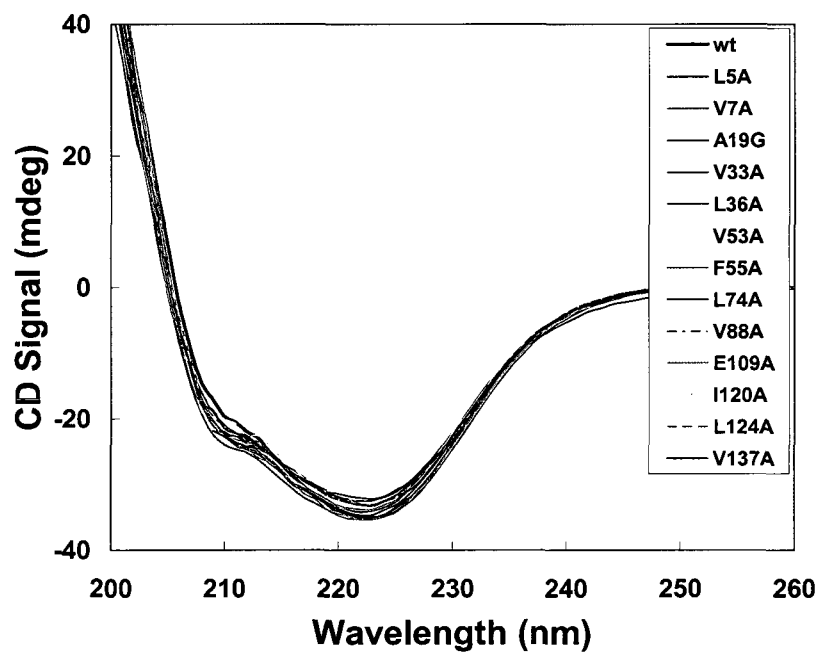


Figure 5.5 – CD spectra of wild-type and mutant apoflavodoxins (20 μ M protein, 100 mM KPi, pH 7, 20 $^{\circ}$ C).



Figure 5.6 – Crystal structure of *D. desulfuricans* flavodoxin solved by Drs. Megan Guelker and Yousif Shamoo (pdb:3f6r) (blue) and *D. vulgaris* flavodoxin (pdb:2fx2) (yellow). FMN cofactor shown in sticks (PyMol).

(Genzor et al., 1996; Steensma and van Mierlo, 1998). Previously, collaborative work done by Dr. Margaret Cheung's lab used *D. vulgaris* flavodoxin in their simulations. The structure provided by Dr. Guelker and Dr. Shamoo has made it possible to simulate the same species of flavodoxin used in my *in vitro* work.

Equilibrium studies of apoflavodoxin variants

As expected, each of the tested point mutants displayed lower thermal (Fig. 5.7) and chemical (Fig. 5.8) equilibrium stability relative to wild-type apoflavodoxin (Table 5.2), although the two-state nature of equilibrium unfolding appeared to be conserved across wild-type and all variants (as verified by overlapping CD and fluorescence data). At the tested buffer condition (100 mM KPi, pH 7), wild-type apoflavodoxin unfolded with a thermal midpoint of 67.8 °C (approximately 20 °C higher than in 10 mM HEPES, pH 7). The free energy of unfolding of wild-type apoflavodoxin was calculated to be 26.4 kJ/mol (compared to 4.4 kJ/mol in 10 mM HEPES, pH 7). These data were expected as apoflavodoxin stability is greatly modulated by ionic conditions (Sedlak et al., 2008a; Sedlak et al., 2008b). The two-state nature of thermal and chemical equilibrium unfolding of apoflavodoxin is further strengthened by the correlation of T_m values (calculated from thermal denaturation) and $\Delta G_U(H_2O)$ values (calculated from urea equilibrium unfolding) (Fig. 5.9).

In addition to lower $\Delta G_U(H_2O)$ values for some mutants calculated by urea equilibrium unfolding, it is also apparent that some mutants have lower m-values (broader slopes in transition regions). It is presumed that changes in m-values

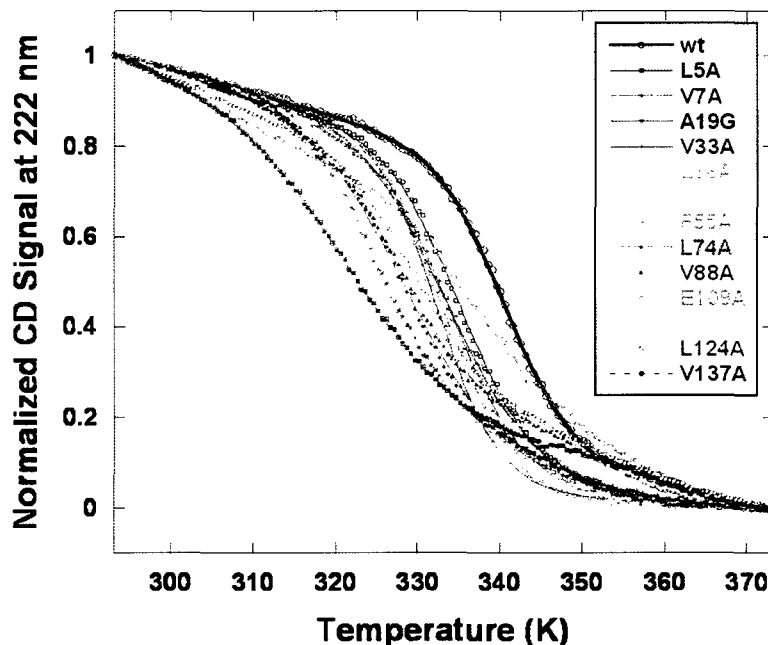


Figure 5.7 – Thermal denaturation of wild-type and mutant apoflavodoxins monitored by CD signal at 222 nm (100 mM KPi, pH 7).

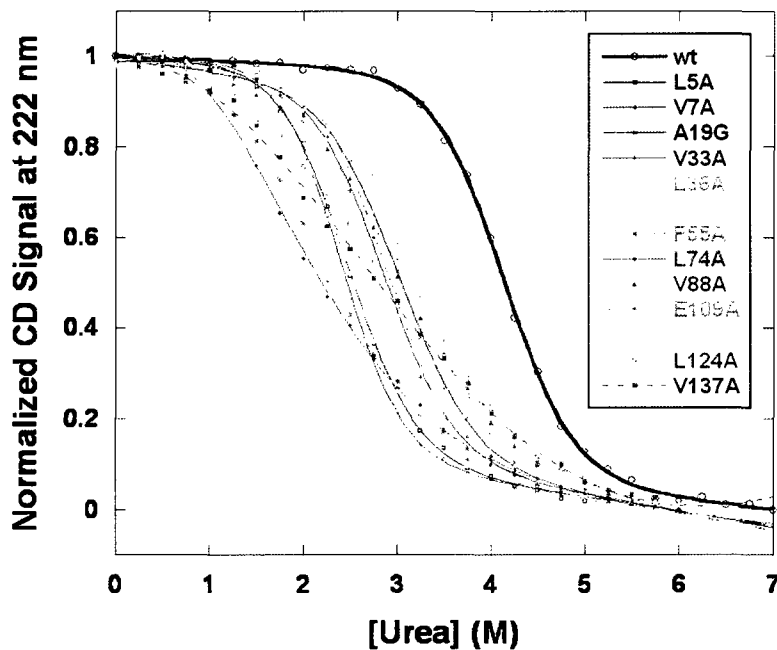


Figure 5.8 – Urea denaturation of wild-type and mutant apoflavodoxins monitored by CD signal at 222 nm (100 mM KPi, pH 7, 20 °C).

Variant	2° Structure	T _m (°C)	ΔG _U (H ₂ O) (kJ/mol)	m-value (kJ/mol,M)	[urea] _{1/2} (M)	T _f (K)
wt	-	67.8 ± 0.1	26.4 ± 1	6.2 ± 0.2	4.2	378.5
L5A	β1	62.7 ± 0.1	15.8 ± 0.7	6.5 ± 0.3	2.4	375.4
V7A	β1	59.6 ± 0.1	17.3 ± 0.6	7.3 ± 0.2	2.4	376
A19G	α1	60.9 ± 0.2	15.2 ± 1.1	5.0 ± 0.3	3.1	373
V33A	β2	61.7 ± 0.1	15.2 ± 0.9	5.3 ± 0.3	2.9	375.5
L36A	β2	60.3 ± 0.1	16.7 ± 0.9	5.7 ± 0.3	2.9	376
V53A	β3	55.7 ± 0.2	13.7 ± 1.5	5.4 ± 0.5	2.5	373
F55A	β3	52.2 ± 0.1	8.0 ± 0.8	3.6 ± 0.3	2.3	373
L74A	α2	56.4 ± 0.1	6.4 ± 1.0	3.1 ± 0.3	2.1	373.5
V88A	β4	54.4 ± 0.1	13.3 ± 0.9	4.5 ± 0.3	3.0	372
E109A	α3	66.7 ± 0.2	14.7 ± 1.7	4.7 ± 0.6	3.1	378.7
I120A	β5	49.1 ± 0.1	5.9 ± 0.9	2.3 ± 0.3	2.6	377
L124A	β5	57.2 ± 0.1	8.1 ± 1.0	2.8 ± 0.3	2.9	376.3
V137A	α4	49.3 ± 0.2	6.5 ± 1.1	2.4 ± 0.6	2.7	373

Table 5.2 – Equilibrium values for wild-type and mutant apoflavodoxins calculated from experiments monitoring CD (100 mM KPi, pH 7). T_f values calculated *in silico* by Cheung group. All errors reported are errors in fit.

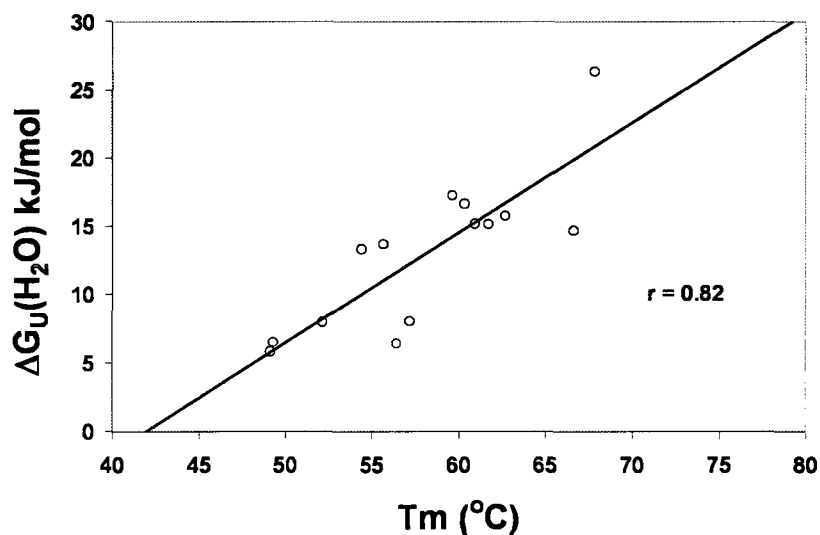


Figure 5.9 – Correlation between free energies of unfolding for wild-type and mutant apoflavodoxins (calculated by urea equilibrium unfolding monitored by CD signal at 222 nm, 20 °C) and thermal midpoints (monitoring CD signal at 222 nm, 100 mM KPi, pH 7).

for point mutants could mean that there is a change in the amount of exposed surface area between the native and unfolded states (Δ ASA) of these mutants relative to the Δ ASA of wild-type apoflavodoxin. It is difficult to say whether or not this is the case for the studied point mutants with very low m -values (L74A, I120A, L124A, and V137A), because each of these mutants have a native-like CD spectrum, and the conservative nature of the point mutations is not expected to alter unfolded state energetics. One explanation could be that the apparent two-state nature of the equilibrium unfolding is not conserved for these mutants (although CD and fluorescence data agree).

In vitro folding analysis of wild-type and mutant apoflavodoxins

In addition to equilibrium experiments, I subjected both wild-type and mutant apoflavodoxins to stopped-flow mixing experiments monitoring CD signal at 222 nm. Previous work done on this species of apoflavodoxin included fluorescence monitored stopped-flow kinetics (Apiyo and Wittung-Stafshede, 2002; Muralidhara et al., 2006). However, the intrinsic fluorophore of apoflavodoxin (Trp60) is situated in a relatively solvent-exposed, loop region of the protein even in the native state, so CD is a better measure of global folding and unfolding events. As seen before by other investigators as well as in my kinetic studies of apoflavodoxin in 10 mM HEPES, pH 7, I noted a sizeable amount of missing amplitude in the folding phase of apoflavodoxin in 100 mM KPi, pH 7 (see Fig. 5.2). After the initial burst phase with missing amplitude in the dead-time of the instrument (approximately a few milliseconds), wild-type and mutant

apoflavodoxins all folded productively with kinetic traces best described by single exponentials.

Semilogarithmic Chevron plots of wild-type and mutant apoflavodoxins were fit to extrapolate folding and unfolding arms back to the zero denaturant condition. All mutant apoflavodoxins (with the exception of E109A) fold slower than wild-type, and all mutant apoflavodoxins unfold faster than wild-type (Fig. 5.10) (Table 5.3). Our assessment of a non-two-state kinetic folding mechanism for apoflavodoxin is evident from the comparison of free energies calculated for wild-type and mutant apoflavodoxins from kinetic experiments ($\Delta G_{U(H_2O)}_{kin}$) versus free energies calculated from equilibrium experiments ($\Delta G_{U(H_2O)}_{eq}$) (Fig. 5.11). A linear correlation between the two sets of data for a true, two-state mechanism (both equilibrium and kinetic) would be expected to pass through the origin. Free energies were calculated for kinetic data as:

$$\Delta G_{U(H_2O)}_{kin} = -RT \ln(k_f^{H_2O} / k_u^{H_2O}) \quad (\text{Eq. 5.1})$$

where R is the gas constant, T is temperature, $k_f^{H_2O}$ and $k_u^{H_2O}$ are the folding and unfolding rates, respectively, extrapolated to zero denaturant from the Chevron plots.

The complicated nature of the folding mechanism makes the calculation of Φ_f values difficult. Folding rates calculated from raw data likely include contributions from the equilibrium between the unfolded state and the off-pathway intermediate. However, the kinetic experiments on wild-type and mutant

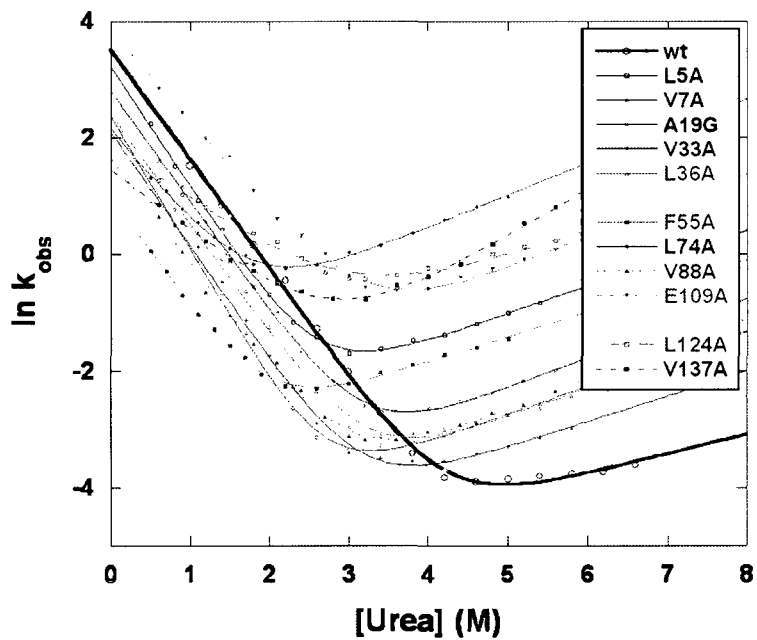


Figure 5.10 – Chevron plots of kinetic folding/unfolding of wild-type and mutant apoflavodoxins (100 mM KPi, pH 7, 20 °C). Folding rates calculated from single exponential step occurring after burst phase.

Variant	2° Structure	Burst amplitude (%)	$k_{f(\text{obs})}$ (s ⁻¹)	k_u (s ⁻¹)	$\Delta G_{U,\text{kin}}(\text{H}_2\text{O})$ (kJ/mol)	Φ_f	$ \eta_{\beta 1} - \eta_{\beta 4} $
wt	-	41.9	33.7 ± 3.8	0.0030 ± 0.001	22.7	-	1.88
L5A	β1	40.1	24.8 ± 1.2	0.0343 ± 0.004	16.0	0.44	0.59
V7A	β1	36.8	10.5 ± 0.9	0.0060 ± 0.001	18.2	0.82	2.44
A19G	α1	61.7	16.4 ± 1.0	0.0080 ± 0.001	18.6	0.79	3.96
V33A	β2	54.2	8.1 ± 0.9	0.0043 ± 0.001	18.4	0.92	3.67
L36A	β2	41.8	10.9 ± 1.1	0.0056 ± 0.002	18.5	0.85	1.57
V53A	β3	46.0	8.6 ± 0.6	0.0055 ± 0.001	17.9	0.88	3.99
F55A	β3	52.5	2.7 ± 0.1	0.0275 ± 0.003	11.2	0.71	4.01
L74A	α2	41.2	8.3 ± 0.5	0.1757 ± 0.02	9.4	0.50	5.36
V88A	β4	65.4	5.1 ± 0.4	0.0052 ± 0.001	16.8	0.90	7.86
E109A	α3	41.1	45.9 ± 2.9	0.0549 ± 0.01	16.4	0.39	3.44
I120A	β5	29.4	9.4 ± 0.5	0.0595 ± 0.01	12.3	0.65	1.89
L124A	β5	65.0	6.6 ± 0.7	0.1029 ± 0.03	10.2	0.53	6.34
V137A	α4	36.1	4.2 ± 0.2	0.0266 ± 0.003	12.3	0.73	2.45

Table 5.3 – Kinetic values for wild-type and mutant apoflavodoxins calculated from stopped-flow mixing experiments (100 mM KPi, pH 7, 20 °C). Φ -values calculated using unfolded rates as described in text. All errors reported are errors in fit. $\eta_{\beta 1}-\eta_{\beta 4}$ calculated as an absolute value from *in silico* work.

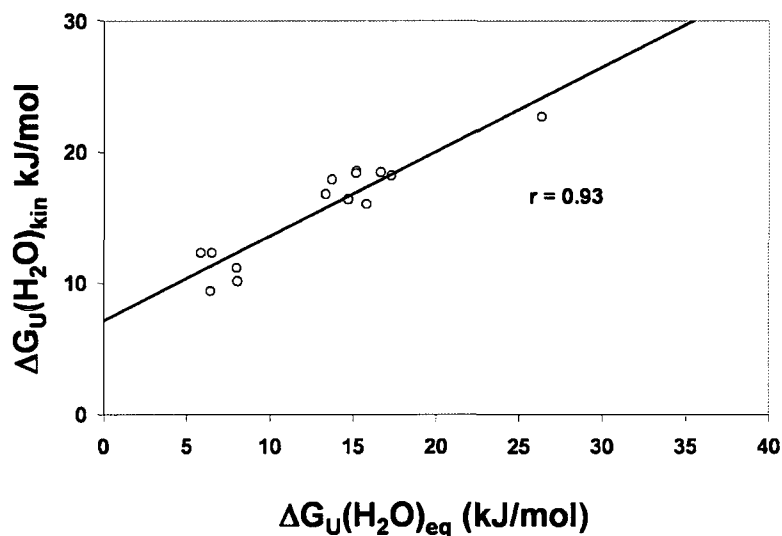


Figure 5.11 – Correlation between free energies of unfolding for wild-type and mutant apoflavodoxins determined by stopped-flow mixing experiments ($\Delta G_{U}(\text{H}_2\text{O})_{\text{kin}}$) and urea equilibrium unfolding experiments ($\Delta G_{U}(\text{H}_2\text{O})_{\text{eq}}$). Linear best-fit equation shown with correlation value.

apoflavodoxins were accompanied by a significantly lower amount of missing amplitude in the unfolding phase in comparison to refolding. This suggests that while the folding mechanism of apoflavodoxin may be complex with an off-pathway intermediate (and presumably an equilibrium between I_{off} and U), it is possible that the unfolding of the apoflavodoxins are two-state with the accumulation of only native and unfolded proteins. If this is the case, it is possible to calculate Φ_u values using unfolding rates as:

$$\Phi_u = [-RT \ln(k_{u,\text{wt}}^{\text{H}_2\text{O}} / k_{u,\text{mut}}^{\text{H}_2\text{O}}) / \Delta\Delta G_{\text{wt} \rightarrow \text{mut}}] \quad (\text{Eq. 5.2})$$

where $\Delta\Delta G_{\text{wt} \rightarrow \text{mut}}$ is the difference in free energies calculated for wild-type and each mutant apoflavodoxin using equilibrium data (as these are apparent two-state processes). Then using the simple relationship of $\Phi_f + \Phi_u = 1$, we can approximate Φ_f values. This approach has been employed previously for another species of apoflavodoxin (Bueno et al., 2006). Φ -values calculated in this manner provide information about the productive transition state between unfolded and folded states of proteins.

Using this approach, I calculated Φ_f values for each of the studied mutants. All of the calculated Φ_f values fell between approximately 0.4 and 0.9 suggesting fractional amounts of native-like contacts dispersed throughout the folding transition state of the protein (Table 5.3). The folding transition state of apoflavodoxin is thus most well described by a “diffuse” transition state. The only other study to date employing Φ -value analysis on an apoflavodoxin (*Anabaena* apoflavodoxin) came to a similar conclusion of a diffuse transition state (Bueno et

al., 2006). The highest Φ_f values calculated in our study were for V7A (β -strand 1), V33 (β -strand 2), L36A (β -strand 2), V53A (β -strand 3), and V88A (β -strand 4). This suggests that while there are at least fractional amounts of native-like interactions formed throughout the folding transition state of apoflavodoxin, the region consisting of the most native-like interactions is the central β -sheet (Fig. 5.12).

Interestingly, although all mutant apoflavodoxins fold via a burst-phase intermediate followed by a single exponential productive folding event, for a number of point mutants the amount of missing amplitude in the folding phase increased relative to wild-type apoflavodoxin. Although it is difficult to say whether this means these mutants (A19G, V33A, F55A, V88A, and L124A) have an increased amount of secondary structure in the burst-phase intermediate or the intermediate is similar in structure but populates to a greater degree, it is reasonable to suggest that the folding mechanism of these mutants could be altered. In order to gain residue-specific information about the folding mechanism of wild-type apoflavodoxin and each mutant, Dr. Cheung's group simulated all of the apoflavodoxins used in our *in vitro* studies.

Discussion

In silico data correlates with in vitro results

Using the newly solved structure of *D. desulfuricans* flavodoxin from the Shamoo lab (pdb:3f6r), Dr. Cheung's group simulated wild-type and each mutant

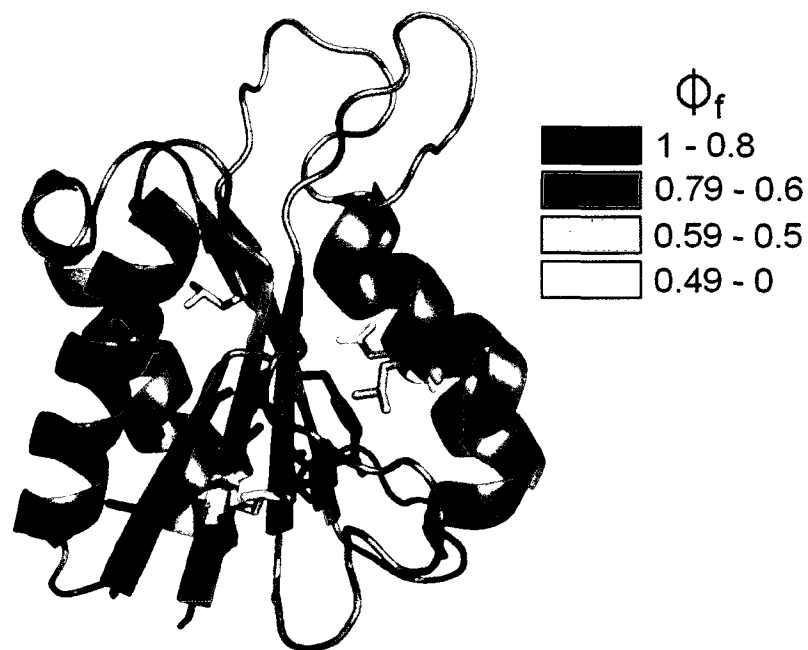


Figure 5.12 – Depiction of apoflavodoxin with sampled residues color-coded based on calculated Φ_f values (in decreasing order: purple, red, orange, yellow showing the primary role of the central, β -sheet in forming the folding transition state (PyMol). Refer to Table 5.3 for exact values.

apoflavodoxin using $C\alpha$ -SCM and Gō-like interactions as before. As a proof-of-principle experiment, the folding temperature (T_f) of each mutant was determined *in silico* (Table 5.2). The simulated T_f values agree well enough qualitatively with experimentally determined T_m values to suggest that Gō-like modeling would be sufficient to gather reliable folding information for the apoflavodoxin variants.

Similarly to our previous studies on the effects of macromolecular crowding on the folding pathway of apoflavodoxin, Dr. Cheung's group followed the evolution of specific secondary structural elements (signified by $\langle Q_i \rangle$; fraction of native-like contacts made by the region of interest) of apoflavodoxin along the reaction coordinate of folding for the entire polypeptide (signified by Q ; fraction of total native-like contacts formed with 1 being exactly like the crystal structure). If the folding process of the protein is homogeneous, the fractions of native contacts in each region of interest ($\langle Q_i \rangle$) will increase linearly with the gain of native-like contacts in the global fold (Q) roughly resembling a unity line. Conversely, deviations from homogeneous folding behavior can suggest topological frustration along the folding pathway. Previous simulations performed by Dr. Cheung (using the crystal structure of *D. vulgaris* flavodoxin) and Φ -values calculated from our *in vitro* data (the highest Φ -values are located in the β -sheet) on apoflavodoxin mutants suggested that the central β -sheet is key for global folding. As a result, Dr. Cheung's group focused on the evolution of native-like contacts formed in the central β -sheet (interactions between β -1 and β -2, β -1 and β -3, β -3 and β -4, and β -4 and β -5) for wild-type apoflavodoxin and all mutants.

Interestingly, what followed was the discovery that three types of folding routes were employed by wild-type and mutant apoflavodoxins (Fig. 5.13). The first of the folding routes of interest is the folding route employed by wild-type apoflavodoxin. Similar to the folding route determined for *D. vulgaris* apoflavodoxin *in silico* (Homouz et al., 2009), it is apparent that early contact formation in the β -sheet (especially by β -strands 1 and 2) causes topological frustration that necessitates the unfolding of those areas in favor of native-like contacts in β -strand 3 to form before a global folding event. This new data allows us to see that especially native-like contacts between β -strands 3 and 4 drive proper folding. Along with wild-type apoflavodoxin, other studied mutants (L5A, V7A, L36A, V53A, L74A, E109A, I120A, and V137A) undergo similar folding events. In addition, the similar folding pathway for *D. desulfuricans* (simulated using pdb:3f6r) and *D. vulgaris* (simulated previously using pdb:2fx2) apoflavodoxins is an excellent proof of principle for earlier simulations relating *D. vulgaris* apoflavodoxin data *in silico* to *D. desulfuricans* data *in vitro* (Homouz et al., 2009; Stagg et al., 2007).

The second folding route employed by an apoflavodoxin variant is that of V33A (β -strand 2) apoflavodoxin. In this unique folding route, early contact formation between β -strands 3 and 4 is evident without the early topological frustration seen in β -strand 1 for wild-type apoflavodoxin. Interestingly, the other

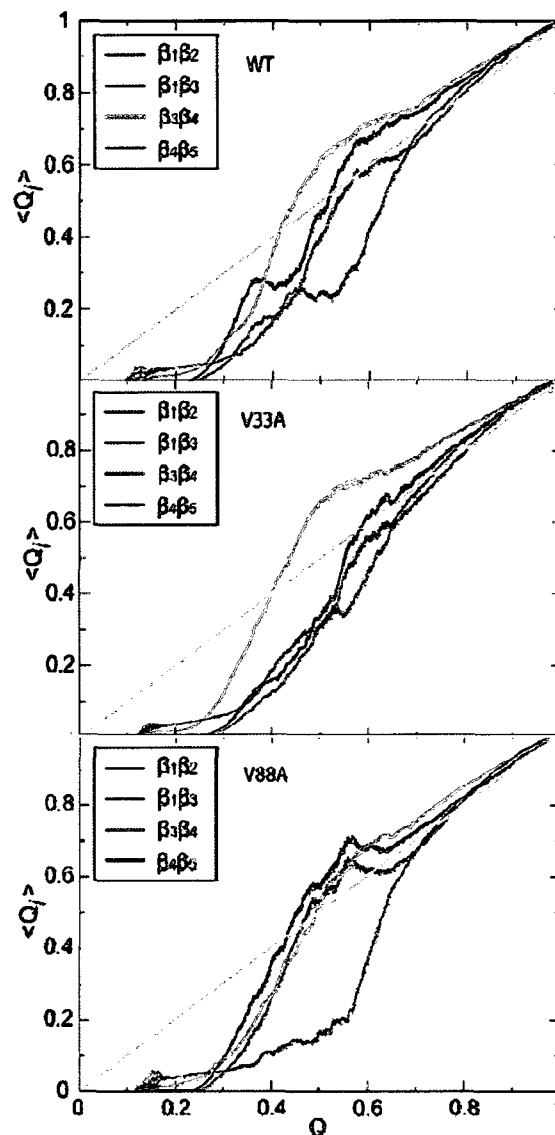


Figure 5.13 – Three unique folding mechanisms for wild-type and mutant apoflavodoxins represented by wild-type (top panel), V33A (middle panel), and V88A (bottom panel). Individual colors represent formation of native-like contacts between specified β -strands.

β -strands seem relatively unformed throughout the transition state region (approximately $Q = 0.4$). The other native-like contacts in the central β -sheet proceed rather homogeneously toward global folding. We believe the V33A mutation causes a loss in β -1 and β -2 contacts which drives folding through β -3 contacts.

The third unique folding route is that employed by V88A apoflavodoxin (also A19G, F55A, and L124A). Similarly to the other two folding routes, native-like contacts form relatively early in β -strands 3 and 4. However, in this folding route, native-like contacts also form between strands 1 and 2 and between strands 1 and 3 simultaneously with contacts between strands 3 and 4. Only native-like contacts between β -strands 4 and 5 lag behind to be formed last.

The similarities in the evolution of native-like contacts formed in the secondary structural elements of *D. vulgaris* apoflavodoxin (Fig. 5.3) (Homouz et al., 2009) and wild-type *D. desulfuricans* apoflavodoxin (Fig. 5.13) (46 % sequence identity) suggest it may be possible to propose a model for the gain of structure over productive folding for proteins adopting the flavodoxin-like fold. However, the significant differences in the interplay of the individual β -strands in *D. desulfuricans* apoflavodoxin as a result of single, conservative point mutations (Fig. 5.13) suggests that even minor changes to the primary sequence can significantly alter the folding pathway. Therefore, attempts to suggest a folding

mechanism for a flavodoxin-like protein based entirely off of its structural similarity to *D. desulfuricans* or *D. vulgaris* apoflavodoxin may be unreasonable.

Competing nuclei in central β -sheet drive apoflavodoxin folding

The elucidation of the folding pathways of wild-type and mutant apoflavodoxins suggests that the driving force behind productive folding lies in the interplay between the β -strands making up apoflavodoxin's central, parallel β -sheet. While some of the mutants display wild-type-like folding pathways, other mutants (especially V33A and V88A) fold through different mechanisms involving slightly different interactions forming in the β -sheet. Taking together *in vitro* and *in silico* data, we began to think about the possibility that there are similar reasons for differences in the amount of missing amplitude in refolding kinetics and divergent folding pathways *in silico*.

The unique folding pathways observed for wild-type and some apoflavodoxin mutants resulting from characteristic sequences of native-like contact evolution in the central β -sheet led us to evaluate the possibility of competing folding nuclei in the sheet (which we also found for *D. vulgaris* apoflavodoxin; (Homouz et al., 2009)). Whereas *in vitro* data lacks the resolution to get at such information, simulations do allow for the calculation of native-like contacts in specific regions of apoflavodoxin at any point in the folding reaction coordinate. In our case, Dr. Cheung's group assessed the native-like contacts formed by apoflavodoxin at $Q = 0.3 - 0.5$, a point near the folding-transition state (roughly correlating to occurrences in the dead-time of *in vitro* sampling). What followed was the

elucidation of two major folding nuclei in the central β -sheet of apoflavodoxin. The two folding nuclei are centered around residue 6 (Ile) of β -strand 1 and residue 90 (Ala) of β -strand 4 (Fig. 5.14). Ile6 and Ala90 were chosen as they were the residues near the center of the two folding nuclei that had fulfilled the most native-like contacts.

By calculating the number of native-like contacts formed in each folding nucleus ($n_{\beta 1}$ and $n_{\beta 4}$) at specific points (relative to Q) in the folding reaction coordinates of wild-type and mutant apoflavodoxins, it was possible to gain insight into the competition of the folding nuclei in each unique folding pathway. Interestingly, we found that $|n_{\beta 1} - n_{\beta 4}|$ (the difference between the number of native-like contacts formed between the two folding nuclei) values calculated for wild-type and mutant apoflavodoxins correlated with the amount of missing amplitude detected in refolding by *in vitro* stopped-flow mixing experiments (Fig. 5.15). For mutants like V33A and V88A where unique folding pathways were observed (presumably a result of the loss of essential interactions made by the native side-chains), $|n_{\beta 1} - n_{\beta 4}|$ values are relatively high suggesting that one folding nucleus dominates over the other. These mutants have larger amounts of missing amplitude in folding experiments. For the wild-type folding pathway, where individual β -strand interactions form rather heterogeneously over the global evolution of Q, the two folding nuclei gain native-like contacts at relatively similar rates. These proteins (wild-type and some variants) have lower amounts

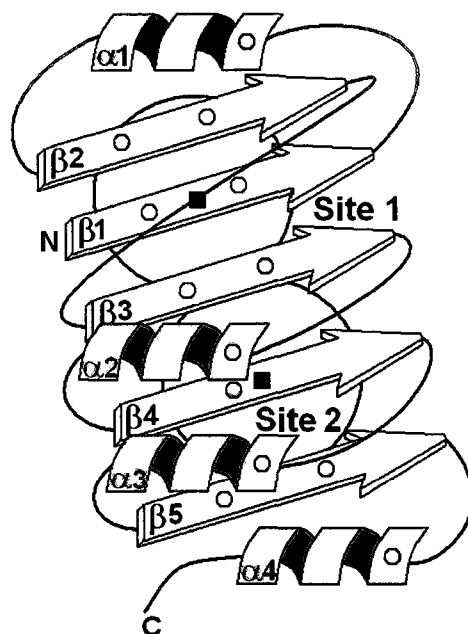


Figure 5.14 – Cartoon depiction of the two proposed folding nuclei (grey spheres) of apoflavodoxin. The centers of the two folding nuclei (Ile6 and Ala90) are shown as black squares, residues with lesser amounts of missing amplitudes ($\leq 50\%$) are shown as white circles, and residues with greater amounts of missing amplitudes ($> 50\%$) are shown as red circles. Refer to Table 5.3 for exact values.

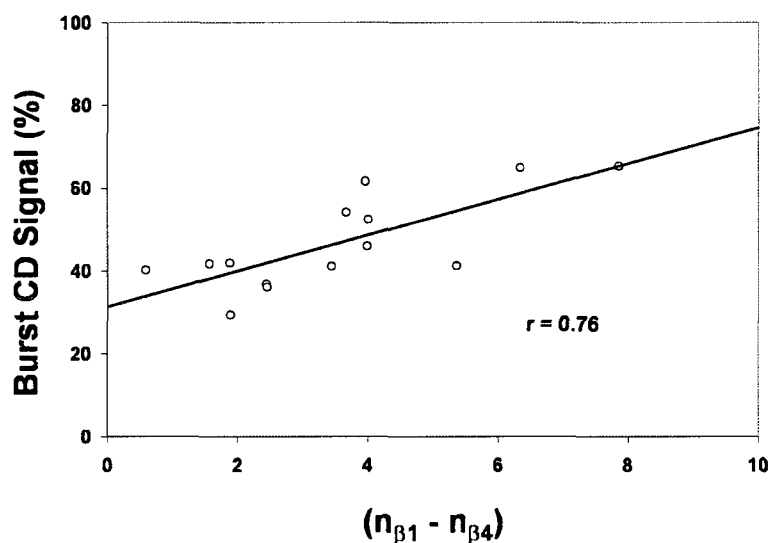


Figure 5.15 – Correlation between % missing amplitude calculated for wild-type and mutant apoflavodoxins (stopped-flow mixing experiments) and disparity in the size of the two competing folding nuclei ($n_{\beta 1} - n_{\beta 4}$; calculated as an absolute value from *in silico* work). Refer to Table 5.3 for exact values.

of missing amplitudes in folding experiments. This suggests that favoring one nucleation site over the other (regardless of which site) promotes early misfolding and thus there is an increase in the amount of missing amplitude in stopped-flow mixing experiments.

Summary

Kinetic experiments using wild-type apoflavodoxin in the presence and absence of spherical Ficoll 70 and rod-like dextran 70 demonstrate that macromolecular crowding increases the folding rate of the protein at the studied concentration of crowding agent (150 mg/ml) by nearly 3-fold which is in agreement with theory and experimental work (Cheung et al., 2005; van den Berg et al., 2000). The presence of a burst-phase intermediate (assumed off-pathway) in the folding mechanism of apoflavodoxin which corresponded roughly to the dead-time of the stopped-flow mixer (about a few milliseconds) allowed us to indirectly probe the population of the intermediate species in the presence and absence of crowding agents. What we found was that the percentage of missing amplitude in the folding phase of apoflavodoxin was unchanged in buffer alone and in the presence of Ficoll 70 (about 30 %). However, for apoflavodoxin folding in the presence of dextran 70, this percentage jumped to approximately 75 %.

In silico work performed by the Cheung group using *D. vulgaris* flavodoxin as a model of *D. desulfuricans* apoflavodoxin corroborated our *in vitro* work. By simulating the formation of native-like contacts in three secondary structural

regions (α -1, β -1, and β -3) over the evolution of global folding, it was found that apoflavodoxin folds via a heterogeneous pathway with ample topological frustration. This heterogeneous folding pathway with topological frustration agrees with work suggesting that members of the flavodoxin-like fold family fold through multiple pathways and often populate misfolded structures that must unfold before productive folding (Bollen and van Mierlo, 2005). In the cases of apoflavodoxin in buffer and in volume occupied by spherical crowding agents (simulating Ficoll 70), the folding pathway of apoflavodoxin was only slightly changed with more native contacts formed in β -1 near $Q = 0.4$ before unfolding in favor of native-like contacts in β -3. This small change is likely due to compaction of the unfolded state into a more prolate conformation favoring local interactions in β 1. However, in the presence of dumb-bell shaped crowding agents (simulating dextran 70), the folding pathway underwent large changes. First, the unfolded ensemble appeared to have more native-like structure. In addition, the topological frustration seen in the early stages of apoflavodoxin in buffer and with spherical crowding agents effectively disappeared as β -1 and β -3 formed relatively homogeneously over the global evolution of Q . The agreement of *in vitro* and *in silico* work suggests that at least in the case of apoflavodoxin, the geometry of crowding agent strongly modulates the folding pathway of the protein. These findings agree with the theoretical hypothesis of Minton who posed that the geometrical shapes of crowding agents may modulate their effects on protein stability (Minton, 1981).

In order to gain residue specific information on the folding mechanism of apoflavodoxin, I constructed a set of 13 point mutants (L5A, V7A, A19G, V33A, L36A, V53A, F55A, L74A, V88A, E109A, I120A, L124A, and V137A) spanning the secondary structural elements of the protein. All the studied mutants displayed a characteristic wild-type-like native CD spectrum and had lower equilibrium stabilities measured by thermal and chemical equilibrium. The studied equilibrium transitions are apparent two-state reactions as reported previously (Apiyo and Wittung-Stafshede, 2002; Perham et al., 2007; Sedlak et al., 2008b; Stagg et al., 2007), although it should be noted that native-like intermediates have been suggested to populate (Muralidhara and Wittung-Stafshede, 2004; Muralidhara and Wittung-Stafshede, 2005). Therefore it is possible that some of the mutants with particularly low equilibrium m -values (L74A, I120A, L124A, and V137A) could unfold via a more complex mechanism at the studied conditions although CD and fluorescence data are in agreement.

Time-resolved folding experiments on wild-type and mutant apoflavodoxins all resulted in the appearance of a significant amount of missing amplitude suggesting a burst-phase intermediate. A number of the studied variants had higher than expected burst-phase amplitudes relative to wild-type (calculated by % missing amplitude in the folding phase). An off-pathway intermediate has been proposed previously for proteins with the flavodoxin-like fold (multiple apoflavodoxins, CheY, and Spo0F) (Apiyo and Wittung-Stafshede, 2002; Bollen et al., 2004; Bueno et al., 2006; Hills and Brooks, 2008a; Hills and Brooks,

2008b; Homouz et al., 2009; Kathuria et al., 2008; Melo et al., 2003; Muralidhara et al., 2006). Taken together with the fact that TIM barrel proteins (another β/α repeat superfamily) also have been found to fold via a mechanism with an off-pathway intermediate (Forsyth et al., 2007; Gu et al., 2007; Wu et al., 2007), this strongly suggests that the native-state topology of the α/β parallel motif is prone to early misfolding. I note that our *in vitro* data does not verify that the burst-phase intermediate is off-pathway. However, the off-pathway nature of the intermediate previously has been argued for *D. desulfuricans* apoflavodoxin (Apiyo and Wittung-Stafshede, 2002) as well as for other members of the flavodoxin-like fold. In addition, computational data both on *D. vulgaris* apoflavodoxin (Homouz et al., 2009) and the current work suggest significant topological frustration early in the folding landscape presumably leading to misfolding.

Φ -values were calculated for each variant using unfolding rates and ranged from $\Phi_f \approx 0.4 - 0.9$ suggesting a diffuse transition state. The area of the protein with the highest Φ -values was the central, β -sheet suggesting the core of the protein is well-formed in the transition state. Similar work undertaken using the apoflavodoxin from *Anabaena* came to the conclusion of a diffuse transition state, however, it was concluded that the transition state was stabilized significantly by packing of three α -helices toward β -strands 3 and 4 (Bueno et al., 2006). Stating conclusively whether or not the transition state structures of *D. desulfuricans* and *Anabaena* apoflavodoxins are appreciably dissimilar is

impossible at this point mostly due to the lack of point mutations in the α -helices of *D. desulfuricans* apoflavodoxin. In contrast to the diffuse transition states of the two apoflavodoxins, the transition state of CheY has been proposed to be polarized with native-like interactions forming in the N-terminus of the central, β -sheet, but with the C-terminal region of the β -sheet remaining largely unstructured (Lopez-Hernandez and Serrano, 1996). It appears that although proteins adopting the flavodoxin-like fold may be prone to early misfolding events (off-pathway intermediates), the productive folding transition state may vary widely among the members of the superfamily as previously predicted (Bueno et al., 2006).

Folding pathways assessed by the Cheung group *in silico* revealed three unique mechanisms employed by the apoflavodoxin variants. While the wild-type folding pathway agreed very closely with that determined previously by the Cheung group for *D. vulgaris* apoflavodoxin, some of the variant apoflavodoxins (in particular V33A and V88A) employed different folding mechanisms presumably dependent upon the loss of interactions due to mutation. The heterogeneity of the folding routes of the variant apoflavodoxins along with the observation of varying amounts of missing amplitudes *in vitro* experiments led us to explore the possibility of two competing folding nuclei in the central, β -sheet. The existence of multiple folding nuclei has been proposed for larger proteins often based on geometrical factors in the native state (Norcross and Yeates, 2006) and was previously found to be the case for *D. vulgaris* apoflavodoxin

(Homouz et al., 2009). For *D. desulfuricans* apoflavodoxin, simulation data suggests one nucleus containing β -1, β -2, and β -3 centered around Ile6 and another nucleus containing β -3, β -4, and β -5 centered around Ala 90 compete for native contacts along the folding reaction coordinate. Interestingly, we found that when strong biases occurred for native-like contacts in one folding nucleus over the other in the folding reactions of variant apoflavodoxins *in silico*, these same mutants displayed greater amounts of missing amplitude in the burst-phase *in vitro*. This suggests that the dominance of one of the competing folding nuclei over the other can lead to increased topological frustration (manifesting in more structure in the burst-phase intermediate). Similarly, recent *in vitro* and *in silico* work done on CheY revealed that native-like contacts near the interface of the two proposed folding nuclei impeded the formation of the proper folding transition state and resulted in a misfolded structure that necessitated unfolding in order for continuing down a productive folding pathway (Hills and Brooks, 2008b; Kathuria et al., 2008) although no variant CheY proteins were studied. To our knowledge, our work is the first time that a connection between topological frustration, competing folding nuclei, and *in vitro* measurements has been clearly made to assess heterogeneity in the early folding events of a protein.

In order to investigate the correlation made between disparity in the sizes of the competing folding nuclei in apoflavodoxin variants ($n\beta_1$ and $n\beta_4$) and the appearance of greater amounts of burst-phase intermediate in time-resolved *in vitro* experiments, Dr. Cheung's group revisited their previous simulations of

apoflavodoxin folding in the presence of dumb-bell shaped crowding agents (simulating dextran 70). Previously, I found that apoflavodoxin folding in the presence of dextran 70 *in vitro* proceeded with a much greater amount of structure in the burst-phase intermediate (demonstrated by significantly increased missing amplitude in the folding kinetics). *In silico* results showed that the presence of crowding agents mimicking dextran 70 greatly altered the folding pathway of apoflavodoxin. Dr. Cheung's group has re-analyzed the original data and found that in the presence of crowding agents mimicking dextran 70, native-like contacts in folding nucleus 2 of apoflavodoxin ($n\beta_4$) was strongly favored over folding nucleus 1. This provides more evidence that in the case of apoflavodoxin, strong bias toward one folding nucleus or the other in early phases of folding leads to formation of the off-pathway intermediate (and thus greater missing amplitude *in vitro*). This also suggests that the folding mechanism of apoflavodoxin *in vivo* may be strongly modulated by macromolecular crowding.

CHAPTER 6: SUMMARY, OVERALL PERSPECTIVE, AND FUTURE DIRECTION

In vitro data suggests intracellular conditions significantly modify properties of apoflavodoxin

Using synthetic crowding agents (Ficoll 70 and dextran 70) and a range of small ions in concentrations similar to those found in the intracellular milieu, we have shown that the biophysical properties of apoflavodoxin can be significantly altered relative to in dilute buffer conditions. In short, we have shown that both macromolecular crowding and small ions (a) greatly increase the thermal midpoint of apoflavodoxin (in certain cases by greater than 25 °C), (b) increase the free energy of unfolding of apoflavodoxin (amount is buffer dependent in case of crowding), (c) increase the amount of secondary structural content in the folded protein, (d) increase the folding rate of the productive folding step of apoflavodoxin, and (e) may alter the folding mechanism of apoflavodoxin, specifically the accumulation of an off-pathway burst-phase intermediate.

Effects of macromolecular crowding on apoflavodoxin properties: proposed mechanism, discussion of current crowding theory, and implications for the future

The effects of macromolecular crowding and thus excluded volume on the structure and stability of apoflavodoxin are numerous and significant. Our *in vitro* data in conjunction with collaborative *in silico* work done by Dr. Margaret Cheung's group has added to, and in some cases changed, the way that protein biophysicists view the contributions of the crowded nature of the cell to protein properties.

One well-accepted, prevailing crowding theory suggests that crowding should increase the stability of folded proteins only indirectly through entropically disfavoring the unfolded state (Minton, 2005b; Zhou, 2004; Zimmerman and Minton, 1993). Therefore, equilibrium values assessing protein stability such as thermal midpoint and free energies of unfolding for proteins in crowded environments should increase relative to the protein in buffer. Minton theorized that increases in thermal midpoints for proteins under crowded conditions relative to in dilute solutions should be on the order of 5 to 20 °C (Minton, 2000a). Previous experimental studies noted moderate increases to thermal midpoints (≤ 5 °C) of studied proteins as a function of increased macromolecular crowding (Hall and Dobson, 2006; Sasahara et al., 2003; Tellam et al., 1983). In contrast to these moderate increases in thermal stability, the thermal midpoint of apoflavodoxin increased dramatically in the presence of 400 mg/ml Ficoll 70 ($\sim + 20$ °C) and dextran 70 ($\sim + 26$ °C) relative to in buffer alone (10 mM HEPES, pH 7). Simulations suggest that the free energy of unfolding for the model WW domain should increase approximately 4.6 kJ/mol at $\phi = 25$ % (Cheung et al., 2005). In agreement with theory, another recent experimental study shows that the free energy of VlsE increases by approximately 5 kJ/mol in the presence of 100 mg/ml Ficoll 70 (Homouz et al., 2008), the free energy of FK506-binding protein was found to increase upon the addition of 160 mg/ml dextran (Spencer et al., 2005), and I also found that the free energy of unfolding of apoflavodoxin increased by 3 – 4 kJ/mol upon the addition of both Ficoll 70 and dextran 70 (10 mM HEPES, pH 7, 20 °C).

Also in agreement with crowding theory, compaction of the unfolded (or disordered) states of proteins has been noted for a variety of proteins by numerous methods. GdmCl-unfolded RNase A has been found to spontaneously refold (as verified by CD, enzyme activity, and measurement of hydrodynamic radius) by the addition of either Ficoll 70 or PEG (Tokuriki et al., 2004). FRET studies on adenylate kinase suggest that partially GdmCl-unfolded protein is compacted in the presence of dextran (Ittah et al., 2004). NMR studies on the intrinsically disordered protein FlgM have shown that crowding can induce spontaneous folding (Dedmon et al., 2002). However, another study has shown that in the case of two intrinsically disordered human protein domains, macromolecular crowding does not induce spontaneous folding (Flaugh and Lumb, 2001). Studies on the unfolded state of VlsE have shown large global changes to the unfolded state of the protein in the presence of crowding agents (Homouz et al., 2008). Our *in vitro* results are ambiguous towards the effects of macromolecular crowding on the unfolded state of apoflavodoxin. In the presence of either Ficoll 70 or dextran 70, the thermally unfolded CD signal of apo- and holoflavodoxin increases, but the shape of the spectrum still appears unfolded. This could potentially mean that the protein is gaining local structure, but the protein is still globally unfolded. In contrast, the secondary structural content of GdmCl-unfolded apo- and holoflavodoxin does not change as monitored by CD in the presence of either Ficoll 70 or dextran 70. The ambiguity of the effects of macromolecular crowding on thermally or chemically unfolded

protein as well as on intrinsically disordered proteins suggests that crowding does not elicit compaction events resulting in proper (or improper) folding in all cases.

Contrary to the theory that crowding affects only the unfolded states of proteins, we have found that for apoflavodoxin, holoflavodoxin, and VisE (Perham et al., 2007), the secondary structural content of the folded states of the proteins increase in the presence of macromolecular crowding. Other unpublished studies in our lab have shown similar results for *Pseudomonas aeruginosa* azurin and horse heart myoglobin. In the cases of apo- and holoflavodoxin, structural prediction algorithms have suggested that crowding increases the amount of α -helical content of the folded proteins while reducing the amount of random coil regions. Predicted secondary structural content of apo- and holoflavodoxin in 400 mg/ml Ficoll 70 closely resembles that of the crystal structure. *In silico* work done by the Cheung group shows that the folded state ensemble of apoflavodoxin gains native-like contacts between α -helices and the central β -sheet, and the protein becomes more compact (in terms of R_g) as a function of increased crowding. Our work suggests that macromolecular crowding affects both the unfolded and native states of proteins. Although not widely accepted, other theory suggests that in the case of large macromolecular crowders, the folded state may directly be stabilized (Hu et al., 2007).

The entropically disfavored unfolded state of proteins in the presence of macromolecular crowding is suggested by theory to result in increases in protein folding rates (Cheung et al., 2005). As expected, experimentalists have shown increases in protein folding rates in the presence of macromolecular crowding in the cases of hen lysozyme (van den Berg et al., 2000) monitored by enzyme activity, apocytochrome b_{562} (Ai et al., 2006) as monitored by NMR spin-relaxation, and VlsE (Homouz et al., 2008) as monitored by stopped-flow mixing. In agreement with these data, I have shown that apoflavodoxin folding rates increase 2 – 3 fold in the presence of 150 mg/ml Ficoll 70 or dextran 70 as monitored by stopped-flow mixing (10 mM HEPES, pH 7, 20 °C). In addition to increases in folding rates, we also found that the presence of dextran 70 (much more so than Ficoll 70) significantly altered the folding mechanism of apoflavodoxin. Minton has postulated that crowding agent geometry may in fact affect the degree of protein stability (Minton, 1981), and our data appears to agree. Both *in vitro* stopped-flow mixing experiments showing an increase in the structure of the off-pathway burst-phase intermediate and *in silico* work showing a change in the heterogeneity of apoflavodoxin folding as a result of the presence of dumb-bell shaped crowding agents demonstrate that crowding agent geometry affects the folding mechanism of apoflavodoxin.

Taken together, our data (both *in vitro* and *in silico*) assessing the effects of macromolecular crowding on apoflavodoxin structure, stability, and folding mechanism suggests that excluded volume due to macromolecular crowding

affects both folded and unfolded protein ensembles. In addition, we have shown that crowding agent geometry can affect local structure in the unfolded state (*in silico* results on apoflavodoxin and spherical crowding agents) as well as modulating the heterogeneity of the folding pathway and the appearance of folding intermediates (dumb-bell shaped crowding agents, dextran 70). Our data in conjunction with other theoretical and experimental efforts focusing on the effects of crowding on protein structure, stability, folding rates, diffusion, and activity strongly suggest that typical *in vitro* experiments may fall short of characterizing proteins relative to their *in vivo* environments.

Effects of Hofmeister ions on apoflavodoxin (and cytochrome c) stability: proposed mechanisms for ion-induced protein stability

The Hofmeister series of ions, although formed in 1888 to explain the effects of various salts on protein solubility (Hofmeister, 1888), has been found to hold true for the effects of ions on protein stability, especially in the cases of anions (Baldwin, 1996; Goto and Aimoto, 1991; Goto et al., 1990; Ramos and Baldwin, 2002). As anions have been found to more strongly affect protein properties than cations, less is known about the Hofmeister effects of cations on proteins (Pace and Grimsley, 1988; Richard et al., 2006). Although the most prevalent theory for the ordering of Hofmeister ions suggests that the ions indirectly affect proteins through affecting the hydrogen-bonding network of bulk water (Baldwin, 1996), recent studies using multiple techniques suggest that ionic effects on water structure extend only as far as the first hydration shell of the ion (Batchelor et al., 2004; Naslund et al., 2005; Omta et al., 2003).

Our work using *D. desulfuricans* apoflavodoxin as a model protein for studying small (chloride) cations showed that at least in the case of this acidic protein, even relatively low amounts (≤ 250 mM) of cations can elicit significant increases in protein stability (T_m increases more than 20 °C and $\Delta G_U(H_2O)$ increases 5-fold). Prior work on another apoflavodoxin (from *Anabaena*) also reported cation-induced increases in protein stability (albeit much more modest than for *D. desulfuricans* apoflavodoxin) and suggested ionic screening of repulsive surface charges as being the primary origin of increased protein stability (Maldonado et al., 2002). Neutralization of negative surface charges has been proposed to be the major mechanism for the stabilization of proteins from halophilic organisms (Elcock and McCammon, 1998), and so it stands to reason that neutralization of surface charges is likely a major contributor to the increase in stability seen in *Desulfovibrio desulfuricans* apoflavodoxin as the host organism has been found living in environments of at or above 4 M salt (Kerkar, 2004). Neutralization of repulsive surface charges on highly charged proteins is believed to occur through three possible mechanisms: (a) the Debye-Hückel ion screening effect, (b) direct ion-pairing, and (c) indirectly affecting water structure (Goto and Aimoto, 1991; Goto et al., 1990; Zhang et al., 2005). Our data suggests that all three possible mechanisms are likely employed in the case of cationic effects on apoflavodoxin stability at low (≤ 250 mM) concentrations. In accord with Debye-Hückel screening affects, and data on *Anabaena* apoflavodoxin (Maldonado et al., 2002), we found that at ion concentrations where the protein is effectively saturated (~ 250 mM), the effects of the various cations on apoflavodoxin stability

are similar regardless of their position in the Hofmeister series. In agreement with ion-pairing, we found that at concentrations below 250 mM, apparent specific binding events occurred for the studied cations and their efficacy depended on their position in the Hofmeister series. Finally, the indirect effects of the studied ions on water structure cannot be negated, as the observed ordering of the ionic effects based on their position in the Hofmeister series suggests an integral role of cation-water interactions.

In order to gain a more general view of the mechanism of ionic effects on protein stability, we extended our project to include both small cations and anions at higher concentrations (300 mM – 1.75 M; where Hofmeister effects should dominate) and proteins with vastly different charges (apoflavodoxin and positively charged cytochrome c). Interestingly, we found that the effects of the studied cations and anions were similar for both proteins regardless of charge. Therefore, the portion of the two proteins modulating protein-ion interactions must be common to both proteins – potentially the peptide group or nonpolar side-chains. This contradicts previous findings suggesting that protein charge plays a major role in modulating ionic effects on protein properties (Bostrom et al., 2005). However, our results agree with studies on model amides suggesting a primary role for direct ion-peptide group interactions (Bello et al., 1966; Nandi and Robinson, 1972b). As with our study of ionic effects on protein stability at low concentrations, we once again found strong correlations for ionic effects on apoflavodoxin and cytochrome c stability at high ion concentrations with ion

hydration properties – specifically ion air/water partitioning coefficients, ion effects on surface tension, and anion charge density. These results agree with a number of other studies suggesting that ionic effects on surface tension (Arakawa and Timasheff, 1982; Breslow and Guo, 1990; Jensen et al., 1995; Kaushik and Bhat, 1999; Lee and Timasheff, 1981) and ion charge-density (Collins, 2006; Collins et al., 2007) are major factors in affecting protein stability.

Taken together, our data on the effects of Hofmeister ions on the stability of apoflavodoxin at low (≤ 250 mM) concentrations and oppositely charged proteins at higher (300 mM – 1.75 M) concentrations strongly suggest a major role for ion hydration in modulating protein properties. At low concentrations, our data suggest that direct protein-ion interactions are modulated by the degree of cation hydration and thus the position of the cation in the Hofmeister series. At high concentrations, the similar effects of cations and anions on oppositely charged proteins, and the correlation of ionic effects on protein properties with intrinsic ion hydration again suggests protein-ion interactions – potentially ion-peptide group interactions. In addition to proposing specific mechanisms of ion-protein interactions modulating protein stability, our work in conjunction with other theoretical and experimental efforts have shown that the presence of Hofmeister ions (in physiologically relevant concentrations) can significantly modulate protein properties. As with the steric effects of macromolecular crowding, we suggest that data accumulated in low ionic strength, dilute buffer conditions may often fall short of characterizing protein properties relative to *in vivo* conditions.

Future direction of this project and implications for future in vitro work

Although many exciting (and in some cases, novel) discoveries have been made on the effects of volume exclusion and small ions on the structure and stability of flavodoxin, much remains to be done. In particular, we would like to resolve the effects of macromolecular crowding on the native state of flavodoxin to the residue level. Preliminary NMR data on doubly-labeled flavodoxin in the presence and absence of Ficoll 70 (collaboration with Drs. Kevin MacKenzie and Adina Maximciuc-Kilpatrick) have shown that NMR spectra even in the presence of high concentrations of synthetic crowding agents are analyzable (not shown). NMR data through our first attempts were promising but complex. The completion of NMR experiments on native flavodoxin in the presence of Ficoll 70 could be coupled with attempts to perform in-cell NMR on flavodoxin-overexpressing bacteria (an emerging method of gathering structural information (Bernado et al., 2004; Dedmon et al., 2002; Serber and Dotsch, 2001)).

On a more immediate timescale, I have completed the *in vitro* portion of a project assessing the effects of 100 mg/ml Ficoll 70 on the equilibrium and kinetic properties of wild-type and mutant apoflavodoxins (included in Appendix). Dr. Cheung's group will once again simulate all the studied variants *in silico* to attempt to couple experimental data with information at a greater level of resolution. Although I am just in the preliminary stages of data analysis, it appears that the folding transition state of apoflavodoxin is not grossly altered by the presence of 100 mg/ml Ficoll 70 (100 mM KPi, pH 7). This result could have

been expected, because our previous work showed that Ficoll 70 did not greatly alter the folding pathway of wild-type apoflavodoxin (10 mM HEPES, pH 7). In the future, it would be interesting to perform equilibrium and kinetic studies on the variant apoflavodoxins in the presence of 100 mg/ml dextran 70 which we have shown *in vitro* and *in silico* to affect the kinetic folding process of apoflavodoxin.

As for the importance of our work (and others) on the often overlooked, *intrinsic properties of the intracellular milieu (macromolecular crowding and ionic nature)*, we would strongly urge that *in vitro* conditions for protein biophysical studies include investigations into the effects of synthetic crowding agents and small ions in physiologically relevant amounts before concluding protein biophysical properties and reaction mechanisms. In addition to our work, the recent work on the “intrinsically disordered” protein FlgM showing spontaneous folding by NMR in the presence of crowding (both with synthetic crowders and by in-cell techniques) (Dedmon et al., 2002) is an excellent cautionary tale describing the missteps that can be made in characterizing purified proteins in the absence of conditions mimicking the intracellular environment.

REFERENCES

Adler, A. J., Greenfield, N. J., and Fasman, G. D. (1973). Circular dichroism and optical rotatory dispersion of proteins and polypeptides. *Methods Enzymol* 27, 675-735.

Ai, X., Zhou, Z., Bai, Y., and Choy, W. Y. (2006). 15N NMR spin relaxation dispersion study of the molecular crowding effects on protein folding under native conditions. *J Am Chem Soc* 128, 3916-3917.

Anfinsen, C. B. (1973). Principles that govern the folding of protein chains. *Science* 181, 223-230.

Apiyo, D., and Wittung-Stafshede, P. (2002). Presence of the cofactor speeds up folding of *Desulfovibrio desulfuricans* flavodoxin. *Protein Sci* 11, 1129-1135.

Arakawa, T., and Timasheff, S. N. (1982). Preferential interactions of proteins with salts in concentrated solutions. *Biochemistry* 21, 6545-6552.

Asakura, S. a. O., F. (1954). Interaction between particles suspended in solutions of macromolecules. *Journ Polym Sci* 33, 183-192.

Bai, Y. (2006). Protein folding pathways studied by pulsed- and native-state hydrogen exchange. *Chem Rev* 106, 1757-1768.

Baldwin, R. L. (1996). How Hofmeister ion interactions affect protein stability. *Biophys J* 71, 2056-2063.

Baldwin, R. L. (2008). The search for folding intermediates and the mechanism of protein folding. *Annu Rev Biophys* 37, 1-21.

Batchelor, J. D., Olteanu, A., Tripathy, A., and Pielak, G. J. (2004). Impact of protein denaturants and stabilizers on water structure. *J Am Chem Soc* 126, 1958-1961.

Becklin, R. R., and Desiderio, D. M. (1995). The amount of ultraviolet absorbance in a synthetic peptide is directly proportional to its number of peptide bonds. *Analyt Lett* 28, 2175-2190.

Bello, J., Haas, D., and Bello, H. R. (1966). Interactions of protein-denaturing salts with model amides. *Biochemistry* 5, 2539-2548.

Bernado, P., Garcia de la Torre, J., and Pons, M. (2004). Macromolecular crowding in biological systems: hydrodynamics and NMR methods. *J Mol Recognit* 17, 397-407.

Bertini, I., Gray, H. B., Lippard, S. J., and Valentine, J. S. (1994). *Bioinorganic Chemistry*: University Science Books, Mill Valley, CA).

Bhuyan, A. K. (2002). Protein stabilization by urea and guanidine hydrochloride. *Biochemistry* 41, 13386-13394.

Bolen, D. W. (2001). Protein stabilization by naturally occurring osmolytes, In *Protein structure, stability, and folding*, K. P. Murphy, ed. (Totowa, New Jersey: Humana Press), pp. 17-36.

Bollen, Y. J., Kamphuis, M. B., and van Mierlo, C. P. (2006). The folding energy landscape of apoflavodoxin is rugged: hydrogen exchange reveals nonproductive misfolded intermediates. *Proc Natl Acad Sci U S A* 103, 4095-4100.

Bollen, Y. J., Sanchez, I. E., and van Mierlo, C. P. (2004). Formation of on- and off-pathway intermediates in the folding kinetics of *Azotobacter vinelandii* apoflavodoxin. *Biochemistry* 43, 10475-10489.

Bollen, Y. J., and van Mierlo, C. P. (2005). Protein topology affects the appearance of intermediates during the folding of proteins with a flavodoxin-like fold. *Biophys Chem* 114, 181-189.

Bostrom, M., Tavares, F. W., Finet, S., Skouri-Panet, F., Tardieu, A., and Ninham, B. W. (2005). Why forces between proteins follow different Hofmeister series for pH above and below pI. *Biophys Chem* 117, 217-224.

Breslow, R., and Guo, T. (1990). Surface tension measurements show that chaotropic salting-in denaturants are not just water-structure breakers. *Proc Natl Acad Sci U S A* 87, 167-169.

Bryngelson, J. D., Onuchic, J. N., Socci, N. D., and Wolynes, P. G. (1995). Funnels, pathways, and the energy landscape of protein folding: a synthesis. *Proteins* 21, 167-195.

Bueno, M., Ayuso-Tejedor, S., and Sancho, J. (2006). Do proteins with similar folds have similar transition state structures? A diffuse transition state of the 169 residue apoflavodoxin. *J Mol Biol* 359, 813-824.

Cacace, M. G., Landau, E. M., and Ramsden, J. J. (1997). The Hofmeister series: salt and solvent effects on interfacial phenomena. *Q Rev Biophys* 30, 241-277.

Campos, L. A., Bueno, M., Lopez-Llano, J., Jimenez, M. A., and Sancho, J. (2004). Structure of stable protein folding intermediates by equilibrium phi-analysis: the apoflavodoxin thermal intermediate. *J Mol Biol* 344, 239-255.

Chaffotte, A. F., Cadieux, C., Guillou, Y., and Goldberg, M. E. (1992). A possible initial folding intermediate: the C-terminal proteolytic domain of tryptophan synthase beta chains folds in less than 4 milliseconds into a condensed state with non-native-like secondary structure. *Biochemistry* 31, 4303-4308.

Chan, H. S., and Dill, K. A. (1998). Protein folding in the landscape perspective: chevron plots and non-Arrhenius kinetics. *Proteins* 30, 2-33.

Chen, Y., and Barkley, M. D. (1998). Toward understanding tryptophan fluorescence in proteins. *Biochemistry* 37, 9976-9982.

Cheung, M. S. (2007). Life in a crowd: macromolecular crowding and confinement effects on protein interactions in living systems. .

Cheung, M. S., Klimov, D., and Thirumalai, D. (2005). Molecular crowding enhances native state stability and refolding rates of globular proteins. *Proc Natl Acad Sci U S A* 102, 4753-4758.

Cheung, M. S., and Thirumalai, D. (2007). Effects of crowding and confinement on the structures of the transition state ensemble in proteins. *J Phys Chem B* 111, 8250-8257.

Clementi, C. (2008). Coarse-grained models of protein folding: toy models or predictive tools? *Curr Opin Struct Biol* 18, 10-15.

Clementi, C., Nymeyer, H., and Onuchic, J. N. (2000). Topological and energetic factors: what determines the structural details of the transition state ensemble and "en-route" intermediates for protein folding? An investigation for small globular proteins. *J Mol Biol* 298, 937-953.

Collins, K. D. (1997). Charge density-dependent strength of hydration and biological structure. *Biophys J* 72, 65-76.

Collins, K. D. (2004). Ions from the Hofmeister series and osmolytes: effects on proteins in solution and in the crystallization process. *Methods* 34, 300-311.

Collins, K. D. (2006). Ion hydration: Implications for cellular function, polyelectrolytes, and protein crystallization. *Biophys Chem* 119, 271-281.

Collins, K. D., Neilson, G. W., and Enderby, J. E. (2007). Ions in water: characterizing the forces that control chemical processes and biological structure. *Biophys Chem* 128, 95-104.

Colombo, G., and Micheletti, C. (2006). Protein folding simulations: combining coarse-grained models and all-atom molecular dynamics. *Theor Chem Acc* 116, 75-86.

Cooper, A. (1999). Thermodynamics of protein folding and stability., In *Protein: a comprehensive treatise.*, G. Allen, ed. (JAI Press, Inc.), pp. 217-270.

Courtenay, E. S., Capp, M. W., and Record, M. T., Jr. (2001). Thermodynamics of interactions of urea and guanidinium salts with protein surface: relationship between solute effects on protein processes and changes in water-accessible surface area. *Protein Sci* 10, 2485-2497.

Courtenay, E. S., Capp, M. W., Saecker, R. M., and Record, M. T., Jr. (2000). Thermodynamic analysis of interactions between denaturants and protein surface exposed on unfolding: interpretation of urea and guanidinium chloride m -values and their correlation with changes in accessible surface area (ASA) using preferential interaction coefficients and the local-bulk domain model. *Proteins Suppl* 4, 72-85.

Cremades, N., Bueno, M., Toja, M., and Sancho, J. (2005). Towards a new therapeutic target: *Helicobacter pylori* flavodoxin. *Biophys Chem* 115, 267-276.

da Costa, M. S., Santos, H., and Galinski, E. A. (1998). An overview of the role and diversity of compatible solutes in Bacteria and Archaea. *Adv Biochem Eng Biotechnol* 61, 117-153.

Dedmon, M. M., Patel, C. N., Young, G. B., and Pielak, G. J. (2002). FlgM gains structure in living cells. *Proc Natl Acad Sci U S A* 99, 12681-12684.

Dennis, P. P., and Shimmin, L. C. (1997). Evolutionary divergence and salinity-mediated selection in halophilic archaea. *Microbiol Mol Biol Rev* 61, 90-104.

Di Stasio, E. (2004). Anionic regulation of biological systems: the special role of chloride in the coagulation cascade. *Biophys Chem* 112, 245-252.

Djikaev, Y. S., and Ruckenstein, E. (2009). First passage time analysis of protein folding via nucleation and of barrierless protein denaturation. *Adv Colloid Interface Sci* 146, 18-30.

Dobson, C. M., and Karplus, M. (1999). The fundamentals of protein folding: bringing together theory and experiment. *Curr Opin Struct Biol* 9, 92-101.

Du, F., Zhou, Z., Mo, Z. Y., Shi, J. Z., Chen, J., and Liang, Y. (2006). Mixed macromolecular crowding accelerates the refolding of rabbit muscle creatine kinase: implications for protein folding in physiological environments. *J Mol Biol* 364, 469-482.

Duan, Y., and Kollman, P. A. (1998). Pathways to a protein folding intermediate observed in a 1-microsecond simulation in aqueous solution. *Science* 282, 740-744.

Edwards, Y. H., Edwards, P. A., and Hopkinson, D. A. (1973). A trimeric structure for mammalian purine nucleoside phosphorylase. *FEBS Lett* 32, 235-237.

Eggers, D. K., and Valentine, J. S. (2001). Molecular confinement influences protein structure and enhances thermal protein stability. *Protein Sci* 10, 250-261.

Eicken, C., Sharma, V., Klabunde, T., Lawrenz, M. B., Hardham, J. M., Norris, S. J., and Sacchettini, J. C. (2002). Crystal structure of Lyme disease variable surface antigen VlsE of *Borrelia burgdorferi*. *J Biol Chem* 277, 21691-21696.

Elcock, A. H., and McCammon, J. A. (1998). Electrostatic contributions to the stability of halophilic proteins. *J Mol Biol* 280, 731-748.

Ellis, R. J. (2001a). Macromolecular crowding: an important but neglected aspect of the intracellular environment. *Curr Opin Struct Biol* 11, 114-119.

Ellis, R. J. (2001b). Macromolecular crowding: obvious but underappreciated. *Trends Biochem Sci* 26, 597-604.

Ellis, R. J., and Minton, A. P. (2003). Cell biology: join the crowd. *Nature* 425, 27-28.

Ellis, R. J., and Minton, A. P. (2006). Protein aggregation in crowded environments. *Biol Chem* 387, 485-497.

Engel, R., Westphal, A. H., Huberts, D. H., Nabuurs, S. M., Lindhoud, S., Visser, A. J., and van Mierlo, C. P. (2008). Macromolecular crowding compacts unfolded apoflavodoxin and causes severe aggregation of the off-pathway intermediate during apoflavodoxin folding. *J Biol Chem* 283, 27383-27394.

Englander, S. W., Mayne, L., and Krishna, M. M. (2007). Protein folding and misfolding: mechanism and principles. *Q Rev Biophys* 40, 287-326.

Fasman, G. D. (1996). *Circular dichroism and the conformational analysis of biomolecules*. (New York: Plenum Press).

Fernandez-Recio, J., Genzor, C. G., and Sancho, J. (2001). Apoflavodoxin folding mechanism: an alpha/beta protein with an essentially off-pathway intermediate. *Biochemistry* 40, 15234-15245.

Fersht, A. R., Kellis, J.T., Matouschek, A., and Serrano, L. (1990). Folding pathway enigma. *Nature (London)* 343, 601.

Fersht, A. R., and Sato, S. (2004). Phi-value analysis and the nature of protein-folding transition states. *Proc Natl Acad Sci U S A* 101, 7976-7981.

Fillat, M. F., Borrias, W. E., and Weisbeek, P. J. (1991). Isolation and overexpression in *Escherichia coli* of the flavodoxin gene from *Anabaena* PCC 7119. *Biochem J* 280 (Pt 1), 187-191.

Fink, A. L. (1999). Chaperone-mediated protein folding. *Physiol Rev* 79, 425-449.

Flaugh, S. L., and Lumb, K. J. (2001). Effects of macromolecular crowding on the intrinsically disordered proteins c-Fos and p27(Kip1). *Biomacromolecules* 2, 538-540.

Forsyth, W. R., Bilsel, O., Gu, Z., and Matthews, C. R. (2007). Topology and sequence in the folding of a TIM barrel protein: global analysis highlights partitioning between transient off-pathway and stable on-pathway folding intermediates in the complex folding mechanism of a (betaalpha)₈ barrel of unknown function from *B. subtilis*. *J Mol Biol* 372, 236-253.

Fromme, P. (1996). Structure and function of photosystem I. *Curr Opin Struct Biol* 6, 473-484.

Gangeswaran, R., and Eady, R. R. (1996). Flavodoxin 1 of *Azotobacter vinelandii*: characterization and role in electron donation to purified assimilatory nitrate reductase. *Biochem J* 317 (Pt 1), 103-108.

Genzor, C. G., Perales-Alcon, A., Sancho, J., and Romero, A. (1996). Closure of a tyrosine/tryptophan aromatic gate leads to a compact fold in apo flavodoxin. *Nat Struct Biol* 3, 329-332.

Georlette, D., Blaise, V., Dohmen, C., Bouillenne, F., Damien, B., Depiereux, E., Gerday, C., Uversky, V. N., and Feller, G. (2003). Cofactor binding modulates the conformational stabilities and unfolding patterns of NAD(+)-dependent DNA ligases from *Escherichia coli* and *Thermus scotoductus*. *J Biol Chem* 278, 49945-49953.

Gibson, J. F., Ingram, D. J., and Perutz, M. F. (1956). Orientation of the four haem groups in haemoglobin. *Nature* 178, 906-908.

Goto, Y., and Aimoto, S. (1991). Anion and pH-dependent conformational transition of an amphiphilic polypeptide. *J Mol Biol* 218, 387-396.

Goto, Y., Takahashi, N., and Fink, A. L. (1990). Mechanism of acid-induced folding of proteins. *Biochemistry* 29, 3480-3488.

Goyer, R. A. (1997). Toxic and essential metal interactions. *Annu Rev Nutr* 17, 37-50.

Grantcharova, V., Alm, E. J., Baker, D., and Horwich, A. L. (2001). Mechanisms of protein folding. *Curr Opin Struct Biol* 11, 70-82.

Greene, R. F., Jr., and Pace, C. N. (1974). Urea and guanidine hydrochloride denaturation of ribonuclease, lysozyme, alpha-chymotrypsin, and beta-lactoglobulin. *J Biol Chem* 249, 5388-5393.

Gruebele, M. (1999). The fast protein folding problem. *Annu Rev Phys Chem* 50, 485-516.

Gu, Z., Zitzewitz, J. A., and Matthews, C. R. (2007). Mapping the structure of folding cores in TIM barrel proteins by hydrogen exchange mass spectrometry: the roles of motif and sequence for the indole-3-glycerol phosphate synthase from *Sulfolobus solfataricus*. *J Mol Biol* 368, 582-594.

Guelker, M., Stagg, L., Wittung-Stafshede, P., and Shamoo, Y. (2009). Pseudosymmetry, high copy number and twinning complicate the structure determination of *Desulfovibrio desulfuricans* (ATCC 29577) flavodoxin. *Acta Crystallogr D Biol Crystallogr* 65, 523-534.

Gulukota, K., and Wolynes, P. G. (1994). Statistical mechanics of kinetic proofreading in protein folding in vivo. *Proc Natl Acad Sci U S A* 91, 9292-9296.

Hagihara, Y., Aimoto, S., Fink, A. L., and Goto, Y. (1993). Guanidine hydrochloride-induced folding of proteins. *J Mol Biol* 231, 180-184.

Hall, D., and Dobson, C. M. (2006). Expanding to fill the gap: a possible role for inert biopolymers in regulating the extent of the 'macromolecular crowding' effect. *FEBS Lett* 580, 2584-2590.

Hall, D. A., Vander Kooi, C. W., Stasik, C. N., Stevens, S. Y., Zuiderweg, E. R., and Matthews, R. G. (2001). Mapping the interactions between flavodoxin and its physiological partners flavodoxin reductase and cobalamin-dependent methionine synthase. *Proc Natl Acad Sci U S A* 98, 9521-9526.

Hargrove, M. S., Krzywda, S., Wilkinson, A. J., Dou, Y., Ikeda-Saito, M., and Olson, J. S. (1994). Stability of myoglobin: a model for the folding of heme proteins. *Biochemistry* 33, 11767-11775.

Hartl, F. U., and Martin, J. (1995). Molecular chaperones in cellular protein folding. *Curr Opin Struct Biol* 5, 92-102.

Hartl, F. U., Martin, J., and Neupert, W. (1992). Protein folding in the cell: the role of molecular chaperones Hsp70 and Hsp60. *Annu Rev Biophys Biomol Struct* 21, 293-322.

Helms, L. R., Krey, G. D., and Swenson, R. P. (1990). Identification, sequence determination, and expression of the flavodoxin gene from *Desulfovibrio salexigens*. *Biochem Biophys Res Commun* 168, 809-817.

Helms, L. R., and Swenson, R. P. (1991). Cloning and characterization of the flavodoxin gene from *Desulfovibrio desulfuricans*. *Biochim Biophys Acta* 1089, 417-419.

Hess, J. F., Oosawa, K., Matsumura, P., and Simon, M. I. (1987). Protein phosphorylation is involved in bacterial chemotaxis. *Proc Natl Acad Sci U S A* 84, 7609-7613.

Hills, R. D., Jr., and Brooks, C. L., 3rd (2008a). Coevolution of function and the folding landscape: correlation with density of native contacts. *Biophys J* 95, L57-59.

Hills, R. D., Jr., and Brooks, C. L., 3rd (2008b). Subdomain competition, cooperativity, and topological frustration in the folding of CheY. *J Mol Biol* 382, 485-495.

Hillson, N., Onuchic, J. N., and Garcia, A. E. (1999). Pressure-induced protein-folding/unfolding kinetics. *Proc Natl Acad Sci U S A* 96, 14848-14853.

Hocker, B., Schmidt, S., and Sterner, R. (2002). A common evolutionary origin of two elementary enzyme folds. *FEBS Lett* 510, 133-135.

Hofmeister, F. (1888). Zur Lehre von der Wirkung der Salze. *Arch Exp Pathol Pharmacol*, 247-260.

Homouz, D., Perham, M., Samiotakis, A., Cheung, M. S., and Wittung-Stafshede, P. (2008). Crowded, cell-like environment induces shape changes in aspherical protein. *Proc Natl Acad Sci U S A* 105, 11754-11759.

Homouz, D., Stagg, L., Wittung-Stafshede, P., and Cheung, M. S. (2009). Macromolecular crowding modulates folding mechanism of alpha/beta protein apoflavodoxin. *Biophys J* 96, 671-680.

Houry, W. A., Rothwarf, D. M., and Scheraga, H. A. (1995). The nature of the initial step in the conformational folding of disulphide-intact ribonuclease A. *Nat Struct Biol* 2, 495-503.

Hoy, J. A., Smagghe, B. J., Halder, P., and Hargrove, M. S. (2007). Covalent heme attachment in *Synechocystis* hemoglobin is required to prevent ferrous heme dissociation. *Protein Sci* 16, 250-260.

Hu, Z., Jiang, J., and Rajagopalan, R. (2007). Effects of macromolecular crowding on biochemical reaction equilibria: a molecular thermodynamic perspective. *Biophys J* 93, 1464-1473.

Hughes, N. J., Chalk, P. A., Clayton, C. L., and Kelly, D. J. (1995). Identification of carboxylation enzymes and characterization of a novel four-subunit pyruvate:flavodoxin oxidoreductase from *Helicobacter pylori*. *J Bacteriol* 177, 3953-3959.

Hukushima, K., and Nemoto, K. (1996). Exchange Monte Carlo method and application to spin glass simulations. *Journ Phys Soc Jpn* 65, 1604-1608.

Ittah, V., Kahana, E., Amir, D., and Haas, E. (2004). Applications of time-resolved resonance energy transfer measurements in studies of the molecular crowding effect. *J Mol Recognit* 17, 448-455.

Itzhaki, L. S., Otzen, D. E., and Fersht, A. R. (1995). The structure of the transition state for folding of chymotrypsin inhibitor 2 analysed by protein engineering methods: evidence for a nucleation-condensation mechanism for protein folding. *J Mol Biol* 254, 260-288.

Jackson, S. E., and Fersht, A. R. (1991). Folding of chymotrypsin inhibitor 2. 1. Evidence for a two-state transition. *Biochemistry* 30, 10428-10435.

Jensen, W. A., Armstrong, J. M., De Giorgio, J., and Hearn, M. T. (1995). Stability studies on maize leaf phosphoenolpyruvate carboxylase: the effect of salts. *Biochemistry* 34, 472-480.

Karplus, M., and Weaver, D. L. (1976). Protein-folding dynamics. *Nature* 260, 404-406.

Kathuria, S. V., Day, I. J., Wallace, L. A., and Matthews, C. R. (2008). Kinetic traps in the folding of beta alpha-repeat proteins: CheY initially misfolds before accessing the native conformation. *J Mol Biol* 382, 467-484.

Kaushik, J. K., and Bhat, R. (1999). A mechanistic analysis of the increase in the thermal stability of proteins in aqueous carboxylic acid salt solutions. *Protein Sci* 8, 222-233.

Kauzmann, W. (1959). Some factors in the interpretation of protein denaturation. *Adv Protein Chem* 14, 1-63.

Kaya, H., and Chan, H. S. (2003). Origins of chevron rollovers in non-two-state protein folding kinetics. *Phys Rev Lett* 90, 258104.

Kelly, S. M., and Price, N. C. (1997). The application of circular dichroism to studies of protein folding and unfolding. *Biochim Biophys Acta* 1338, 161-185.

Kerker, S. (2004) Studies on bacteria of the dissimilatory reductive processes of the sulphur cycle from the salt pans of Goa., Goa University.

Kerker, S. (2005). Ecology of hypersaline microorganisms, In *Marine Microbiology: Facets & Opportunities*, N. Ramaiah, ed. (National Institute of Oceanography, Goa), pp. 37-47.

Kiefhaber, T. (1995). Kinetic traps in lysozyme folding. *Proc Natl Acad Sci U S A* 92, 9029-9033.

Kim, D. E., Fisher, C., and Baker, D. (2000). A breakdown of symmetry in the folding transition state of protein L. *J Mol Biol* 298, 971-984.

Kolinski, A. a. S., J. (2004). Reduced models of proteins and their applications. *Polymer* 2, 511-524.

Koonin, E. V., Wolf, Y. I., and Karev, G. P. (2002). The structure of the protein universe and genome evolution. *Nature* 420, 218-223.

Korzhev, D. M., Salvatella, X., Vendruscolo, M., Di Nardo, A. A., Davidson, A. R., Dobson, C. M., and Kay, L. E. (2004). Low-populated folding intermediates of Fyn SH3 characterized by relaxation dispersion NMR. *Nature* 430, 586-590.

Lakowitz, J. R. (1999). Principles of fluorescence spectroscopy. (New York: Kluwer Academic / Plenum).

Laurent, T. C. (1963). The Interaction between Polysaccharides and Other Macromolecules. 5. the Solubility of Proteins in the Presence of Dextran. *Biochem J* 89, 253-257.

Lee, J. C., and Timasheff, S. N. (1981). The stabilization of proteins by sucrose. *J Biol Chem* 256, 7193-7201.

Leopold, P. E., Montal, M., and Onuchic, J. N. (1992). Protein folding funnels: a kinetic approach to the sequence-structure relationship. *Proc Natl Acad Sci U S A* 89, 8721-8725.

Levinthal, C. (1968). Are there pathways for protein folding? . *Journ Chem Phys* 65, 44.

Li, Z., and Scheraga, H. A. (1987). Monte Carlo-minimization approach to the multiple-minima problem in protein folding. *Proc Natl Acad Sci U S A* 84, 6611-6615.

Liang, F. T., Steere, A. C., Marques, A. R., Johnson, B. J., Miller, J. N., and Philipp, M. T. (1999). Sensitive and specific serodiagnosis of Lyme disease by enzyme-linked immunosorbent assay with a peptide based on an immunodominant conserved region of *Borrelia burgdorferi* vlsE. *J Clin Microbiol* 37, 3990-3996.

Lim, W. K., Rosgen, J., and Englander, S. W. (2009). Urea, but not guanidinium, destabilizes proteins by forming hydrogen bonds to the peptide group. *Proc Natl Acad Sci U S A* 106, 2595-2600.

Lindorff-Larsen, K., Vendruscolo, M., Paci, E., and Dobson, C. M. (2004). Transition states for protein folding have native topologies despite high structural variability. *Nat Struct Mol Biol* 11, 443-449.

Lopez-Hernandez, E., and Serrano, L. (1996). Structure of the transition state for folding of the 129 aa protein CheY resembles that of a smaller protein, Cl-2. *Fold Des* 1, 43-55.

Lopez-Llano, J., Campos, L. A., Bueno, M., and Sancho, J. (2006). Equilibrium phi-analysis of a molten globule: the 1-149 apoflavodoxin fragment. *J Mol Biol* 356, 354-366.

Lopez-Llano, J., Maldonado, S., Bueno, M., Lostao, A., Angeles-Jimenez, M., Lillo, M. P., and Sancho, J. (2004). The long and short flavodoxins: I. The role of the differentiating loop in apoflavodoxin structure and FMN binding. *J Biol Chem* 279, 47177-47183.

Lostao, A., El Harrou, M., Daoudi, F., Romero, A., Parody-Morreale, A., and Sancho, J. (2000). Dissecting the energetics of the apoflavodoxin-FMN complex. *J Biol Chem* 275, 9518-9526.

Luby-Phelps, K. (2000). Cytoarchitecture and physical properties of cytoplasm: volume, viscosity, diffusion, intracellular surface area. *Int Rev Cytol* 192, 189-221.

Lumry, R., and Biltonen, R. (1966). Validity of the "two-state" hypothesis for conformational transitions of proteins. *Biopolymers* 4, 917-944.

- Luo, J., Iwakura, M., and Matthews, C. R. (1995). Detection of a stable intermediate in the thermal unfolding of a cysteine-free form of dihydrofolate reductase from *Escherichia coli*. *Biochemistry* 34, 10669-10675.
- Maldonado, S., Irun, M. P., Campos, L. A., Rubio, J. A., Luquita, A., Lostao, A., Wang, R., Garcia-Moreno, E. B., and Sancho, J. (2002). Salt-induced stabilization of apoflavodoxin at neutral pH is mediated through cation-specific effects. *Protein Sci* 11, 1260-1273.
- Maldonado, S., Lostao, A., Irun, M. P., Fernandez-Recio, J., Gustavo Genzor, C., Begona Gonzalez, E., Rubio, J. A., Luquita, A., Daoudi, F., and Sancho, J. (1998). Apoflavodoxin: structure, stability, and FMN binding. *Biochimie* 80, 813-820.
- Mani, R. S., and Kay, C. M. (1976). Physicochemical studies on the creatine kinase M-line protein and its interaction with myosin and myosin fragments. *Biochim Biophys Acta* 453, 391-399.
- Marcus, Y. (1997). *Ion properties* (New York: Marcel Dekker).
- Mason, P. E., Brady, J. W., Neilson, G. W., and Dempsey, C. E. (2007). The interaction of guanidinium ions with a model peptide. *Biophys J* 93, L04-06.
- Matouschek, A., Kellis, J. T., Jr., Serrano, L., Bycroft, M., and Fersht, A. R. (1990). Transient folding intermediates characterized by protein engineering. *Nature* 346, 440-445.
- Matouschek, A., Kellis, J. T., Jr., Serrano, L., and Fersht, A. R. (1989). Mapping the transition state and pathway of protein folding by protein engineering. *Nature* 340, 122-126.
- Maxwell, K. L., Wildes, D., Zarrine-Afsar, A., De Los Rios, M. A., Brown, A. G., Friel, C. T., Hedberg, L., Horng, J. C., Bona, D., Miller, E. J., *et al.* (2005). Protein folding: defining a "standard" set of experimental conditions and a preliminary kinetic data set of two-state proteins. *Protein Sci* 14, 602-616.
- Mayr, L. M., and Schmid, F. X. (1993). Stabilization of a protein by guanidinium chloride. *Biochemistry* 32, 7994-7998.

Medalia, O., Weber, I., Frangakis, A. S., Nicastro, D., Gerisch, G., and Baumeister, W. (2002). Macromolecular architecture in eukaryotic cells visualized by cryoelectron tomography. *Science* 298, 1209-1213.

Melo, E. P., Chen, L., Cabral, J. M., Fojan, P., Petersen, S. B., and Otzen, D. E. (2003). Trehalose favors a cutinase compact intermediate off-folding pathway. *Biochemistry* 42, 7611-7617.

Mevarech, M., Frolow, F., and Gloss, L. M. (2000). Halophilic enzymes: proteins with a grain of salt. *Biophys Chem* 86, 155-164.

Minton, A. P. (1981). Excluded volume as a determinant of macromolecular structure and reactivity. *Biopolymers* 20, 2093-2120.

Minton, A. P. (2000a). Effect of a concentrated "inert" macromolecular cosolute on the stability of a globular protein with respect to denaturation by heat and by chaotropes: a statistical-thermodynamic model. *Biophys J* 78, 101-109.

Minton, A. P. (2000b). Implications of macromolecular crowding for protein assembly. *Curr Opin Struct Biol* 10, 34-39.

Minton, A. P. (2001). The influence of macromolecular crowding and macromolecular confinement on biochemical reactions in physiological media. *J Biol Chem* 276, 10577-10580.

Minton, A. P. (2005a). Influence of macromolecular crowding upon the stability and state of association of proteins: predictions and observations. *J Pharm Sci* 94, 1668-1675.

Minton, A. P. (2005b). Models for excluded volume interaction between an unfolded protein and rigid macromolecular cosolutes: macromolecular crowding and protein stability revisited. *Biophys J* 88, 971-985.

Moore, G. R. a. P., G.W. (1990). *Cytochromes c: evolutionary, structural, and physicochemical aspects.* (New York: Springer-Verlag).

Muller, F. (1992). *Chemistry and biochemistry of flavoenzymes:* CRC Press, Boca Raton, FL).

Muralidhara, B. K., Chen, M., Ma, J., and Wittung-Stafshede, P. (2005). Effect of inorganic phosphate on FMN binding and loop flexibility in *Desulfovibrio desulfuricans* apo-flavodoxin. *J Mol Biol* 349, 87-97.

Muralidhara, B. K., Rathinakumar, R., and Wittung-Stafshede, P. (2006). Folding of *Desulfovibrio desulfuricans* flavodoxin is accelerated by cofactor fly-casting. *Arch Biochem Biophys* 451, 51-58.

Muralidhara, B. K., and Wittung-Stafshede, P. (2003). Can cofactor-binding sites in proteins be flexible? *Desulfovibrio desulfuricans* flavodoxin binds FMN dimer. *Biochemistry* 42, 13074-13080.

Muralidhara, B. K., and Wittung-Stafshede, P. (2004). Thermal unfolding of Apo and Holo *Desulfovibrio desulfuricans* flavodoxin: cofactor stabilizes folded and intermediate states. *Biochemistry* 43, 12855-12864.

Muralidhara, B. K., and Wittung-Stafshede, P. (2005). FMN binding and unfolding of *Desulfovibrio desulfuricans* flavodoxin: "hidden" intermediates at low denaturant concentrations. *Biochim Biophys Acta* 1747, 239-250.

Murzin, A. G., Brenner, S. E., Hubbard, T., and Chothia, C. (1995). SCOP: a structural classification of proteins database for the investigation of sequences and structures. *J Mol Biol* 247, 536-540.

Myers, J. K., Pace, C. N., and Scholtz, J. M. (1995). Denaturant m values and heat capacity changes: relation to changes in accessible surface areas of protein unfolding. *Protein Sci* 4, 2138-2148.

Nabuurs, S. M., Westphal, A. H., and van Mierlo, C. P. (2008). Extensive formation of off-pathway species during folding of an alpha-beta parallel protein is due to docking of (non)native structure elements in unfolded molecules. *J Am Chem Soc* 130, 16914-16920.

Nandi, P. K., and Robinson, D. R. (1972a). The effects of salts on the free energies of nonpolar groups in model peptides. *J Am Chem Soc* 94, 1308-1315.

Nandi, P. K., and Robinson, D. R. (1972b). The effects of salts on the free energy of the peptide group. *J Am Chem Soc* 94, 1299-1308.

Naslund, L. A., Edwards, D. C., Wernet, P., Bergmann, U., Ogasawara, H., Pettersson, L. G., Myneni, S., and Nilsson, A. (2005). X-ray absorption spectroscopy study of the hydrogen bond network in the bulk water of aqueous solutions. *J Phys Chem A* *109*, 5995-6002.

Neudecker, P., Zarrine-Afsar, A., Choy, W. Y., Muhandiram, D. R., Davidson, A. R., and Kay, L. E. (2006). Identification of a collapsed intermediate with non-native long-range interactions on the folding pathway of a pair of Fyn SH3 domain mutants by NMR relaxation dispersion spectroscopy. *J Mol Biol* *363*, 958-976.

Nielsen, S. O., Lopez, C.F., Srinivas, G., and Klein, M.L. (2004). Coarse grain models and the computer simulation of soft materials. *Journ Phys Cond Matter* *16*, R481-512.

Nogues, I., Hervas, M., Peregrina, J. R., Navarro, J. A., de la Rosa, M. A., Gomez-Moreno, C., and Medina, M. (2005). Anabaena flavodoxin as an electron carrier from photosystem I to ferredoxin-NADP⁺ reductase. Role of flavodoxin residues in protein-protein interaction and electron transfer. *Biochemistry* *44*, 97-104.

Norcross, T. S., and Yeates, T. O. (2006). A framework for describing topological frustration in models of protein folding. *J Mol Biol* *362*, 605-621.

Northey, J. G., Di Nardo, A. A., and Davidson, A. R. (2002). Hydrophobic core packing in the SH3 domain folding transition state. *Nat Struct Biol* *9*, 126-130.

Oliveberg, M. (2001). Characterisation of the transition states for protein folding: towards a new level of mechanistic detail in protein engineering analysis. *Curr Opin Struct Biol* *11*, 94-100.

Ollivier, B., Caumette, P., Garcia, J. L., and Mah, R. A. (1994). Anaerobic bacteria from hypersaline environments. *Microbiol Rev* *58*, 27-38.

Omta, A. W., Kropman, M. F., Woutersen, S., and Bakker, H. J. (2003). Negligible effect of ions on the hydrogen-bond structure in liquid water. *Science* *301*, 347-349.

Onuchic, J. N., Luthey-Schulten, Z., and Wolynes, P. G. (1997). Theory of protein folding: the energy landscape perspective. *Annu Rev Phys Chem* *48*, 545-600.

Pace, C. N., and Grimsley, G. R. (1988). Ribonuclease T1 is stabilized by cation and anion binding. *Biochemistry* 27, 3242-3246.

Pace, C. N., Vajdos, F., Fee, L., Grimsley, G., and Gray, T. (1995). How to measure and predict the molar absorption coefficient of a protein. *Protein Sci* 4, 2411-2423.

Pegram, L. M., and Record, M. T., Jr. (2007). Hofmeister salt effects on surface tension arise from partitioning of anions and cations between bulk water and the air-water interface. *J Phys Chem B* 111, 5411-5417.

Perham, M., Stagg, L., and Wittung-Stafshede, P. (2007). Macromolecular crowding increases structural content of folded proteins. *FEBS Lett* 581, 5065-5069.

Pozdnyakova, I., Guidry, J., and Wittung-Stafshede, P. (2001). Copper stabilizes azurin by decreasing the unfolding rate. *Arch Biochem Biophys* 390, 146-148.

Privalov, P. L. (1979). Stability of proteins: small globular proteins. *Adv Protein Chem* 33, 167-241.

Privalov, P. L. (1982). Stability of proteins. Proteins which do not present a single cooperative system. *Adv Protein Chem* 35, 1-104.

Privalov, P. L., and Khechinashvili, N. N. (1974). A thermodynamic approach to the problem of stabilization of globular protein structure: a calorimetric study. *J Mol Biol* 86, 665-684.

Qu, Y., and Bolen, D. W. (2002). Efficacy of macromolecular crowding in forcing proteins to fold. *Biophys Chem* 101-102, 155-165.

Ramos, C. H., and Baldwin, R. L. (2002). Sulfate anion stabilization of native ribonuclease A both by anion binding and by the Hofmeister effect. *Protein Sci* 11, 1771-1778.

Record, M. T., Jr., Courtenay, E. S., Cayley, D. S., and Guttman, H. J. (1998a). Responses of *E. coli* to osmotic stress: large changes in amounts of cytoplasmic solutes and water. *Trends Biochem Sci* 23, 143-148.

Record, M. T., Jr., Courtenay, E. S., Cayley, S., and Guttman, H. J. (1998b). Biophysical compensation mechanisms buffering E. coli protein-nucleic acid interactions against changing environments. *Trends Biochem Sci* 23, 190-194.

Rhee, Y. M., Sorin, E. J., Jayachandran, G., Lindahl, E., and Pande, V. S. (2004). Simulations of the role of water in the protein-folding mechanism. *Proc Natl Acad Sci U S A* 101, 6456-6461.

Richard, A. J., Liu, C. C., Klinger, A. L., Todd, M. J., Mezzasalma, T. M., and LiCata, V. J. (2006). Thermal stability landscape for Klenow DNA polymerase as a function of pH and salt concentration. *Biochim Biophys Acta* 1764, 1546-1552.

Robinson, D. R., and Jencks, W. P. (1965). The Effect of Compounds of the Urea-Guanidinium Class on the Activity Coefficient of Acetyltetraglycine Ethyl Ester and Related Compounds. *J Am Chem Soc* 87, 2462-2470.

Rogers, L. J., and Sykes, G. A. (1990). Conformational changes in *Chondrus crispus* flavodoxin on dissociation of FMN and reconstitution with flavin analogues. *Biochem J* 272, 775-779.

Romero, A., Caldeira, J., Legall, J., Moura, I., Moura, J. J., and Romao, M. J. (1996). Crystal structure of flavodoxin from *Desulfovibrio desulfuricans* ATCC 27774 in two oxidation states. *Eur J Biochem* 239, 190-196.

Rose, G. D., Fleming, P. J., Banavar, J. R., and Maritan, A. (2006). A backbone-based theory of protein folding. *Proc Natl Acad Sci U S A* 103, 16623-16633.

Rothman, J. E. (1989). Polypeptide chain binding proteins: catalysts of protein folding and related processes in cells. *Cell* 59, 591-601.

Sali, A., Shakhnovich, E., and Karplus, M. (1994). How does a protein fold? *Nature* 369, 248-251.

Sanbonmatsu, K. Y., and Garcia, A. E. (2002). Structure of Met-enkephalin in explicit aqueous solution using replica exchange molecular dynamics. *Proteins* 46, 225-234.

Sanchez-Ruiz, J. M. (1992). Theoretical analysis of Lumry-Eyring models in differential scanning calorimetry. *Biophys Journ* 61, 921-935.

Sanchez, I. E., and Kiefhaber, T. (2003). Origin of unusual phi-values in protein folding: evidence against specific nucleation sites. *J Mol Biol* 334, 1077-1085.

Sancho, J. (2006). Flavodoxins: sequence, folding, binding, function and beyond. *Cell Mol Life Sci* 63, 855-864.

Santoro, M. M., and Bolen, D. W. (1988). Unfolding free energy changes determined by the linear extrapolation method. 1. Unfolding of phenylmethanesulfonyl alpha-chymotrypsin using different denaturants. *Biochemistry* 27, 8063-8068.

Sasahara, K., McPhie, P., and Minton, A. P. (2003). Effect of dextran on protein stability and conformation attributed to macromolecular crowding. *J Mol Biol* 326, 1227-1237.

Schaefer, M., and Gitlin, J. D. (1999). Genetic disorders of membrane transport. IV. Wilson's disease and Menkes disease. *Am J Physiol* 276, G311-314.

Schellman, J. A. (1987). The thermodynamic stability of proteins. *Annu Rev Biophys Chem* 16, 115-137.

Scheraga, H. A., Khalili, M., and Liwo, A. (2007). Protein-folding dynamics: overview of molecular simulation techniques. *Annu Rev Phys Chem* 58, 57-83.

Sedlak, E., Stagg, L., and Wittung-Stafshede, P. (2008a). Effect of Hofmeister ions on protein thermal stability: Roles of ion hydration and peptide groups? *Arch Biochem Biophys* 479, 69-73.

Sedlak, E., Stagg, L., and Wittung-Stafshede, P. (2008b). Role of cations in stability of acidic protein *Desulfovibrio desulfuricans* apoflavodoxin. *Arch Biochem Biophys* 474, 128-135.

Semisotnov, G. V., Rodionova, N. A., Razgulyaev, O. I., Uversky, V. N., Gripas, A. F., and Gilmanshin, R. I. (1991). Study of the "molten globule" intermediate state in protein folding by a hydrophobic fluorescent probe. *Biopolymers* 31, 119-128.

Serber, Z., and Dotsch, V. (2001). In-cell NMR spectroscopy. *Biochemistry* 40, 14317-14323.

Shakhnovich, E. I., and Finkelstein, A. V. (1989). Theory of cooperative transitions in protein molecules. I. Why denaturation of globular protein is a first-order phase transition. *Biopolymers* 28, 1667-1680.

Shea, J. E., and Brooks, C. L., 3rd (2001). From folding theories to folding proteins: a review and assessment of simulation studies of protein folding and unfolding. *Annu Rev Phys Chem* 52, 499-535.

Shukla, N., Bhatt, A. N., Aliverti, A., Zanetti, G., and Bhakuni, V. (2005). Guanidinium chloride- and urea-induced unfolding of FprA, a mycobacterium NADPH-ferredoxin reductase: stabilization of an apo-protein by GdmCl. *Febs J* 272, 2216-2224.

Silow, M., and Oliveberg, M. (1997). Transient aggregates in protein folding are easily mistaken for folding intermediates. *Proc Natl Acad Sci U S A* 94, 6084-6086.

Spencer, D. S., Xu, K., Logan, T. M., and Zhou, H. X. (2005). Effects of pH, salt, and macromolecular crowding on the stability of FK506-binding protein: an integrated experimental and theoretical study. *J Mol Biol* 351, 219-232.

Stagg, L., Zhang, S. Q., Cheung, M. S., and Wittung-Stafshede, P. (2007). Molecular crowding enhances native structure and stability of alpha/beta protein flavodoxin. *Proc Natl Acad Sci U S A* 104, 18976-18981.

Steensma, E., and van Mierlo, C. P. (1998). Structural characterisation of apoflavodoxin shows that the location of the stable nucleus differs among proteins with a flavodoxin-like topology. *J Mol Biol* 282, 653-666.

Stok, J. E., and De Voss, J. (2000). Expression, purification, and characterization of Biol: a carbon-carbon bond cleaving cytochrome P450 involved in biotin biosynthesis in *Bacillus subtilis*. *Arch Biochem Biophys* 384, 351-360.

Street, T. O., Bolen, D. W., and Rose, G. D. (2006). A molecular mechanism for osmolyte-induced protein stability. *Proc Natl Acad Sci U S A* 103, 13997-14002.

Stryer, L. (1968). Fluorescence spectroscopy of proteins. *Science* 162, 526-533.

Tellam, R. L., Sculley, M. J., Nichol, L. W., and Wills, P. R. (1983). The influence of poly(ethylene glycol) 6000 on the properties of skeletal-muscle actin. *Biochem J* 213, 651-659.

Timasheff, S. N. (1992). Water as ligand: preferential binding and exclusion of denaturants in protein unfolding. *Biochemistry* 31, 9857-9864.

Tokuriki, N., Kinjo, M., Negi, S., Hoshino, M., Goto, Y., Urabe, I., and Yomo, T. (2004). Protein folding by the effects of macromolecular crowding. *Protein Sci* 13, 125-133.

Ueda, Y., Taketomi, H., and Go, N. (1975). Studies on protein folding, unfolding and fluctuations by computer simulation. I. The effect of specific amino acid sequence represented by specific inter-unit interactions. *Int Journ Pept Prot Res* 7, 445-459.

Ueda, Y., Taketomi, H., and Go, N. (1978). Studies on protein folding, unfolding and fluctuations by computer simulation. A three-dimensional lattice model of lysozyme. *Biopolymers* 17, 1531-1548.

Unneberg, P., Merelo, J. J., Chacon, P., and Moran, F. (2001). SOMCD: method for evaluating protein secondary structure from UV circular dichroism spectra. *Proteins* 42, 460-470.

Uversky, V. N., and Ptitsyn, O. B. (1996). All-or-none solvent-induced transitions between native, molten globule and unfolded states in globular proteins. *Fold Des* 1, 117-122.

van den Berg, B., Wain, R., Dobson, C. M., and Ellis, R. J. (2000). Macromolecular crowding perturbs protein refolding kinetics: implications for folding inside the cell. *Embo J* 19, 3870-3875.

Vargas, J. (2003). *Stem cell research* (New York: The Rosen Publishing Group, Inc.).

Veitshans, T., Klimov, D., and Thirumalai, D. (1997). Protein folding kinetics: timescales, pathways and energy landscapes in terms of sequence-dependent properties. *Fold Des* 2, 1-22.

Venturoli, D., and Rippe, B. (2005). Ficoll and dextran vs. globular proteins as probes for testing glomerular permselectivity: effects of molecular size, shape, charge, and deformability. *Am J Physiol Renal Physiol* 288, F605-613.

Von Hippel, P. H., and Hamabata, A. (1973). Model studies on the effects of neutral salts on the conformational stability of biological macromolecules. *J Mechanochem Cell Motil* 2, 127-138.

Watenpaugh, K. D., Sieker, L. C., Jensen, L. H., Legall, J., and Dubourdieu, M. (1972). Structure of the oxidized form of a flavodoxin at 2.5-Angstrom resolution: resolution of the phase ambiguity by anomalous scattering. *Proc Natl Acad Sci U S A* 69, 3185-3188.

Wenner, J. R., and Bloomfield, V. A. (1999). Crowding effects on EcoRV kinetics and binding. *Biophys J* 77, 3234-3241.

Wetlaufer, D. B. (1973). Nucleation, rapid folding, and globular intrachain regions in proteins. *Proc Natl Acad Sci U S A* 70, 697-701.

Wetlaufer, D. B., Malik, S.K., Stoller, L., and Coffin, R.I. (1964). *J Am Chem Soc*, 508.

Woody, R. W. (1995). Circular dichroism. *Methods Enzymol* 246, 34-71.

Wright, P. E., and Dyson, H. J. (1999). Intrinsically unstructured proteins: re-assessing the protein structure-function paradigm. *J Mol Biol* 293, 321-331.

Wu, H. (1931). Studies on denaturation of proteins. *Chin J Physiol* *xiii*, 321-344.

Wu, Y., Vadrevu, R., Kathuria, S., Yang, X., and Matthews, C. R. (2007). A tightly packed hydrophobic cluster directs the formation of an off-pathway sub-millisecond folding intermediate in the alpha subunit of tryptophan synthase, a TIM barrel protein. *J Mol Biol* 366, 1624-1638.

Yankovskaya, V., Horsefield, R., Tornroth, S., Luna-Chavez, C., Miyoshi, H., Leger, C., Byrne, B., Cecchini, G., and Iwata, S. (2003). Architecture of succinate dehydrogenase and reactive oxygen species generation. *Science* 299, 700-704.

Zhang, Y., Furyk, S., Bergbreiter, D. E., and Cremer, P. S. (2005). Specific ion effects on the water solubility of macromolecules: PNIPAM and the Hofmeister series. *J Am Chem Soc* 127, 14505-14510.

Zhou, H. X. (2004). Protein folding and binding in confined spaces and in crowded solutions. *J Mol Recognit* 17, 368-375.

Zimmerman, S. B., and Minton, A. P. (1993). Macromolecular crowding: biochemical, biophysical, and physiological consequences. *Annu Rev Biophys Biomol Struct* 22, 27-65.

Zurbriggen, M. D., Tognetti, V. B., and Carrillo, N. (2007). Stress-inducible flavodoxin from photosynthetic microorganisms. The mystery of flavodoxin loss from the plant genome. *IUBMB Life* 59, 355-360.

APPENDIX

Effects of macromolecular crowding on apoflavodoxin folding mechanism

In order to assess the effects of excluded volume on apoflavodoxin folding, I used the apoflavodoxin variants from the previous studies along with 100 mg/ml Ficoll 70. The reason for choosing this concentration of crowding agent was simply because of limitations due to reagent volumes as a result of the amounts of stock protein, stock KPi buffer, and 10 M urea. Unfortunately at the time this manuscript is being written, only the *in vitro* data has been completed, and Dr. Cheung's group will simulate the variants with spherical crowding agents in the near future.

Effects of crowding on wild-type and mutant apoflavodoxin equilibrium stability

As with our previous studies, we expect that macromolecular crowding should stabilize wild-type and mutant apoflavodoxins against thermal and chemical equilibrium denaturation. Using the thermal transition data from Stagg et. al (2007), we postulated that thermal transitions for wild-type and mutant apoflavodoxins should increase on average 1-2 °C in 100 mg/ml Ficoll 70 compared to the buffer condition (100 mM KPi, pH 7) (using data from Table 3.2 assessing increase in T_m upon addition of 100 mg/ml Ficoll in 20 mM KPi and 40 mM KPi, 250 mM NaCl conditions). In fact, the average change in T_m for all the studied variants is + 1.8 °C upon the addition of 100 mg/ml Ficoll 70 (monitored by CD signal at 222 nm) (Table A.1). For a few of the mutants (L5A, V7A, and

Variant	2° Structure	T _m (°C)	ΔT _m (°C)	ΔG _U (kJ/mol)	ΔΔG _U (kJ/mol)	m-value (kJ/mol,M)	Δm-value (kJ/mol,M)	[urea] _{1/2} (M)	Δ[urea] _{1/2} (M)
wt	-	69.7 ± 0.1	1.8	26.5 ± 1.8	0.2	5.7 ± 0.5	-0.6	4.66	0.4
L5A	β1	62.3 ± 0.1	-0.4	17.7 ± 1.1	1.9	6.3 ± 0.4	-0.1	2.80	0.4
V7A	β1	59.3 ± 0.1	-0.3	18.0 ± 0.6	0.7	6.7 ± 0.2	-0.5	2.66	0.3
A19G	α1	61.5 ± 0.1	0.5	16.7 ± 0.4	1.5	5.0 ± 0.1	0	3.36	0.3
V33A	β2	61.5 ± 0.1	-0.3	16.0 ± 0.5	0.8	5.2 ± 0.2	-0.1	3.08	0.2
L36A	β2	64.2 ± 0.1	3.8	17.6 ± 0.9	0.9	5.4 ± 0.3	-0.3	3.22	0.3
V53A	β3	56.8 ± 0.1	1.1	14.0 ± 1.0	0.3	5.7 ± 0.4	0.3	2.48	-0.1
F55A	β3	52.9 ± 0.1	0.8	6.7 ± 0.3	-1.3	2.7 ± 0.1	-0.9	2.51	0.3
L74A	α2	58.5 ± 0.1	2.1	7.9 ± 1.4	1.4	4.1 ± 0.5	1.0	1.91	-0.2
V88A	β4	57.8 ± 0.1	3.4	15.0 ± 0.8	1.7	4.3 ± 0.3	-0.2	3.52	0.6
E109A	α3	67.2 ± 0.1	0.6	16.5 ± 0.8	1.8	4.8 ± 0.2	0.1	3.44	0.3
I120A	β5	53.1 ± 0.1	3.9	8.4 ± 0.8	2.5	2.8 ± 0.3	0.6	2.96	0.4
L124A	β5	61.2 ± 0.1	4.1	10.2 ± 1.6	3.1	4.3 ± 0.6	0.7	2.36	0.2
V137A	α4	52.6 ± 0.2	3.3	7 ± 0.3	0.5	2.4 ± 0.1	0	2.95	0.2
Average			1.8		1.1		0.0		0.3

Table A.1 – Equilibrium values calculated for wild-type and mutant apoflavodoxins in the presence of 100 mg/ml Ficoll 70 (100 mM KPi, pH 7). ΔT_m, ΔΔG_U, Δm-value, and Δ[urea]_{1/2} values calculated as value_{100mg/ml Ficoll 70} – value_{buffer}. All values calculated from experiments monitoring CD signal at 222 nm.

V33A), the calculated T_m in 100 mg/ml Ficoll 70 decreased slightly, however, the decreases are small and may not be significant.

Similarly, we would expect that 100 mg/ml Ficoll 70 should stabilize the studied variants against urea denaturation. As touched on earlier in Chapter 3, we noted that the calculated $\Delta G_U(H_2O)$ value for wild-type apoflavodoxin did not increase significantly in the presence of 100 mg/ml Ficoll 70 using 100 mM KPi, pH 7 as the buffer condition (likely a result of a slightly lower m -value). However, the midpoint of unfolding for wild-type apoflavodoxin does increase (approximately + 0.4 M urea). On average, the calculated $\Delta G_U(H_2O)$ values for the studied apoflavodoxins modestly increased (+ 1.1 kJ/mol) in the presence of 100 mg/ml Ficoll 70. In addition, calculated urea midpoints of unfolding increased on average by 0.3 M urea. Calculated m -values fluctuated approximately ± 1 kJ/mol, M for the studied apoflavodoxins, however, the average m -value for the entire set of variants did not change as a result of 100 mg/ml Ficoll 70.

Effects of crowding on kinetic folding/unfolding of wild-type and mutant apoflavodoxins

Efforts to assess the effects of crowding (100 mg/ml Ficoll 70) on the kinetic folding mechanism of wild-type and mutant apoflavodoxins were muddied by the presence of significant rollover in the folding arms of many of the studied proteins (and at least some rollover in all proteins). Rollover (non-Arrhenius) kinetics are difficult to analyze and draw conclusions. Rollover in the folding arms of Chevron

plots may mean that an additional intermediate state is populating or that the transition state is moving along the reaction coordinate (Houry et al., 1995; Kaya and Chan, 2003; Kiefhaber, 1995; Matouschek et al., 1990; Silow and Oliveberg, 1997). In order to attempt to analyze the data as accurately and thoroughly as possible, I assessed the Chevron plots in two ways: (1) I excluded data points in the non-linear portions of the folding arm and fit the Chevrans in a fundamental manner (Fig. A.1), and (2) I introduced a variable into the fit to describe the curvature of the folding arm to extrapolate the curved folding arm to zero denaturant (Fig. A.2) (fit adapted from (Maxwell et al., 2005)):

$$\ln k_{\text{obs}} = \ln[e^{((A + m_f[D] / RT) + c_f[D]^2)} + e^{((B + m_u[D] / RT) + c_u[D]^2)}] \quad (\text{Eq. A.1})$$

where A is $\ln k_f^{\text{H}_2\text{O}}$, B is $\ln k_u^{\text{H}_2\text{O}}$, m_f and m_u are the slopes of the linear portions of the Chevron, and c_f and c_u are constants describing the curvature of the folding and unfolding phases.

Thus we have two sets of folding and unfolding rates for the studied variants and two sets of Φ -values (Table A.2). I again calculated Φ -values using unfolding rates and equilibrium $\Delta\Delta G_U$ values, and as the unfolding phases of these Chevrans are roughly linear, we expect the Φ -values calculated using linear and curved fits to be in close agreement. Interestingly, although a few of the Φ -values do change as a result of the addition of 100 mg/ml Ficoll 70 (especially A19G), qualitatively, the Φ -values calculated by both linear and curved fits suggest that the transition state of apoflavodoxin is largely unchanged as a result of crowding. We could have predicted as much based on the fact that

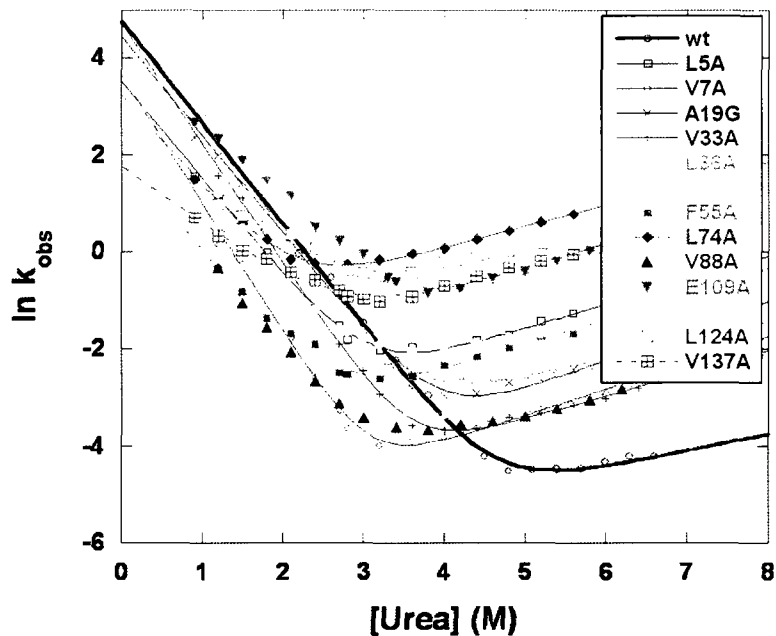


Figure A.1 – Chevron plots of wild-type and mutant apoflavodoxins in the presence of 100 mg/ml Ficoll 70 excluding data points in rollover portion of folding arm (100 mM KPi, pH 7, 20 °C).

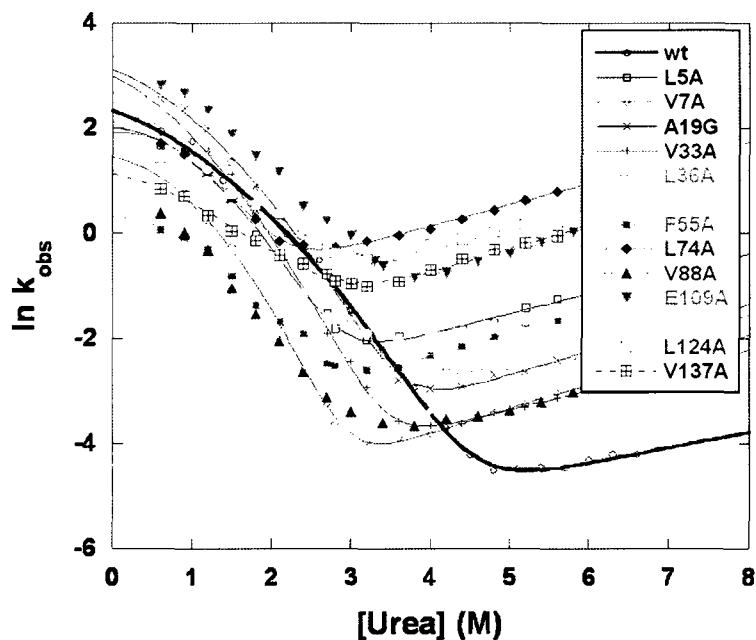


Figure A.2 – Chevron plots for wild-type and mutant apoflavodoxins containing all data points from stopped-flow mixing experiments with apparent rollover in folding arms (100 mM KPi, pH 7, 20 °C).

<i>Linear Fits</i>						
Variant	2° Structure	% Miss. Amp. (Ref.)	$k_{f(\text{obs})}$ (s ⁻¹)	k_u (s ⁻¹)	$\Delta G_{U,\text{kin}}$ (kJ/mol)	Φ_f
wt	-	40.9	115.7 ± 31.7	0.0015 ± 0.0010	27.4	-
L5A	β1	56.4	33.6 ± 4.5	0.0174 ± 0.0048	18.4	0.33
V7A	β1	67.0	38.8 ± 11.8	0.0023 ± 0.0010	23.7	0.88
A19G	α1	15.6	83.3 ± 11.7	0.0028 ± 0.0015	25.1	0.85
V33A	β2	21.1	109.9 ± 12.4	0.0030 ± 0.0007	25.6	0.84
L36A	β2	40.9	186.8 ± 65.7	0.0117 ± 0.0016	23.6	0.44
V53A	β3	30.8	38.8 ± 4.4	0.0109 ± 0.0021	19.9	0.62
F55A	β3	48.4	6.2 ± 1.2	0.0108 ± 0.0025	15.5	0.76
L74A	α2	35.8	25.2 ± 2.8	0.1830 ± 0.0177	12.0	0.37
V88A	β4	41.4	7.9 ± 0.7	0.0045 ± 0.0005	18.2	0.77
E109A	α3	30.5	62.0 ± 6.0	0.0259 ± 0.0072	18.9	0.31
I120A	β5	36.4	53.3 ± 6.0	0.0453 ± 0.0077	17.2	0.54
L124A	β5	37.8	12.5 ± 3.0	0.1024 ± 0.0406	11.7	0.33
V137A	α4	37.0	5.8 ± 0.8	0.0547 ± 0.0138	11.4	0.55

<i>Rollover Fits</i>						
Variant	2° Structure	% Miss. Amp. (Ref.)	$k_{f(\text{obs})}$ (s ⁻¹)	k_u (s ⁻¹)	$\Delta G_{U,\text{kin}}$ (kJ/mol)	Φ_f
wt	-	40.9	10.2 ± 1.6	0.0022 ± 0.0012	20.6	-
L5A	β1	56.4	7.4 ± 1.4	0.0317 ± 0.0056	13.3	0.26
V7A	β1	67.0	4.2 ± 0.3	0.0034 ± 0.0009	17.3	0.87
A19G	α1	15.6	22.1 ± 2.9	0.0071 ± 0.0016	19.6	0.71
V33A	β2	21.1	19.7 ± 3.2	0.0052 ± 0.0012	20.1	0.80
L36A	β2	40.9	8.2 ± 0.5	0.0171 ± 0.0041	14.4	0.43
V53A	β3	30.8	14.5 ± 4.4	0.0135 ± 0.0043	17.0	0.64
F55A	β3	48.4	1.3 ± 0.3	0.0145 ± 0.0028	11.0	0.77
L74A	α2	35.8	6.5 ± 1.2	0.2295 ± 0.0186	8.1	0.39
V88A	β4	41.4	3.3 ± 0.5	0.0055 ± 0.0009	15.6	0.80
E109A	α3	30.5	28.3 ± 3.8	0.0452 ± 0.0097	15.7	0.26
I120A	β5	36.4	23.6 ± 1.7	0.0582 ± 0.0135	14.6	0.56
L124A	β5	37.8	3.8 ± 0.2	0.1551 ± 0.0276	7.8	0.32
V137A	α4	37.0	3.0 ± 0.5	0.0778 ± 0.0148	8.9	0.55

Table A.2 – Kinetic folding (apparent) and unfolding rates, free energies of unfolding, and Φ -values calculated by linear fits (top panel) and fits to the rollover kinetics (bottom panel) for wild-type and mutant apoflavodoxins in the presence of 100 mg/ml Ficoll 70 (100 mM KPi, pH 7, 20 °C). Φ -values calculated using unfolding rates as described in text.

the presence of 150 mg/ml Ficoll 70 did not change the amount of observed off-pathway burst-phase intermediate nor did it significantly change the *in silico* folding pathway of apoflavodoxin (Homouz et al., 2009). Calculated missing amplitudes do appear to change for a number of the variant apoflavodoxins in the presence of 100 mg/ml Ficoll 70 relative to the buffer condition, but assessing this data relative to folding pathway heterogeneity is impossible at this point without *in silico* data.